PREDICTING SPATIAL DISTRIBUTION OF CRITICAL PORE TYPES AND THEIR INFLUENCE ON RESERVOIR QUALITY, CANYON (PENNSYLVANIAN) REEF RESERVOIR, DIAMOND M FIELD, TEXAS

A Thesis

by

AARON JAY FISHER

Submitted to the Office of Graduate Studies of
Texas A&M University
in partial fulfillment of the requirements for the degree of

MASTER OF SCIENCE

December 2005

Major Subject: Geology

PREDICTING SPATIAL DISTRIBUTION OF CRITICAL PORE TYPES AND

THEIR INFLUENCE ON RESERVOIR QUALITY, CANYON

(PENNSYLVANIAN) REEF RESERVOIR, DIAMOND M FIELD, TEXAS

A Thesis

by

AARON JAY FISHER

Submitted to the Office of Graduate Studies of
Texas A&M University
in partial fulfillment of the requirements for the degree of

MASTER OF SCIENCE

Approved by:

Chair of Committee,   Wayne Ahr
Committee Members,   John Spang
                          Duane McVay
Head of Department,   Richard Carlson

December 2005

Major Subject: Geology

ABSTRACT

Predicting Spatial Distribution of Critical Pore Types and Their Influence on

Reservoir Quality, Canyon (Pennsylvanian) Reef Reservoir,

Diamond M Field, Texas. (December 2005)

Aaron Jay Fisher, B.S., University of Nebraska, Lincoln

Chair of Advisory Committee: Dr. Wayne M. Ahr

This study examined the stratigraphic architecture, depositional and diagenetic

histories, and resulting reservoir characteristics that have influenced the occurrence,

distribution, and quality of flow units in the Diamond M field, Scurry County, Texas.

The study area is located in the Midland Basin. The field has production from the

Canyon (Pennsylvanian) Horseshoe Atoll carbonate buildup. Recent drilling in the

Diamond M field was done to evaluate ways to improve recovery by water flooding.

Classification of depositional texture based on detailed petrologic and petrographic

studies on three cores was done. Subsequent genetic classification of pore types by thin

section petrography revealed three dominant pore types: intramatrix, moldic, and vuggy.

The reservoir was zoned according to dominant pore type and log signatures to evaluate

correlations at field scale by using neutron logs. Equations determined from core

analyses provided equations used for estimating porosity and permeability, which were

used to develop a ranking scheme for reservoir quality based on good, intermediate, and

poor flow units at field scale. Ultimately slice maps of reservoir quality at a 10 ft

interval for a 150 ft section of the Canyon Reef reservoir were developed. These

reservoir quality maps will provide a useful tool for the design and implementation of

accurate and profitable development programs.

ACKNOWLEDGMENTS

NOMENCLATURE AND ABBREVIATIONS

Production:
bbls = barrels
Mcf = million cubic feet

Permeability Data:
k = permeability in μm^2 or md ($1md = 9.871* 10^{-4}$ μm^2

Porosity Types:
V = vuggy
M = moldic
F = fracture
S = styolitic
CRIC = cement reduced intercrystalline
SEIM = solution enhanced intramatrix
SEIP = solution enhanced intraparticle

TABLE OF CONTENTS

LIST OF FIGURES

LIST OF TABLES

INTRODUCTION

Definition of the Problem

Porosity in carbonate reservoirs occurs in three end-member genetic categories;

depositional, diagenetic, and fracture. Depositional porosity in detrital rocks can be

comparatively simple to interpret and map at field scale. Porosity in reefs may be

fracture or non fracture depositional, hybrid, or purely diagenetic and in its simplest

form, it follows biological fabrics that have neither intuitive distribution patterns nor

simple pore geometries. This study examines a phylloid algal mound complex in which

a sponsor company, Parallel Petroleum Co. identified remaining bypassed oil after

secondary recovery by water flooding therefore, an infill drilling program has been

initiated to recover the remaining oil. This thesis is aimed at finding solutions to the

problems of where the bypassed oil resides and how it can be recovered in the most cost-

effective way. The answers to these problems lie in finding ways to identify and quality-

rank reservoir flow units, baffles, and barriers to provide critical information for

improved recovery efforts. Ebanks et al. (1993) defined flow units as zones of the

reservoir that exhibit intermediate to high combined porosity/permeability values and

can be correlated from well to well. Baffles are zones that contain poor to low

porosity/permeability values and can be correlated from well to well. Barriers are zones

---

This thesis follows the style and format of the American Association of Petroleum
Geologists Bulletin.

of rock that contain poor porosity/permeability values and can be correlated across the field. Barriers are usually mud supported rocks that are correlatable over the entire field.

The presence of bypassed oil was confirmed when: 1) that it was discovered that the reservoir has undergone several poorly understood episodes of diagenesis, 2) that oil below the original oil/water contact was discovered and produced, and 3) that the stratigraphic architecture at field scale includes several unconformities (the total effects of which on Diamond M reservoir quality are not well understood). This study focuses on pore types, relationships between pore types and unconformities, the influence of unconformities on stratigraphic continuity across the field and their impact on total porosity and permeability across the field, on genetic pore types within flow units, baffles and barriers, and the relationship to reservoir quality. Unconformities are a focal point because they represent time markers, they are generally recognizable in cores and on logs, and they represent times of major change in the environmental regimes that govern deposition and diagenesis.

Thin section study revealed that porosity within the study area is a result of selective grain and pore-wall dissolution related to burial diagenesis. Additionally, saddle dolomite is irregularly distributed throughout the reservoir, indicating that late burial diagenesis contributed to the complexity of the reservoir pore system.

Hammel (1996) determined reservoir quality by a ranking system which utilizes values of porosity and permeability together with the genetic classification of pore types to identify flow units, baffles and barriers. In addition, a slice mapping technique is used

to identify overlying reservoir flow units, baffles, and barriers within the field (Hammel, 1996).

Objective of the Study

The primary objective of this study is to identify and rank flow units in the Pennsylvanian "Canyon Reef" at Diamond M field. Top ranked flow units should be targets for infill drilling as well as models for use in other Canyon reef-type fields. A more general goal of this study is to develop a more reliable method for carbonate reservoir characterization that will enable other operators to find and extract bypassed oil in the vast number of Upper Paleozoic carbonate reservoirs of West Texas and New Mexico. The significance of this study is highlighted by the fact that 17 % of all oil production in the USA during 2002 came from the "Permian Basin" of West Texas and New Mexico (Dutton et al., 2005).

Location of Study Area

The study area, Diamond M Field, is located in southwestern Scurry County 13 miles west southwest of Snyder, Texas (Figure 1). The field produces from the Horseshoe Atoll, an arcuate mound complex 70 to 90 miles in areal extent that occurs in the northern part of the Midland Basin (Stafford, 1959). Canyon Fm. rocks alone in the complexes have depositional relief of approximately 1,000 feet (Wermund, 1975). The reservoir consists primarily of the phylloid algal *Eugonophyllum* along with pockets of detrital grainstones and packstones that contain the red algae *Archeolithophyllum*. The reservoir is a 250 ft. thick sequence known locally as the "Canyon reef."
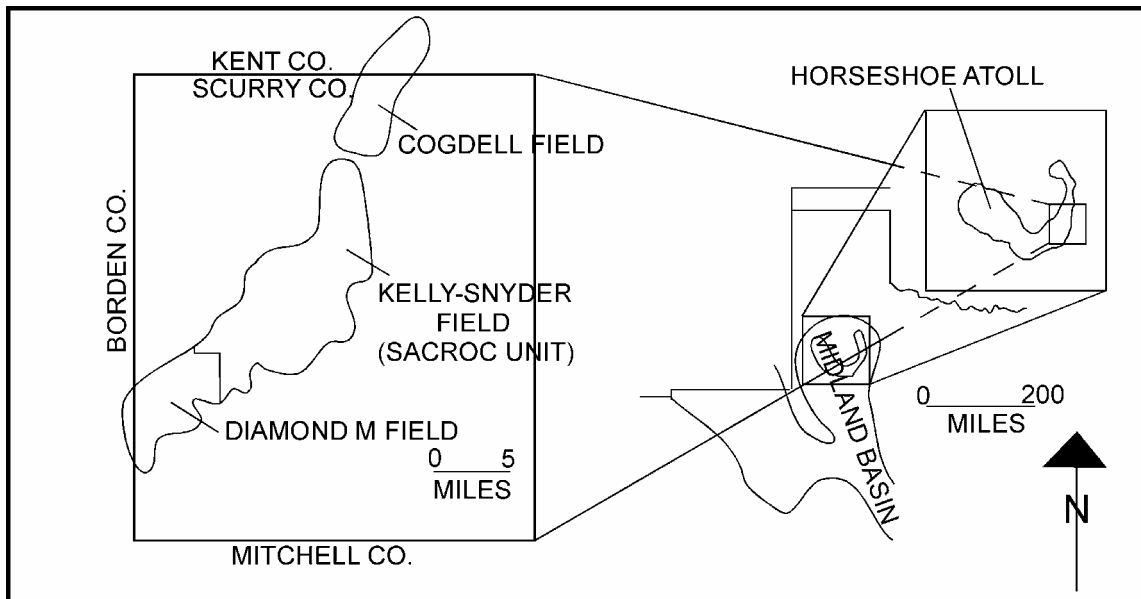
Figure 1. Map of West Texas showing the Horseshoe Atoll

Materials Available for Study

Three borehole cores, well information including production history, completion reports, geological studies, existing base maps and cross sections, and gamma-ray/neutron logs along with modern gamma-ray, spontaneous potential, caliper, neutron, and litho-density logs were provided by Parallel Petroleum Co. and the Harold Vance Department of Petroleum Engineering at Texas A&M University. Parallel Petroleum Co. provided approximately 500 ft of core taken from three recently drilled wells, core analysis by way of Rotary Labs Inc., wireline logs from more than 50 wells, basemaps, as well as calculated porosity, permeability, water saturation, oil saturation, bulk density, and fluoresence on the three cored wells.

REGIONAL GEOLOGIC SETTING

Structural Setting

The Permian Basin is an asymmetric structural basin that formed during the Gondwana-Laurassia collision. Reactivation of pre-existing zones of weakness caused division into sub-basins and topographic highs (Ross, 1986). The Midland Basin, which forms the northern portion of the Permian Basin, is located in the foreland of the Marathon-Ouachita fold and thrust belt (Tai, 2001). Geographically, the Midland Basin is bounded to the east by the Fort Chadbourne Fault Zone and to the west by the Central Basin Platform. The Midland Basin is asymmetrical in an east-west profile with the depocenter located to the west, adjacent to the Central Basin Platform. Compared to other sub-basins in the Permian Basin, such as the Delaware Basin, the Midland Basin had a very gentle profile and was much shallower. There has been little deformation across the Permian Basin since Early Permian time (Hammel, 1996). The region has been tectonically stable, and only minor tilting occurred along its edges (Ward et al., 1986; Frenzle et al, 1988; Ewing, 1993; Mazzullo, 1995).

Diamond M Field, one of many fields located within the structural limits of the Horseshoe Atoll, is located in the northern part of the Midland Basin (Figure 1). Pre-erosional reconstructions of shelf profiles indicate that by upper Pennsylvanian time, the ramps and distally-steepened ramps of the Strawn had evolved into rimmed platforms of considerable shelf-to-basin relief (Mazzullo and Reid, 1988). Lack of terrigenous sediment input along the ramp aided in creating a starved depositional environment.

Stratigraphic Setting

Late Pennsylvanian (Canyon) age rocks comprise the producing interval at the

Diamond M field. The reservoir interval at Diamond M field is dated as Late

Pennsylvanian in age based on fusilinids (Reid, 1998). These rocks overlay Early to

Middle Pennsylvanian siliciclastic rocks of Strawn age (Figure 2). During the Late

Pennsylvanian, shallow water-carbonate deposition dominated the Northwest Shelf,

much of the Central Basin Platform, portions of the Matador Arch, and the shelf margin

along the southeastern margin of the basin (Schatzinger, 1988).

System	Epoch/ Series/ Stage	Time (Ma)	Delaware basin	NW Shelf New Mexico	NW Shelf Texas	Central Basin Platform	Midland basin
Permian	Leonardian		Bone Spring	Abo	Abo	Abo/Wichita	Dean
Permian	Wolfcampian		Wolfcamp	Wolfcamp	Wolfcamp	Wolfcamp	Wolfcamp
Pennsylvanian	Virgilian	302	Cisco	Cisco	Cisco	Cisco	Cisco
Pennsylvanian	Missourian		Canyon	Canyon	Canyon	Canyon	Canyon
Pennsylvanian	Desmoinesian		Strawn	Strawn	Strawn	Strawn	Strawn
Pennsylvanian	Atokan		Atoka	Atoka	Atoka	Atoka	Atoka
Pennsylvanian	Morrowan	323	Morrow	Morrow	Morrow	Morrow	Morrow
Mississippian	Chesterian		Barnett	Barnett	Barnett	Barnett	Barnett
Mississippian	Meramecian		Mississippian				
Mississippian	Osagean						
Mississippian		363					

Figure 2. Stratigraphic column, ages, and geographical areas of West Texas and New Mexico

The Horseshoe Atoll rests conformably on top of Strawn siliciclastic sandstones and basinal shales. Overlying the Horseshoe Atoll are Permian (Wolfcamp) sandstones and shales that form the top seal of the reservoir. However, these shales are not the only reservoir barriers in the field. Baffles linked to Canyon age unconformities may exist at greater depths within Horseshoe Atoll.

The Horseshoe Atoll is generally classified as a carbonate buildup and referred to as the "Canyon Reef" or "Scurry Reef" referring to Scurry County. Facies variations exist in the reef at different geographic and stratigraphic locations. Facies are dominated by phylloid algal rich automicritic reef rock. Packstone and grainstone pockets occur within the reef, but they are not correlatable from well to well. The Horseshoe Atoll is not an ecological reef. Previous classifications such as Dunham (1962) defined rocks mainly by their depositional texture. Embry and Klovan (1971) extended Dunham's classification to include reef framework and associated detrital associations. Phylloid algal buildups are commonly included as bafflestones, sensu Embry and Klovan (1971) because phylloid algae grew in very shallow water atop a structure and were thought to have acted as baffles much like sea grass does today. This baffling lowered the depositional energy and allowed for small amounts of micritic mud to settle. However, the study area was starved of siliciclastic input during the late paleozoic. Therefore autochthonous automicrite provides the stable substrate for the buildup. Typically phylloid algae stood two to ten cm in height and only about 0.5 to one mm in thickness, however rarely are they preserved upright, as most of the algae fell and were preserved as fragments (Scholle and Ulmer-Scholle, 2003).

PREVIOUS WORK

Diamond M Field is located in southwestern Scurry County about 13 miles west southwest of Snyder Texas. It was discovered in 1948 by Lion Oil Company and is currently operated by Parallel Petroleum Company, which purchased the field in 2000 from Burlington Resources. After discovery in 1948, 111 wells were drilled between 1948 and 1951, including one water injection well. Secondary recovery by water flooding has been in effect since the beginning of field development. The field has produced over 3.6 million barrels of oil since it's discovery in 1948 (Figure 3). In 2002 Parallel Petroleum Company drilled four wells named the Gemstone wells (Emerald, Garnet, Jade, and Topaz) based on a 3-D seismic survey shot in 1992. The company was in search of what they classified "attic" oil locations. Three of the four wells were cored in the producing Canyon Formation were accompanied by core analyses.

Modern log suites consisting of gamma ray, spontaneous potential, caliper, neutron, and litho-density logs were also run on the four wells. This project utilizes the modern logs and cores in conjunction with older logs to identify flow units baffles and barries in the reservoir.

Similar studies have been done on other fields within the Permian Basin. Hammel (1996) conducted a study on the Happy Spraberry Field located in Garza County, Texas. His study was aimed at defining a method to better characterize reservoirs by predicting reservoir quality and flow unit spatial distribution by integrating stratigraphic and petrographic analyses applied in a "slice-map" technique (Hammel

1996). Layman (2002) followed Hammel's work on the Happy Spraberry field by

relating pore geometry determined by petrographic image analysis to reservoir quality

Diamond M Fluid Production History
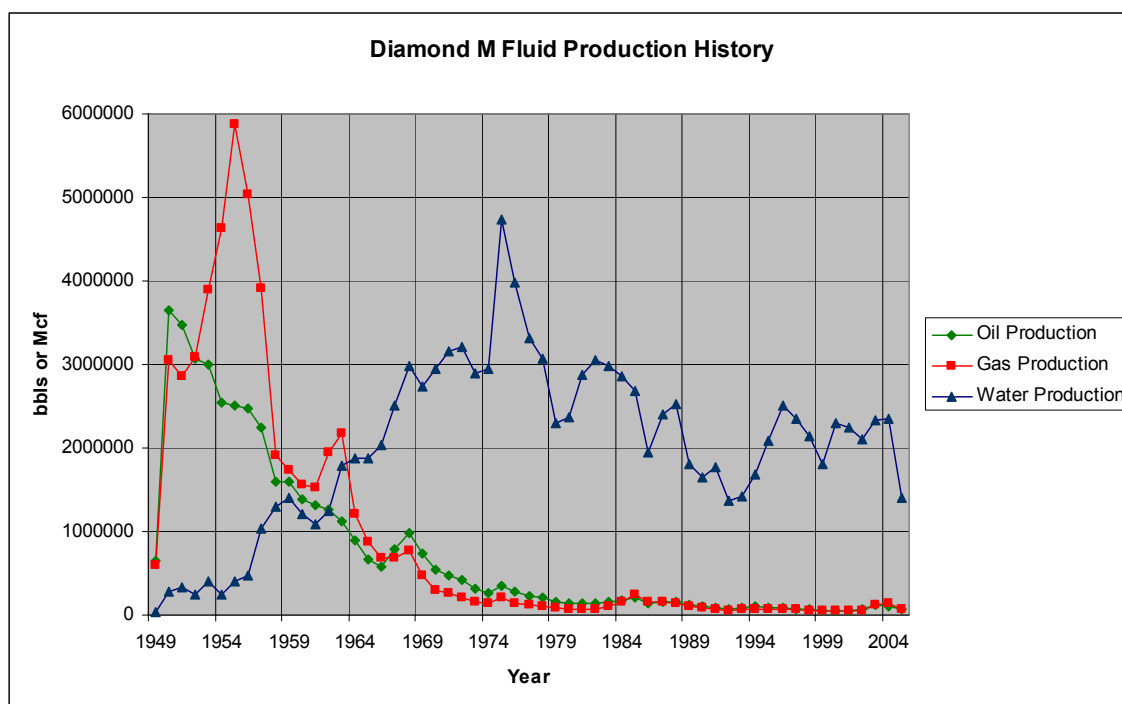
Figure 3. Fluid production history of Diamond M Field

standards established by Hammel (1996).

Important early papers on the Horseshoe Atoll include those of Myers et al.

(1956), Stafford (1959) Burnside (1959), and Vest (1970). These works were concerned

mainly with regional biostratigraphic aspects and discussed the "reefal" nature of the

buildup (Schatzinger, 1983). More recent studies have focused on facies mapping,

biostratigraphy, and depositional environments, most recently by Schatzinger (1988) and

Reid (1998). Schatzinger (1988) focused on the complex mound-to-basin and along-the-

trend transition of facies and depositional environments from the eastern portion of the Horseshoe Atoll.

Work was also done on the nearby Kelly-Snyder Field and the Higgins Ranch Field, as well as on reefs in adjacent Borden, Howard, and Kent counties (Burnside 1959), Myers, Stafford (1959), and Vest (1970). However the majority of previous work done in these papers focused only on basic petrology, structure and stratigraphy of the Horseshoe Atoll. This study builds on the previous work and incorporates new information on pore types, porosity and permeability, and how the combined data relate to reservoir quality.

METHODS OF STUDY

This study is divided into four parts: 1) lithological study of cores, 2) thin section petrography, 3) petrophysical interpretation of reservoir properties from core analyses and wireline logs, and 4) predictive mapping of quality ranked flow units across the study area. Petrologic and petrographic studies were done to classify reservoir rocks according to depositional texture for detrital rocks according to Dunham's (1962) classification, and binding and lithification mechanism for reef rocks according to Riding's (2002) classification. Carbonate pore types were classified according to the genetic pore classification (found on page 29) of Ahr et al. (Oilfield review, 2005), and rock and pore types were compared in order to identify rock and pore characteristics that determined reservoir behavior in quality ranked flow units across a sector of the Diamond M field. Three cores, core analysis, gamma ray, spontaneous potential, caliper, neutron, and litho-density logs were used along with basemaps, cross-sections, and reports from Reid (1998).

Lithologic Study of Cores

Approximately 500 feet of full diameter slabbed core from three wells were examined wet using a binocular microscope after all samples had been etched in dilute HCl to dissolve any debris and to provide a fresh rock surface for evaluation. Detailed core descriptions included identification of constituent components, depositional textures, sedimentary structures, visible porosity, and significant facies changes (Appendix A). These descriptions were used to identify depositional facies in order to generate a working model to explain the depositional and diagenetic history of the

Canyon Formation carbonates in the study area. Once descriptions were completed depositional facies were identified by identifying boundaries of lithogenetic units in cores. Four depositional facies were identified from core descriptions and compared with wireline log signatures to establish a basis for correlating the facies across the field.

Routine core analyses by Rotary Laboratories Inc. included porosity, permeability, water saturation, oil saturation, grain density, fluorescence, lithology, and routine lithological descriptions. Measured porosity values were compared to visual porosity estimates from core descriptions, as well as to porosity values calculated from wireline logs. Graphs were constructed using Microsoft Excel to note similarities and differences between measured and calculated values of porosity. Porosity-permeability crossplots (found on pages 35-37) provided the main source of information with which to identify the best, intermediate, and poor poroperm zones within the field. After examining permeability vs porosity graphs, it was recognized that all but five values were below 50 md. Those five points were excluded when figuring permeability for intramatrix, moldic, and vuggy porosity. By eliminating these points a better porosity/permeability relationship was achieved.

Structural and depositional facies maps were constructed, along with stratigraphic and structural cross sections. Ranked poroperm zones were plotted on the cross sections and were mapped in 10-foot stratigraphic slices at field scale to identify and map flow units, baffles, and barriers (Appendix C).

Thin Section Petrography

Fifty two thin section billets were impregnated with blue epoxy, thin sectioned, and stained with Alizarin Red S in order to distinguish between calcite and other non-stain-susceptible minerals. Sites for thin sections were chosen to represent facies changes, unconformities, and porosity types throughout the reservoir.

Thin section petrography was performed using a binocular microscope in plane and polarized light. Depositional texture, grain type, porosity type and percentage, mineralogy, and diagenetic processes were described. Owing to the limited number and type of pores in the Canyon Reef reservoir, it was determined that quantitative petrographic image analysis was not necessary to discriminate between pore types and depositional facies characteristics. Appendix B contains thin section descriptions as well as photomicrographs illustrating depositional texture, mineralogy, porosity, and notable diagenetic changes.

Borehole log interpretation

Logs used in the study include older gamma-ray/neutron logs along with modern gamma-ray, spontaneous potential, caliper, neutron, and litho-density logs from the gemstone wells. A prominent log trace marks the top of the Canyon Reef on both old and new logs. This trace is characterized by a decrease of approximately 75-90 API units and a well correlatable neutron log signature.

Typically gamma-ray or spontaneous potential are used when doing well to well correlations. However, they are only of limited use in this field due to the lack of large

radiation readings. Therefore, neutron and litho-density logs were used for well to well correlations.

Subsurface mapping

Maps were produced from logs and core analyses; they include structure maps, slice maps, porosity and permeability maps, facies maps, and stratigraphic and structural cross sections that highlight poro-perm zones, and unconformities. Present structure maps help to identify structures that may correspond to variations in depositional or diagenetic porosity and permeability, which in turn may help identify causes of compartmentalization in the reservoir (Hammel, 1996). An interval isopach map of total reef thickness could not be made because most wells did not penetrate through the reef.

Slice mapping: Why necessary, how to do it, what it shows

Slice mapping is a method to incorporate a variety of petrologic, petrographic, and petrophysical data to determine the 3-D distribution of quality ranked poroperm units within a stratigraphic framework Porosity and permeability were averaged over ten-foot thick slices across the study area. Where core analysis was not available porosity and permeability was calculated from logs. Porosity and permeability equations were derived by plotting porosity vs. permeability from the three cored wells. Porosity values were then inputed into the equations in order to obtain permeability values. The average values for each parameter were then contoured to identify porosity and permeability zones across the field. The top of the first slice was taken at the top of the Canyon reef; therefore, these are stratigraphic slices rather than structural slices. By

stacking slices it is possible to identify the spatial distribution of porous and permeable

zones within the reservoir and construct flow units based on the superimposed slices.

CANYON FM. ROCK PROPERTIES

Petrology

In many modern reefs, scleractinian corals provide the rigid framework that is necessary in building a hard, stable substrate in which other organisms live. In contrast, during Pennsylvanian times, the phylloid algae *Eugonophyllum* was a common contributor to carbonate buildups. In the past it was thought that baffling and trapping of sediment by *Eugonophyllum* caused growth of carbonate buildups by passive sediment trapping. However, recent studies have shown that phylloid algae *Eugonophyllum* is capable of providing a complex framework when combined with the calcareous binding organisms *Tubiphytes* and *Archaeolithoporella* (Forsythe, 2003). Phylloid algae provided the stable substrate known as the pioneer community which was followed by encrusting and climax communities (Forsythe, 2003). The absence of Tubiphytes, Archaeolithoporella, other encrusters, and sponges provides strong evidence that the buildups in the study area consist mainly of the phylloid algal pioneer community. Approximately 50-60% of all rocks described in this study were classified as phylloid algal dominated automicritic reef facies. The remaining rocks consist of detrital (mainly skeletal) packstones and grainstones, along with some "pockets" of intraclastic packstones and grainstones interpreted to have been formed by submarine erosion along paleohighs. Core descriptions from the three gemstone wells reveal four dominant facies that are interpreted to be part of the pioneer community.

Reef Facies One

Color, Composition, Texture

The reef facies is light brown to gray in color. Micrite makes up greater than 50% of this rock type. The remaining 50% consists of the phylloid algae *Eugonophyllum*; skeletal grains consist of algae fragments, bivalves, brachiopods, bryozoans, crinoids, forams (pellets, benthic, and encrusting), fusulinids, gastropods, sponge spicules and rare trilobite shells. Non-skeletal grains consisting of micritic clasts, peloids, and unidentifiable grains. Brachiopods, forams, and phylloid algae represent the bulk of the rock (60-70%) while bryozoans and gastropods contribute the least (<5%) to total grain volume.

Facies one is classified as an automicritic reef rock with erosional packstone and grainstone pockets less than 4 ft in thickness. Rock in facies one is generally massive with a mottled appearance showing little or no sedimentary structures or bedding with the exception of parallel bedding and erosional truncation associated in the detrital intervals.

Grainstone Facies

Color, Composition, Texture

The grainstone facies varies in color from light tan to dark gray. Forams and phylloid algal fragments make up greater than 65% of this rock type. Skeletal grains consist of bivalves, brachiopods, crinoids, forams (mainly pellet forams) occasional

fusulinids, gastropods, phylloid algal fragments, and sponge spicules. Forams generally range in size from 0.1mm to 0.5 mm in diameter. Phylloid algal fragments can range in size from 0.5 mm to 5 mm in length. These grainstones are generally moderate to well sorted.

These grainstones are generally massive but often have bedding character near the bottom erosional surface. Phylloid algal pockets less than 4 ft thick are present in one well and show faint bedding structures. This facies also contains intercrystalline porosity and accessory minerals pyrite and chert. Styolites are not commonly found in grainstone and packstone facies.

Reef Facies Two

Color, Composition, Texture

Reef facies two is light to dark gray in color. Micrite accounts for more than 70% of the total rock volume in this facies. The remaining 30% consists of primarily skeletal grains however non-skeletal grains are present in the form of micritic clasts, peloids, and unidentifiable grains. Skeletal grains are dominated by forams and phylloid algae, however there is a considerably higher percentage of crinoid fragments. These three grain types account for over 70% of skeletal grains. Additional skeletal grains include bivalves, brachiopods, bryozoans, fusulinids, gastropods, phylloid algal fragments, and sponge spicules.

Reef facies two is classified as an automicritic reef rock with erosional packstone and grainstone pockets less than 4 ft in thickness. Rocks in facies two have a massive

appearance showing little or no sedimentary structures or bedding with the exception of parallel bedding and erosional truncation associated in the detrital intervals. Micritic clasts and irregular erosional surfaces are associated with erosional packstone and grainstone pockets.

Debris Facies

Color, Composition, Texture

The debris facies is gray to dark gray in color. The debris facies is composed of the same grains and particles that compose the erosional packestones and grainstones but with the addition of angular intraclasts derived from the reef mounds. Clasts and fragments make up more then 65-70% of this rock. Micritic matrix as well as micritic clasts are volumetrically significant (20-30%). Volumetrically insignificant, this debris rich rock is neither common nor correlatable from well to well but represents fragments and debris shed from updip erosion.

Texturally the debris facies is massive and shows no sedimentary structures or bedding characteristics. Styolites are present as well as abundant saddle dolomite and pyrite.

Before modern research on non-framework reefs, phylloid algal rich micritic rocks were classified as "boundstones" following the classification of Dunham (1962). Extensive studies on Permo-Carboniferous and other Paleozoic carbonate buildups that lack framebuilding or binding organisms has let to a variety of new reef classification.

One such scheme is that of Riding (2002), which includes micritic mounds of the type inhabited by phylloid algae.

During Pennsylvanian times, the top of the reef was irregular due to erosional events caused by eustatic sea-level lows (Reid and Reid, 1999). These irregularities combined with fluctuations in relative sea level (Reid and Reid, 1999) left many zones or possibly the entire upper surface exposed and subjected to erosion during low stands. Structurally low zones on top of the atoll were filled with erosional skeletal and intraclastic packstones and grainstones. Though very common, these packstone and grainstone pockets are difficult to correlate because they were laterally and vertically discontinuous, and they lack a log signature that clearly identifies them.

Late diagenetic emplacement of saddle dolomite (Figure 4) occurred irregularly throughout the field. It is interpreted to have formed by chemical compaction and thermochemical sulfate reduction (Machel, 1987). Saddle dolomite can form in true hydrothermal regimes or burial diagenetic (60-200°C) regimes with temperatures in the 100's of C° (Ahr, 2004). Machel (1987) concluded that low temperature saddle dolomite is commonly found in deep carbonate oil bearing reservoirs as a by-product of two processes 1) chemical compaction of dolomitized reef rock, and 2) increase in carbonate alkalinity via thermochemical sulfate reduction.

Petrography

In all, 52 thin sections were collected to represent depositional texture, facies types, and pore types. Sample locations were chosen in order to best represent rock characteristics and porosity trends within the field. After thin section examination it was

concluded that all porosity is a hybrid of depositional and diagenetic processes and no

fracture porosity was found to be evident. It is evident that at least two early stages of

cementation and dissolution have taken place. Dissolution of reservoir rock is a

diagenetic feature, however dissolution is often governed or controlled by depositional

characteristics. Saller et al. (1999) concluded that dissolution enlarged vugs are a

common feature associated with long term subaerial exposure in West Texas upper

Paleozoic shelf limestones. Pore boundaries commonly cut across grains, shells, and
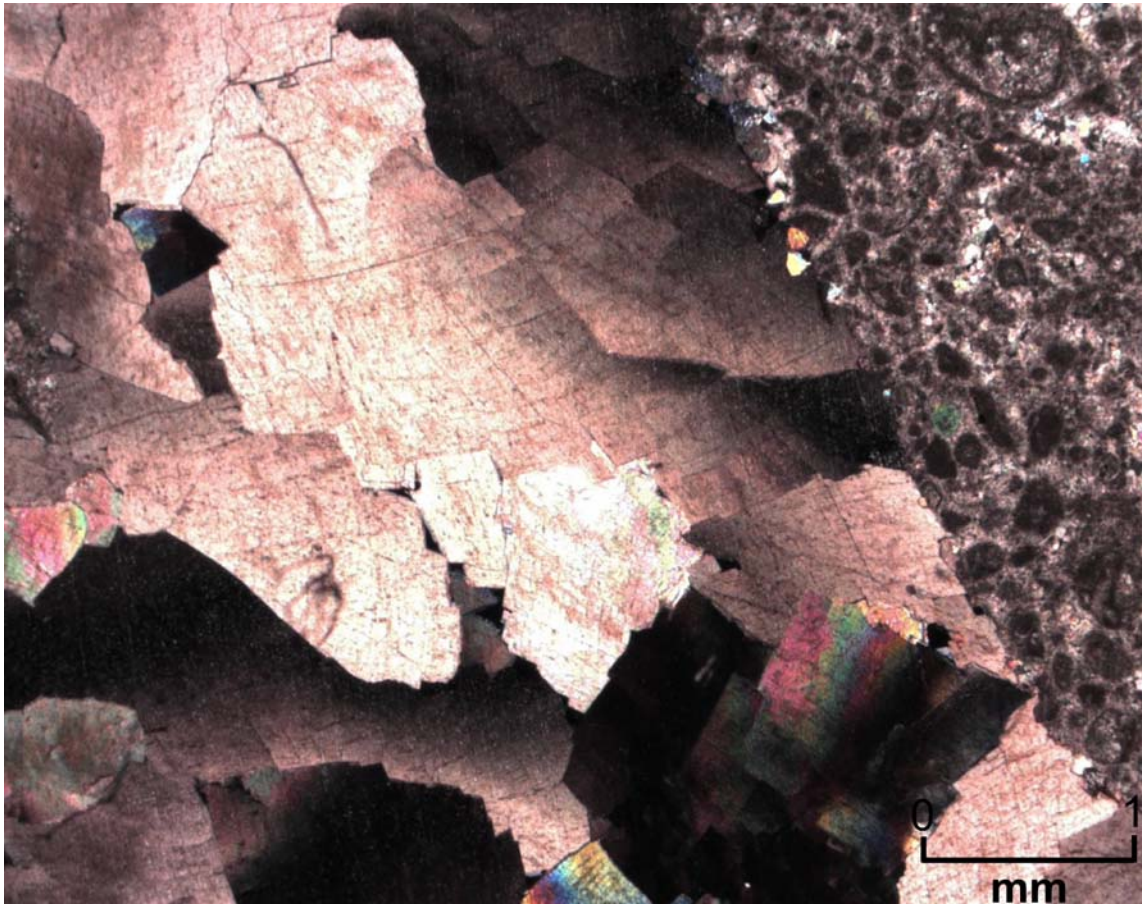
Figure 4. Thin section photograph of saddle dolomite

fragments adding to the argument that they are secondary dissolution events. Vuggy

porosity is also commonly associated with fine grained matrix, is purely diagenetic, and

lacks depositional characteristics. The most common types of porosity include solution

enhanced intramatrix, moldic, and vuggy porosity. There were also small occurrences of

interparticle and intraparticle porosity which constitute 10-15% of porosity as well as

fracture, intercrystalline, cement reduced porosity, styolitic porosity, and microporosity

that combine to produce 1-3% of porosity.

Saddle dolomite is present in all three cores and indicates late burial diagenesis.

Thermochemical saddle dolomite is interpreted to form in a temperature range of 60-

150°C (Radke and Mathis, 1980) and 60-200°C (Ahr, 2004).

Reservoir Properties from Core Analyses

Porosity in the field generally ranges from less than 1% to 30%. Visible porosity

has been estimated to average about 6% overall (Stafford, 1957) while reservoir zones

only exhibit average visible porosity of about 10% (Stafford, 1959). Core analyses data

provided data on porosity, permeability, bulk density, water saturation, fluorescence, and

lithology.

Intramatrix, moldic, and vuggy porosity comprise the major pore types that

dominate porosity in the three gemstone wells. Small amounts of intraparticle, fracture,

and intercrystalline porosity are present. Porosity ranges from 0.1% to 19.7% and

permeability ranges from 0.05 md to 141.83 md from core analysis (Figure 5).

Thin section studies showed that three porosity types dominate. 1) Intramatrix

and moldic were grouped together and 2) vuggy porosity classified separately because it
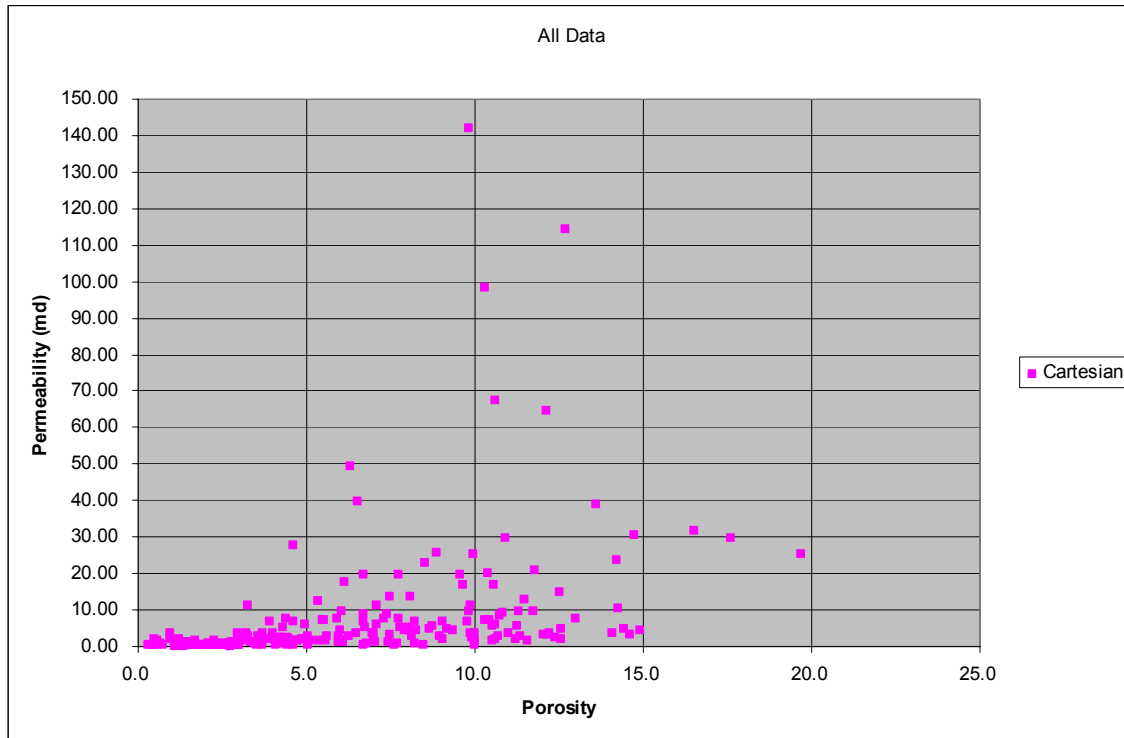
Figure 5. Cartesian plot of porosity vs. permeability

generally corresponds to high K values. Intramatrix and moldic porosity types were

classified together because they are commonly associated together, and it is difficult to

determine which of the two dominate by thin section examination. Poroperm values for

vuggy pores range from approximately 1% to 20% porosity and approximately 0.50 md

to 142 md permeability (Figure 6). Poroperm values for intramatrix and moldic pores

range from 1% to 15% porosity and approximately 0.10 md to 10.0 md permeability

(Figure 7).

Porosity and permeability vary widely. Poro/perm plots were made to illustrate the different trends of intramatrix, moldic, and vuggy porosity. Porosity and permeability plots for vuggy porosity were noticeably skewed towards high values. R^2 values were noticeably lower for vuggy porosity when compared to intramatrix and moldic porosity. These values were expected due to the wide range of vug sizes and whether the vugs are touching or separate. Touching vugs show elevated poro-perm values.

Reservoir quality slices 1-4 (Appendix C) show higher quality reservoir zones located in the southern portion of the field. These high quality zones correspond to high percentages of vuggy porosity. Flow units dominated by intramatrix and moldic porosity rarely have porosity values greater than 13.3 and permeability values over 10 md. Reservoir quality is less predictably distributed in remaining slices. Thick intervals with abundant vuggy porosity or intramatrix/moldic are not common in the lower portions of the reef.
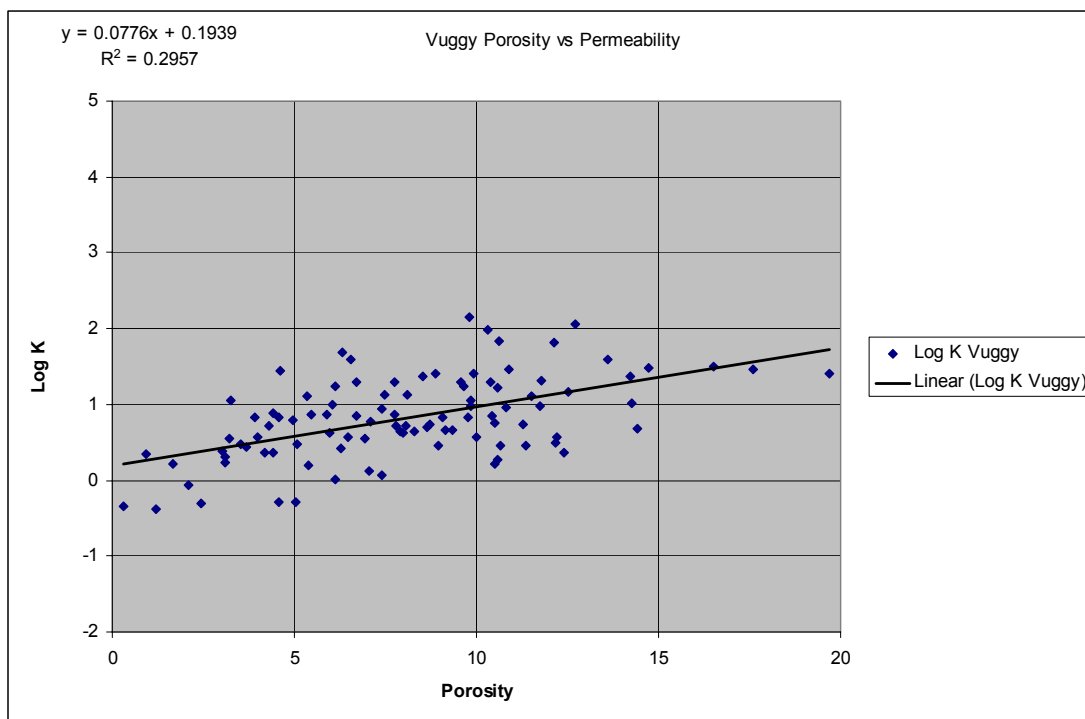
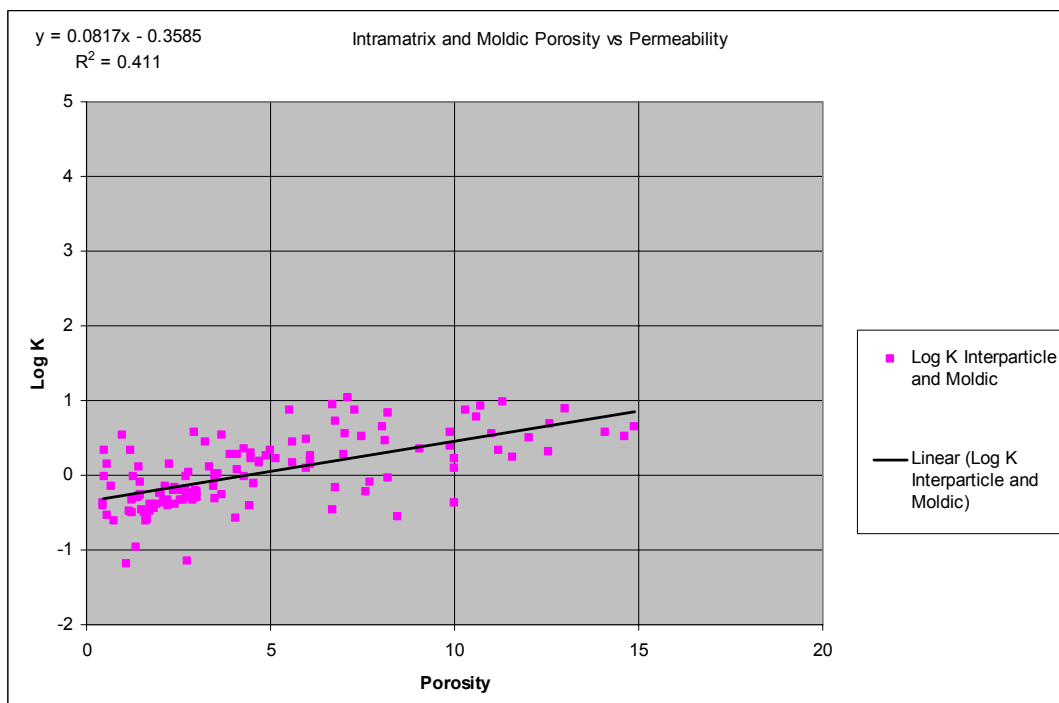**Figure 6. Graph of vuggy porosity vs. permeability**

Figure 7. Graph of intramatrix and moldic porosity vs. permeability

DISCUSSION AND INTERPRETATION

Significance of Unconformities

The Horseshoe Atoll was subjected at least four times to subareal exposure and consequent erosion during Canyon time (Reid, 1998). Emergence is interpreted to have been associated due to fluctuations in glacio-eustatic sea levels (Reid and Reid, 1999). The erosional episodes produced unconformities that have been correlated across the field by Reid (1998) and are evident in core. Reid (1998) identified and correlated at least four such unconformities in the Canyon interval. In addition to weathering and eroding the phylloid algal reef, these unconformities created porosity as a result of dissolution of the underlying rock.

Dissolution porosity and permeability were the result of subareal exposure rather than porosity created during deposition. Depositional porosity is generally low due to pore and void filling automicrite, short hand for "autochthonous micrite" (Riding, 2002). Reservoir rocks in this study area have undergone multiple stages of diagenesis including early and late stage burial dissolution and cementation that resulted in the present porosity and permeability. Saller et al. (1999) suggested that moderate to prolonged subaerial exposure (estimated at 50,000-130,000 yr) may create dissolution vugs, fractures, and fissures. However, oil reservoirs in the Midland Basin of West Texas from Pennsylvanian limestones were affected by mesogenic cementation that resulted in virtually complete loss of porosity (Mazzullo and Harris, 1992). Dissolution porosity resulting in formation of vugs accounts for approximately 40-50% of porosity

in the field. Therefore, porosity must have been created during burial diagenesis, possibly even developing in original cemented pores. Thin sections petrography revealed that multiple stages of dissolution and cementation have taken place since deposition. Micritization of forams, fusulinids, brachiopods, and phylloid algae is interpreted to be early diagenesis. Following micritization burial dissolution and cementation by small blocky calcite crystals occured. Cross cutting relationships involving partial dissolution of micritized grains and cementation of dissolution pores conclude that first stage burial dissolution and pore filling small blocky calcite cement occurred after micritization. A second stage of dissolution is observed cutting irregularly across small blocky calcite as well as micritized grains and shells and cementing pore space with large blocky calcite crystals.

Facies Categories and Spatial Distribution

Due to the homogeneity of rock associated with the Horseshoe Atoll, there are only four distinctive facies identified in the study area. The four separate facies vary from grainstones to automicrite reef rock. Detrital rocks were classified according to Dunham (1962). The phylloid algal and micritic reefs are autochthonous deposits that require a different classification scheme of the type given in Riding (2002). Riding's scheme focuses on bedding characteristics, skeletal allochem content, and type of structure-supporting materials such as micrite, cement, or grains.

Irregular bathymetry created by variations in relief of the reefs above the seabed resulted in deposition of "pockets" of debris deposits within the reef complex. As these pockets are local, they are difficult to correlate from well to well. Reef facies dominate

the algal mound however large variations exist in rock texture, color, grain size and shape, and bedding characteristics. When we correlate from one well to another we are correlating similar reef facies, not necessarily rock type.

Parallel bedding structures as well as truncations are present in grainstones and packstones and easily identified in core and thin section descriptions. Graded bedding was also identified when looking at grainstone and packstone thin section locations indicating that sufficient depositional energy to remove grains from the reef was present. Energy needed for the deposition of grainstones and packstones is interpreted to have been present during sea-level lowstands or erosional events thus removing material from the atoll basinward and filling depressions or low lying areas on top or within the reef structure. Reid and Reid (1999) and Vail et al. (1977) documented transgressive and regressive stages that took place during the Late Pennsylvanian and that can be correlated with the presence of erosional unconformities.

Depositional environments were relatively uniform but the facies that developed in them vary widely. During sea-level lowstands erosion removed material from the atoll basinward and filled depressions or low lying areas on top or within the reef structure. These low lying areas were locations served as small depositional pockets where grainstones and packstones were preserved. These pockets create large variations in rock type and texture across the field (Table 1). However these variations are difficult to correlate from well to well.

Table 1. Facies and common constituent grains

Facies	Common Constituent Grains
Grainstone	Phylloid Algal Fragments, Foram pellets
Grainstone	Phylloid Algae Fragments
Packstone	Bivalves, Brachiopods, Crinoids, Bryozoans, Benthic Forams, Encrusting Forams, Fusulinids, Gastropods, Peloids, Phylloid Algal Fragments, Sponge Spicules, Trilobite Shells
Wackestone	Bivalves, Brachiopods, Crinoids, Bryozoans, Benthic Forams, Encrusting Forams, Fusulinids, Gastropods, Peloids, Phylloid Algal Fragments, Sponge Spicules, Trilobite Shells
Mudstone	Bivalves, Brachiopods, Crinoids, Bryozoans, Benthic Forams, Encrusting Forams, Fusulinids, Gastropods, Peloids, Phylloid Algal Fragments, Sponge Spicules, Trilobite Shells
Phylloid Algal Automicrite (Reef Facies)	Bivalves, Brachiopods, Crinoids, Bryozoans, Benthic Forams, Encrusting Forams, Fusulinids, Gastropods, Peloids, Phylloid Algae, Phylloid Algal Fragments, Sponge Spicules, Trilobite Shells
Breccia	Bivalves, Brachiopods, Crinoids, Bryozoans, Benthic Forams, Encrusting Forams, Fusulinids, Gastropods, Peloids, Phylloid Algal Fragments, Sponge Spicules, Trilobite Shells

Pore Types and Relationship to Depositional and Diagenetic History

Multiple classification schemes have been created to classify pore types. Choquette and Pray (1970) created a classification that placed 15 pore types into three groups depending on whether they were fabric selective or not. Lucia (1995) classified all pore types as either intergranular or vuggy and their relationship with Archie's m value and other characteristics such as pore size, porosity, and permeability. For this study the Ahr et al. (2005) genetic classification is used (Figure 8). The end-member pore types are classified on the basis of their modes of origin: depositional, diagenetic, and fracture. Intermediate categories are classified as hybrids. For this study most pores have been classified as a depositional-diagenetic hybrid. In addition to hybrid pores, purely diagenetic vugs are common and tend to increase porosity (5-10%) and permeability (5-15 md) values significantly (Appendix B).

During the beginning stages of the project it was hypothesized that porosity was mainly hybrid diagenetically altered depositional pores. Further study revealed that purely diagenetic vugs are common in addition to hybrid pores. Porosity is interpreted to have been both enhanced by dissolution and reduced by cementation. Cementation occurs in two forms: 1) Small blocky calcite and 2) Large blocky calcite. Cementation by small blocky calcite is interpreted to occur first due to the fact that it is often dissolved resulting in pore filling by large blocky calcite.

The result of diagenesis and depositional characteristics created multiple hybirid and diagenetic pore types of which solution enhanced intramatrix, moldic, and vuggy
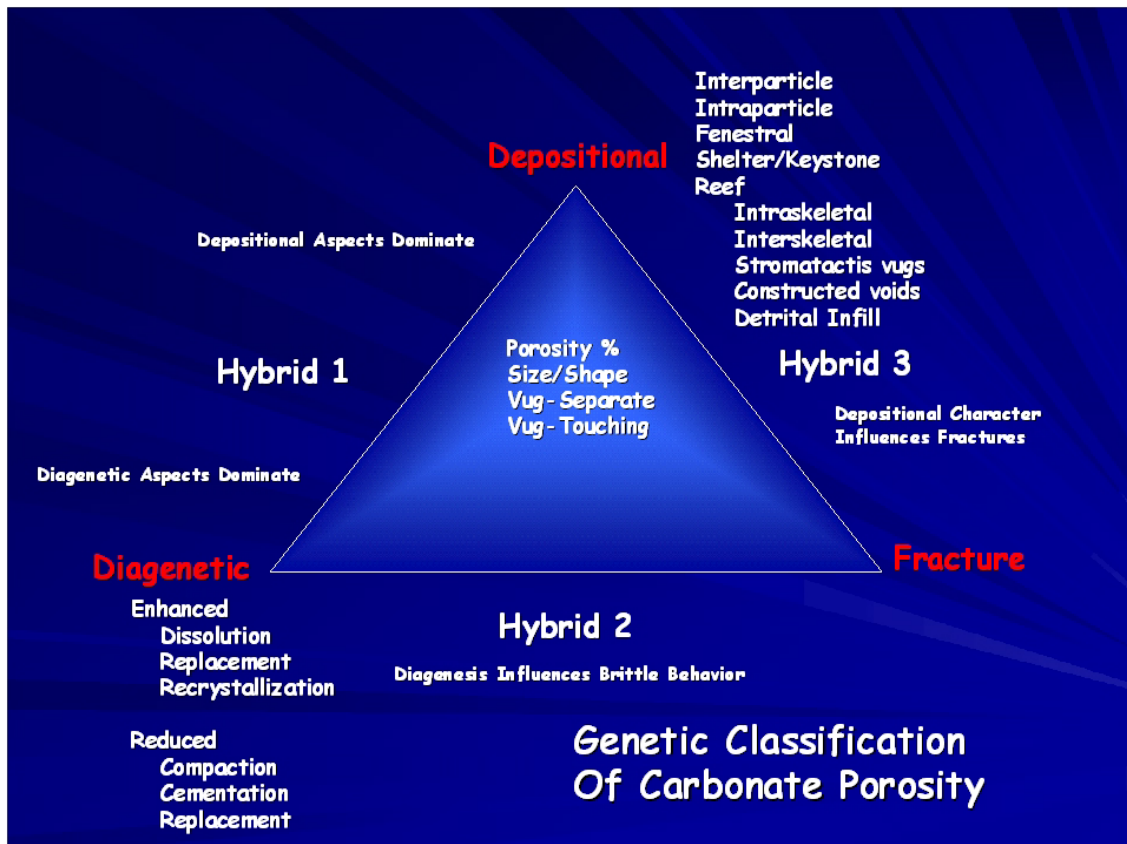
Figure 8. Pore classification scheme from Ahr (2005)

pores are the most common. Solution enhanced intraparticle, fracture, and porosity

associated with styolites is present, but to a much lesser degree.

Pore Types

  Vuggy (V)

Vugs are the result of dissolution enlargement of an existing pore or combination of

pores of which the origin can no longer be identified. Vugs exhibit irregular shapes

which do not conform to any grain type. Vugs are larger than all grain sizes with the

exception of few large brachiopods, fusulinids, and phylloid algal fragments. Vugs are

very common in this study, constituting 40-50% of porosity. Elevated permeability values are associated with vugs.

Solution Enhanced Intramatrix (SEIM)

These pores are created by the dissolution of matrix material during burial diagenesis. It is important to note that SEIM porosity is often found with in non-micritic supported rocks; however it is not intergranular porosity. SEIM pores are irregular in shape (such as V pores) but are on a smaller scale always less then 1mm in diameter. SEIM occurs commonly in muddier reef facies and often found associated with moldic pores. SEIM porosity occurs frequently and accounts for 15-20% of porosity. SEIM pores are seen represented in all facies types.

Moldic (M)

Moldic porosity is created by the dissolution of constituent grains. These pores conform to original casts or molds of dissolved grains and fossils. Moldic pores show very sharp boundaries of where previous fossils and grains were deposited. These pores are commonly associated with SEIM pores and share the same abundance and frequency accounting for 15-20% of total porosity. Moldic pores are very common and seen in all facies types.

Solution Enhanced Intraparticle (SEIP)

Occurs commonly as small pore spaces within constituent grains and fossils. SEIP is usually a depositional characteristic, however many of the pores are diagenetically altered by reducing cement or enhancing dissolution of the particle. SEIP is present in

all facies categories although it is of smaller percentages (less than 10%) when looking

at total porosity.

Cement Reduced Intercrystalline (CRIC)

Cement reduced intercrystalline porosity is pore space that remains after cementation of

rock. CRIC is found only in grainstone facies that have been almost completely

cemented by blocky calcite. Pore shapes are very irregular as calcite crystals form sharp

contacts. These pores are volumetrically insignificant (less than 1%) when looking at

total porosity.

Fracture (F)

Fracture porosity is found sporadically throughout the study area. This type of pore

space is very uncommon and volumetrically insignificant (less than 1%) when looking at

total porosity. Fracture porosity is relatively small, usually 1/10 of a mm of space exists

as it may have been induced during drilling.

Styolite (S)

Porosity associated with styolites is rare due the fact that most styolites visible are tight

with no porosity. However, rare occurrences of dissolution porosity along styolites are

present in cores.   These pores are most commonly associated in reef facies and are

volumetrically insignificant (less than 1%) when looking at total porosity.

Flow Unit Definition and Quality Ranking

A major objective of the study is to identify and rank flow units in the studied

sector of the Diamond M field. Ahr and Hammel (1999) defined flow units as reservoir

zones with combined high porosity and permeability values with the least amount of

resistance to fluid flow. However, we also define baffles and barriers. Baffles are local

zones within reservoirs where beds with low poroperm rank interfere with, but do not

totally block vertical or horizontal flow. Barriers prevent vertical and horizontal flow.

They are, in other words, similar to seals but are found as zones within reservoirs.

Therefore it is essential to utilize cored intervals and thin sections in use with borehole

logs to obtain the best porosity and permeability zones. Once these zones are located

one can map them using the slice map technique.

Porosity and permeability ranges from 0.1% to 19.7% and 0.07 md to 141.81 md

respectively from core analyses. Contoured slice maps for porosity and permeability

were constructed from core analysis for each 10-foot stratigraphic interval (Appendix

C). In order to map flow units across the field including wells that lacked cores and core

analyses, porosity and permeability values were obtained by calculating values from

neutron density logs.

In order to properly classify flow units to numerical categories, porosity and

permeability ranges had to be set up. A reservoir classification was created which uses

porosity and permeability values to classify reservoir quality. For this classification

porosity and permeability ranges were divided into nine reservoir quality pairs. Figure 9

shows the reservoir rankings and ranking classification based on porosity and permeability values.

Three pore types dominated porosity in the cored wells; the pore types include intramatrix, moldic, and vuggy. Porosity and permeability values were separated and
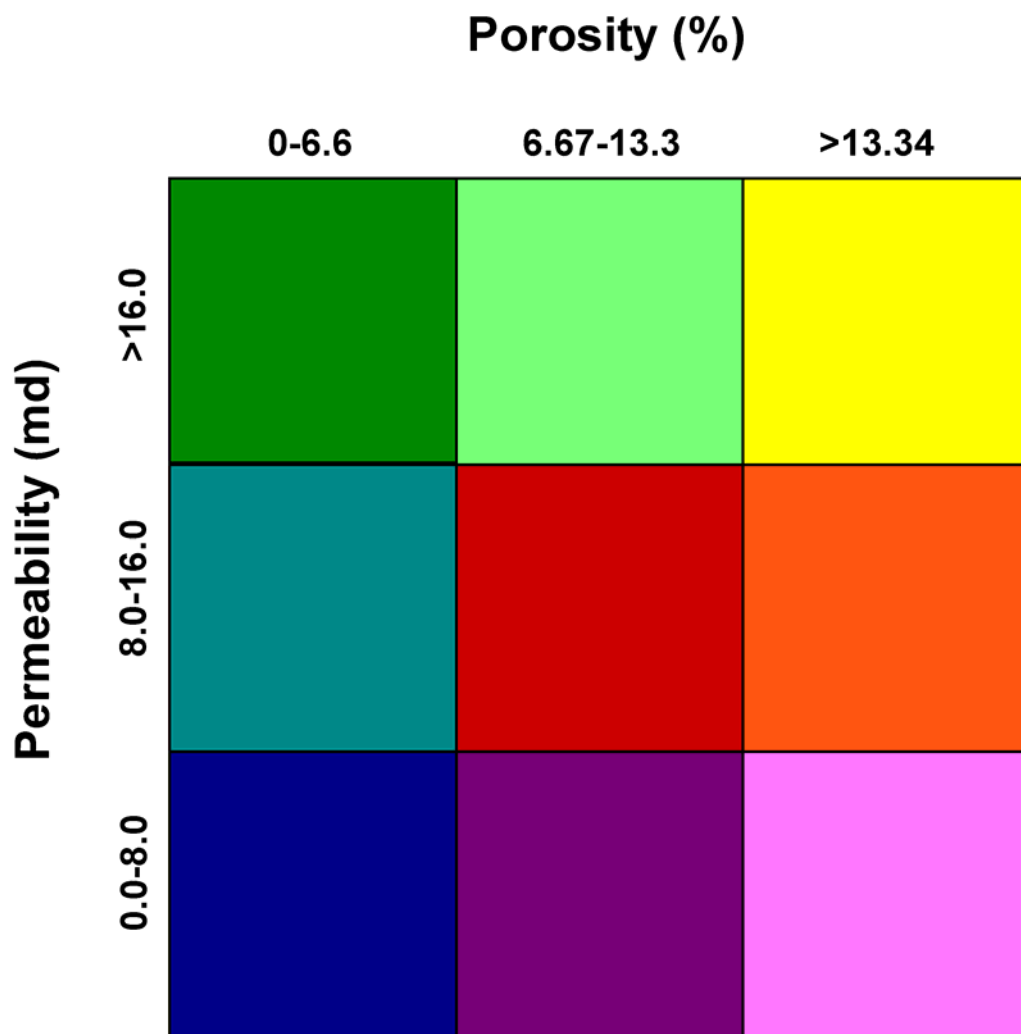

Figure 9. Flow unit diagram

plotted in excel based on the most abundant pore type. Intramatrix and moldic pores

occur with the same frequency in thin sections; therefore it was not possible to

distinguish which pore type constituted the higher amount of total porosity. Porosity and

permeability data were scatter-plotted to test for correspondence with a linear regression

equation. The equation, in $y = mx + b$ form, made it possible to identify the relationship

between vuggy, and intramatrix and moldic pores and permeability in each of the wells

for (Figures 3 and 4). $Y = 0.0817x – 0.3585$ is the linear equation used for calculating

permeability for intramatrix and moldic pores where core analyses is not available. $Y =$

$0.0776x + 0.1939$ is the linear equation used for calculating permeability for vuggy pores

where core analyses is not available. It is important to note that all but five data points

for permeability were below 50 md. In order to achieve an acceptable relationship

between porosity and permeability we eliminated these five outlying points from our

intramatrix/moldic and vuggy permeability equations.

After all plots were made porosity was classified as vuggy, or intramatrix, or

moldic. These zones were then correlated across the field.

Typically well to well structural and stratigraphic correlations are done using

gamma ray or spontaneous potential log traces. However, rocks in Diamond M Field do

not exhibit wide variations in gamma-ray traces that facilitate stratigraphic correlation.

In order to correlate these porosity zones we used neutron logs scaled in counts in which

more counts indicate lower porosity and vice a versa. The basis for this concept is that

neutrons interact with hydrogen in the rock such that greater interaction correlates to a

greater loss of energy, and ultimately, lower amounts of energy that ultimately reaches

the recording device in the borehole. A logarithmic porosity scale was constructed by geologists at Parallel Petroleum Co. Their proprietary method yielded estimates of porosity that were used in all wells in this study except those wells which have core analysis porosity and permeability. Once porosity is obtained that value can been entered into one of the two equations to get permeability. Neutron log traces were then correlated across the field with their respective porosity values entered into one of the two equations. These calculations provided the porosity and permeability values that were used to create our flow unit slice maps.

Distribution of Ranked Flow Units in the Study Area

Flow units within the Diamond M Field do not conform to facies boundaries, nor do they correlate to unconformities. Tracing flow unit correspondence with unconformities is difficult because neutron and gamma ray provide the only information for most of the wells in the field; and that data is generally not sufficient to discriminate between facies and pore types. Quality ranking of flow units in this field depends upon the type and extent of diagenetic alteration of the original depositional texture and fabric. Those changes can be identified in thin sections and the results can be correlated at inter well spacing by overlaying porosity and structure maps, and by correlating facies from well to well.

Porosity, permeability, and reservoir quality maps are presented in Appendix C. Slice maps of ranked flow units are constructed as 10 foot intervals hung on top of the Canyon reef. The first slice represents the interval 0-10 feet below the reef crest, whether that crest has been eroded or not. As previously indicated, the presence of

erosional unconformities that did not remove large stratigraphic thicknesses are difficult to identify with only the old wireline logs. Examination of slice maps in conjunction with structural and stratigraphic cross sections (Plates 1-6), and thin section data revealed which pore types dominate each slice as well as the geological cause-effect mechanisms that created the pores.

Reservoir slice 1 is dominated by intramatrix/moldic pores in the northern portion of the field (in wells H-1, H-2, H-3, H-4, and all other well locations to the north). The dominant pore types outside that area and in the southern portion of the field are vugs. Facies diagrams 1 and 2 show that the northwest portion of the field is reef facies and the southeast portion is grainstone and packstone facies. Reservoir quality slices 2 through 5 show more vuggy pores across the entire study area, but overall quality rankings are lower than in the uppermost five slices. The decrease in combined poroperm values is interpreted to indicate that higher poroperm values occur in closer proximity to unconformities. Facies slices 3 and 4 are dominated by reef facies with approximately the eastern 1/3 of the field represented by grainstones and packstones. Slices 6-8 show moderate amounts of high quality zones primarily located near the three cored wells in the study area. Because those wells are the only ones for which cores exist, it is possible that the old wireline log data is inadequate for quality measurements. In such cases, it is possible that greater porosity and permeability may exist outside the cored well zones. Facies maps 6 and 7 show the southeastern portion of the field represented by reef facies and the northwest dominated by grainstones and packstones. Facies slices 8-15 are dominated by reef facies with the exception of slices 11 and 12

which contain small grainstone and debris pockets in the northwest. Slices 9 and 10 reveal a greater volume of high quality zones which in this case are dominated by vuggy porosity. These zones are also within 20 vertical feet below the overlying Early Middle Canyon Unconformity. Below slice 10 are only scattered zones of reservoir quality; however most of the wells in the study area do not penetrate more than 100 ft. into the reef interval, therefore complete coverage of reservoir quality is not possible at those depths.

CONCLUSIONS

Completion of this thesis resulted in the following conclusions:

● Diamond M Field produces from a diagenetically altered depositional pore system

  (hybrid porosity) in a micritic, platy algal, skeletal wackestones to grainstone

  reservoir.

● Pore types can be identified in thin section and correlated across the field,

  resulting in detailed reservoir quality maps.

● Pore types (V, SEIM, and M) are readily identifiable in thin section and can be

  correlated across the field using poroperm values and neutron log traces.

● Methods used in the study may be applied to other West Texas Paleozoic

  reef fields with similar depositional and diagenetic characteristics.

● Core material should be taken from future wells to aid in identifying reservoir quality.

REFERENCES CITED

Ahr, W.M., 2004, Hydrothermal dolomite and hydrocarbon reservoirs: AAPG Annual Meeting Abstracts, April 18-21, 2004; Dallas Texas.

Ahr, W.M., and B.S. Hammel, 1999, Identification and mapping of flow units in carbonate reservoirs: An example from the Happy Spraberry (Permian) field, Garza County, Texas, USA: Energy Exploration and Exploitation, v. 17, p. 311-334.

Ahr, W.M., D. Allen, A. Boyd, H.N. Bachman, T. Smith, et al, 2005, Confronting the carbonate conundrum: Schlumberger Oilfield Review, Spring 2005, p. 18-29.

Burnside, R.J., 1959, Geology of part of the Horseshoe Atoll in Borden and Howard Counties, Texas: U.S. Geol. Survey, Prof. Paper 315-B, 34 p.

Choquette, P.W., and L.C. Pray, 1970, Geologic nomenclature and classification of porosity in sedimentary carbonates: AAPG Bulletin, v. 54, p. 207-250.

Dunham, R. J., 1962, Classification of carbonate rocks according to depositional texture, *in* W. E. Ham, ed., Classification of carbonate rocks-a symposium: AAPG Memoir 1, p. 108-121.

Dutton, S. P., E. M. Kim, R. F. Broadhead, W. D. Raatz, C. L. Breton, et al, 2005, Play analysis and leading-edge oil-reservoir development methods in the Permian Basin: Increased recovery through advanced technologies: AAPG Bulletin, v. 89, No. 5, p. 553-576.

Ebanks, W.J., Jr., M.H. Schiching, and C.D. Atkinson, 1993, Flow units for reservoir Characterization, *in* Morton-Thompson, D., and A.M. eds., Development Geology Reference Manual: AAPG Methods in Exploration Series, no. 10, p. 282-285.

Embry, A.F. and Klovan, J.E., 1971, A Late Devonian reef tract on northeastern Banks Island, Northwest Territories: Canadian Petroluem Geology Bulletin, p. 730-781.

Ewing, T. E., 1993, Erosional margins and pattern of subsidence in the Late Paleozoic West Texas Basin and adjoining basins of West Texas and New Mexico: New Mexico Geological Society Guidebook, 44th Field Conference, p. 155-166.

Forsythe, G.T.W., 2003, A new synthesis of Permo-Carboniferous phylloid algal reef ecology: SEPM Special Publication n. 78, p. 173-188.

Frenzel, H. N., R. R. Bloomer, R. B. Cline, J. E. Cys, J. E. Galley, W. R. Gibson, J. M. Hills, W. E. King, W. R. Seager, F. E. Kottlowski, S. Thompson lll, G. C. Luff, B. T. Pearson, and D. C. Van Siclan, 1988, The Permian Basin region, *in* L. L. Sloss, ed., The Geology of North America, v. D-2, Sedimentary cover-North American Craton: United States, Geological Society of America, p. 261-306.

Hammel, B. S., 1996, High resolution characterization of the Permian (Upper Leonardian) Spraberry Formation, Happy Spraberry Field, Garza County, Texas. M.S. thesis, Texas A&M University, College Station, Texas, 176 p.

Layman, J.M., 2002, Porosity characterization utillizing petrographic image analysis: Implications for identifying and ranking reservoir flow units, Happy Spraberry Field, Garza County, Texas: M.S. thesis, Texas A&M University, Texas, 102 p.

Lucia, F.J., 1995, Rock-fabric/petrophysical classification of carbonate pore space for reservoir characterization: AAPG Bulletin, v. 79, no.9, p. 1275-1300.

Machel, H.G., 1987, Saddle dolomite as a by-product of chemical compaction and thermochemical sulfate reduction: Geology, v. 15, p. 936-940.

Mazzullo, S. J., 1995, Permian stratigraphy and facies, Permian Basin (Texas-New Mexico) and adjoining areas in the Midcontinent United States, *in* P. A. Scholle, T. M. Peryt, D. S. Ulmer-Scholle, eds., The Permian of Northern Pangea: Sedimentary Basins and Economic Resources, New York Springer-Verlag, v. 2, p. 41-60.

Mazzullo, S.J., and P.M. Harris, 1992, Mesogenetic Dissolution: It's role in porosity development in carbonate reservoirs: AAPG Bulletin v. 76, no. 5, p. 607-620.

Mazzullo, S.J., and A. M. Reid, 1988, Stratigraphic architecture of Pennsylvanian and Lower Permian Facies, Northern Midland Basin, Texas, *in* B. K. Cunningham, ed., Permian and Pennsylvanian Stratigraphy, Midland Basin, West Texas: Studies to aid hydrocarbon exploration, Midland, Texas, West Texas Geological Society, Permian Basin Section, SEPM Publication 88-28, p. 1-6.

Myers, D. A., P. T. Stafford and R.J. Burnside, 1956, Geology of the Late Paleozoic Horseshoe Atoll in West Texas: Univ. of Texas, Bureau of Eco. Geol., Publication No. 5607, 113 p.

Radke, B.M., and R.L. Mathis, 1980, On the formation and occurrence of saddle dolomite: Journal of Sedimentary Petrology, v. 50, p. 1149-1168.

Reid, A. and S.T. Reid, 1999, Glacio-Eustatic sea level fluctuations and the formation of Pennsylvanian age carbonate reservoirs in the Permian Basin of West Texas:

West Texas Geological Society, Publication No 99-106, p. 71-79.

Reid, S. T., 1998, Diamond M Canyon Unit Study, unpublished from Harold Vance Department of Petroleum Engineering, Texas A&M University.

Riding, R., 2002, Structure and composition of organic reefs and carbonate mud mounds; concepts and categories: Earth Science Reviews, 58, p 163-231.

Ross, C. A., 1986, Paleozoic evolution of southern margin of Permian Basin: Geological Society of America Bulletin, v. 97, p. 536-554.

Saller, A.H., J.A.D. Dickson, and F. Matsuda, 1999, Evolution and distribution of porosity associated with subaerial exposure in Upper Paleozoic platform limestones, West Texas: AAPG Bulletin, V. 83, No. 11, p. 1835-1854.

Schatzinger, R. A., 1983, Phylloid algal and sponge-bryozoan mound-to-basin transition: A Late Paleozoic facies tract from the Kelly-Snyder Field, West Texas: SEPM Core Workshop no. 4, p. 244-303.

Schatzinger, R.A., 1988, Changes in facies and depositional environments along and across the trend of the Horseshoe Atoll, Scurry and Kent Counties, Texas: PBS-SEPM Research Seminar Number One, p. 79-105.

Scholle, P.A., and D.S. Ulmer-Scholle, A color guide to the petrography of carbonate rocks: Grains, textures, porosity, diagenesis: AAPG Memoir no. 77, 474 p.

Stafford, P.T., 1957, Scurry Field, *in* Herald, F. A., ed., Occurrence of oil and gas in West Texas, Austin, Univ. of Texas, Bureau of Eco. Geol., Publication no. 5716, p. 295-302.

Stafford, P.T., 1959, Geology of part of the Horseshoe Atoll in Scurry and Kent Counties, Texas: U.S. Geol. Survey, Prof. Paper 315-A, 20 p.

Tai, P. C., 2001, Late Paleozoic foreland deformation in the Southwestern Midland Basin and adjacent areas: Implications for tectonic evolution of the Permian Basin, West Texas: Ph.D. dissertation, Texas A&M University, College Station, Texas, 193 p.

Vail, P.R., R.M. Mitchum, Jr. and S. Thompson, III, 1977, Seismic stratigraphy and global changes of sea level, Part 4: Global cycles of relative changes of sea level: AAPG Memoir 26, p. 83-97.

Vest, E. L., 1970, Oil fields of Pennsylvanian-Permian Horseshoe Atoll, West Texas: *in* Halbouty, M. T., ed., Geology of Giant Petroleum Fields: Amer. Assoc.

Petrol. Geologist Memoir 14, p. 185-203.

Ward R. F., C. G. St. C. Kendall, and P. M. Harris, 1986, Upper Permian (Guadalupian) facies and their association with hydrocarbons-Permian Basin, West Texas and New Mexico: AAPG Bulletin, v. 70, p. 239-262.

Wermund, E.G., 1975, Upper Pennsylvanian limestone banks, north-central Texas: Bureau of Economic Geology, Circular 75-3, 34 p.

APPENDIX A

CORE DESCRIPTIONS AND PHOTOGRAPHS

Core Description
Parallel Petroleum
Topaz #1
Diamond M Field
Scurry County, Texas
Core Interval 6706.0'- 6750.0'

Depth (ft.)	Thickness (ft.)	Description
6706.0	3.0	Limestone. Light gray to dark brown, fine to coarse grained grainstone, moderately to well sorted, bivalves, forams, fusulinids, gastropods, phylloid algae, alternating calcite cement and micritic layers, styolites present, dissolution porosity.
6709.0	2.0	Limestone. Light gray, medium to coarse grained grainstone, poorly sorted, forams, fusulinids, massive, styolites present.
6711.0	3.0	Limestone. Gray, medium to coarse grained packestone, poorly sorted, brachiopods, forams, fusulinids, phylloid algae, massive.
6714.0	7.0	Limestone. Light gray to light brown, automicrite, bivalves, forams, fusulinids, phylloid algae, sponge spicules, grains compose 15% of rock, dissolution porosity.
6721.0	1.0	Preserved.
6722.0	4.0	Limestone. Light gray to light brown, automicrite, bivalves, forams, fusulinids, phylloid algae, sponge spicules, grains compose 15% of rock, styolites present, dissolution porosity.
6726.0	24.0	Not Recovered.

Core Description
Parallel Petroleum
Topaz #1 (cont.)
Diamond M Field
Scurry County, Texas
Core Interval 6750.0'- 6820.0'

Depth (ft.)	Thickness (ft.)	Description
6750.0	3.5	Limestone. Light gray to light brown, automicrite, bivalves, brachiopods, forams, phylloid algae, sponge spicules, trilobite fragments, styolites present, dissolution porosity, quartz replacement.
6753.5	0.9	Limestone. Light gray to light brown, automicrite, bivalves, brachiopods, forams, fusulinids, phylloid algae, sponge spicules, dissolution porosity.
6754.4	0.3	Preserved.
6754.7	1.3	Limestone. Light gray to light brown, automicrite, bivalves, brachiopods, forams, fusulinids, phylloid algae, sponge spicules, dissolution porosity.
6756.0	0.8	Limestone. Light gray to light brown, automicrite, bivalves, brachiopods, forams, fusulinids, phylloid algae, sponge spicules, chert nodules, dissolution porosity.
6756.8	0.4	Preserved.
6757.2	4.3	Limestone. Light gray to light brown, automicrite, bivalves, brachiopods, crinoids forams, fusulinids, phylloid algae, chert nodules, dissolution porosity.
6761.5	58.5	Drilled, not recovered.

Core Description
Parallel Petroleum
Topaz #1 (cont.)
Diamond M Field
Scurry County, Texas
Core Interval 6820.0'- 6836.5'

Depth (ft.)	Thickness (ft.)	Description
6820.0	6.4	Limestone. Brown, automicrite, laminated, micrite, bivalves, brachiopods, crinoid fragments, forams, fusulinids, phylloid algae, pyrite and silica replacement, leached styolites, dissolution and fracture porosity.
6826.4	9.8	Limestone. Light gray to light brown, automicrite, foram grains present, phylloid algae, replacement by calcite and silica, chert nodules, virtually no porosity.
6836.2	0.3	Limestone. Brown, poorly sorted packstone, laminated, abundant fusulinids, chert nodules, low porosity.
6836.5	-----	END OF CORE.

Core Description
Parallel Petroleum
Jade #1
Diamond M Field
Scurry County, Texas
Core Interval 6745.0'- 6772.0'

Depth (ft.)	Thickness (ft.)	Description
6745.0	4.5	Limestone. Brown to gray, automicrite, mottled, micrite, bivalves, brachiopods, crinoids, forams, fusulinids, phylloid algae, sponge spicules, styolites, low porosity.
6750.5	2.0	Limestone. Brown, grainstone, massive, moderate to well sorted, brachiopods, crinoids, forams, fusulinids, phylloid algal fragments, low porosity.
6752.5	10.5	Limestone. Brown to gray, automicrite, mottled, bivalves, brachiopods, crinoids, forams, fusulinids, phylloid algae, sponge spicules, styolites present, low porosity.
6763.0	3.5	Limestone. Brown to tan, automicrite, fine grained, brachiopods, crinoids, forams, fusulinids, phylloid algae, sponge spicules, micritic clasts, low porosity.
6766.5	5.5	Limestone. Tan to light brown, grainstone to packstone, moderate to well sorted, contains layers of poorly sorted, highly micritic, fossiliferous wackestone. Grainstone consists of skeletal and non-skeletal grains which are primarily peloids. Bivalves, brachiopods, crinoids, forams, phylloid algae fragments, sponge spicules and gastropods. Styolites present, porosity higher 10-12% in wackestone, considerably lower in grainstone.

Core Description
Parallel Petroleum
Jade #1 (cont.)
Diamond M Field
Scurry County, Texas
Core Interval 6772.0'- 6808.0'

Depth (ft.)	Thickness (ft.)	Description
6772.0	12.5	Limestone. Light gray to tan, automicrite, thin zones of grainstone. Poor to moderate sorting, highly micritic, bivalves, brachiopods, crinoids, forams, fusulinids, gastropods, phylloid algae, sponge spicules, micritic clasts which resemble burrows, dissolution and fracture porosity common, approximately 5-7%.
6784.5	13.5	Limestone. Tan, grainstone to packstone, moderate to well sorting, skeletal and non-skeletal grains primarily peloids. Bivalves, brachiopods, crinoids, echnoids, forams, fusulinids, phylloid algae fragments, sponge spicules, hydrocarbon staining, variable porosity, well sorted grainstones contain low porosity, moderately sorted packstone layers contain 5-15% dissolution porosity.
6798.0	10.0	Limestone. Gray, light gray, and tan, grainstone, well sorted, composed primarily of phylloid algae and occasional forams and gastropods, calcite cemented, micritic lenses on phylloid algae. Porosity ranges from 5-10%. Bottom five feet moderately to poorly sorted, contains parallel bedding of phylloid algae and forams, abundant micrite.

Core Description
Parallel Petroleum
Jade #1 (cont.)
Diamond M Field
Scurry County, Texas
Core Interval 6808.0'- 6864.0'

Depth (ft.)	Thickness (ft.)	Description
6808.0	8.0	Limestone. Light gray, grainstone to packstone, moderate to well sorted, rounded grains, dominated (75%) by forams, bivalves, brachiopods, crinoids, gastropods, phylloid algae fragments, and sponge spicules all common. Micritic clasts present at 6,813 ft. Highly cemented by calcite, porosity decreases from top (3-5%) to bottom (0%). Dissolution porosity.
6816.0	22.0	Limestone. Gray to dark gray, automicrite, abundant phylloid algae, bivalves, brachiopods, crinoids, forams, gastropods, phylloid algal fragments, sponge spicules, micritic clasts, saddle dolomite, porosity ranges from 3-15%, primarily from 6822-6835. Dissolution and fracture porosity visible.
6838.0	12.0	Limestone. Gray, automicrite, grains well sorted, dominated by forams, bivalves, brachiopods, crinoids, phylloid algae, sponge spicules all common. Low porosity, 1-3%.
6850.0	14.0	Limestone. Gray to dark gray, automicrite, primarily composed of micrite cement, grains common, primarily large crinoids and forams, bivalves, brachiopods, phylloid algae and sponge spicules all present, no visible porosity with the exception of occasional small fracture, styolites present. Highly cemented with calcite.

Core Description
Parallel Petroleum
Jade #1 (cont.)
Diamond M Field
Scurry County, Texas
Core Interval 6864.0'- 6872.0'

Depth (ft.)	Thickness (ft.)	Description
6864.0	8.0	Limestone, dolostone, shades of gray and brown, debrite, poorly sorted, angular to round grains, composed of bivalves, brachiopods, crinoids, forams, gastropods, phylloid algae fragments, sponge spicules, micrite, saddle dolomite, styolites, pyrite. Dissolution porosity, ranges from 1-7%.
6872.0	0.0	End of core.

Core Description
Parallel Petroleum
Emerald #1
Diamond M Field
Scurry County, Texas
Core Interval 6613.0'-6626.0'

Depth (ft.)	Thickness (ft.)	Description
6613.0	1.7	Limestone. Tan, grainstone, poorly sorted, fine to coarse grained, massive, bivalves, brachiopods, crinoids, forams, fusulinids, sponge spicules, 5-7% porosity.
6614.7	0.3	Preserved.
6615.0	3.4	Limestone. Tan, grainstone/packstone, poorly sorted, fine to coarse grained, massive, bivalves, brachiopods, crinoids, forams, fusulinids (increasing in size and abundance to 6618.4ft), sponge spicules. Rock transitions from grainstone to packstone gradually at approximately 6617 ft, 1-2% porosity.
6618.4	2.6	Limestone. Brownish gray, packstone/wackestone, moderately sorted, fine to coarse grained, massive, bivalves, brachiopods, crinoids, forams, fusulinids, phylloid algae, sponge spicules, possible chert nodules and dolomite, styolites, transitions from packstone to wackestone gradually at approximately 6620.0 ft, 5% porosity evident at 6620.6 ft.
6621.0	5.0	Limestone. Tan to gray, automicrite, moderately sorted, fine to coarse grained, irregular bedding surfaces, calcite cemented and micritic layers, bivalves, brachiopods, crinoids, forams, fusulinids, phylloid algae, sponge spicules, possible dolomite and chert, styolites, 2-4% porosity.

Core Description
Parallel Petroleum
Emerald #1 (cont.)
Diamond M Field
Scurry County, Texas
Core Interval 6626.0'- 6635.6'

Depth (ft.)	Thickness (ft.)	Description
6626.0	4.0	Limestone. Gray to brown, automicrite, poorly sorted, fine to coarse grained, bivalves, brachiopods, crinoids, forams, fusulinids, micritic clasts, phylloid algae, sponge spicules, dolomite inclusions, chert possible as well as anhydrite inclusions, pyrite crystals present as well as pyrite replacement of crinoids, unusual replacement by dolomite, 1-2% porosity.
6630.0	2.0	Limestone. Dark gray, grainstone, well well sorted, coarse grained, well rounded, massive, brachiopods, crinoids, forams, phylloid algal fragments, sponge spicules, pyrite present, intermound grainstone, well cemented, no porosity.
6632.0	2.5	Limestone. Dark gray, automicrite, poorly sorted, fine to coarse grained, bivalves, brachiopods, crinoids, forams, fusulinids, micritic clasts, phylloid algae, sponge spicules, dolomite inclusions, chert possible as well as anhydrite inclusions, pyrite present, unusual replacement by dolomite, 1-2% porosity, irregular styolite forms lower boundary.
6634.5	1.1	Limestone. Gray to tan, grainstone, moderate to well sorted, coarse grained, bivalves, brachiopods, crinoids, forams, phylloid algal fragments, sponge spicules, 4-7% porosity, increasing toward bottom.
6635.6	0.4	Preserved.

Core Description
Parallel Petroleum
Emerald #1 (cont.)
Diamond M Field
Scurry County, Texas
Core Interval 6635.6'- 6671.4'

Depth (ft.)	Thickness (ft.)	Description
6636.0	4.4	Limestone. Tan to gray, grainstone, well sorted, coarse grained, becoming finer grained towards bottom, massive, bivalves, brachiopods, crinoids, forams, phylloid algal fragments, sponge spicules, styolites present below 6638.2 as well as odd dolomitic inclusions, approximately 10% porosity.
6640.4	2.6	Core absent.
6643.0	5.0	Limestone. Dark gray to brown, packstone moderate sorting, composed mainly of forams, fusulinids, and micritic mud, shaly texture, phylloid algal fragments, brachiopods, and crinoids all present, styolites present, low porosity.
6648.0	7.0	Limestone. Tan to gray, grainstone, moderate to poor sorting, fine to coarse, grained, well rounded, bivalves, brachiopods, crinoids, forams, fusulinids, phylloid algal fragments, sponge spicules, 1-2% porosity, oil staining at 6649 ft.
6655.0	16.0	Limestone. Gray to brown, automicrite, mainly micrite, mottled, few grains, forams, fusulinids, brachiopods, bivalves, phylloid algae, 80% micrite, styolites, fracture as well as vuggy porosity evident, 3-5%.
6671.0	0.4	Preserved.

Core Description
Parallel Petroleum
Emerald #1 (cont.)
Diamond M Field
Scurry County, Texas
Core Interval 6671.4'- 6690.4'

Depth (ft.)	Thickness (ft.)	Description
6671.4	4.6	Limestone. Gray to light brown, automicrite, mottled, poor to moderate sorting near bottom, bivalves, brachiopods, crinoids, forams, fusulinids, phylloid algae, sponge spicules, possible bryozoan at 6676, styolites, pyrite, possible chert or dolomite inclusions, porosity variable, 20% near top to 3% at bottom. Porosity dominated by interparticle, vuggy, and moldic porosity.
6676.0	6.5	Limestone. Gray to light brown, packstone, moderately sorted, parallel bedding present, bivalves, brachiopods, crinoids, forams, fusulinids, phylloid algal fragments, sponge spicules, bryozoans, possible oil staining, chert nodule at 6681 porosity 3-5%, mainly interparticle and moldic.
6682.5	0.7	Preserved.
6682.9	7.1	Limestone. Gray to brown, automicrite, moderate to well sorted, grains are skeletal, highly micritic, bivalves, brachiopods, crinoids, forams, fusulinids, gastopods, phylloid algae, sponge spicules, dark staining at 6686.6 ft, primarily solution enhanced interparticle to vuggy, and moldic porosity, up to 20% in areas containing large vugs, 15% total porosity.
6690.0	0.4	Preserved.

Core Description
Parallel Petroleum
Emerald #1 (cont.)
Diamond M Field
Scurry County, Texas
Core Interval 6690.4'- 6704.2'

Depth (ft.)	Thickness (ft.)	Description
6690.4	4.6	Limestone. Light tan to gray, automicrite, micritic, well sorted, fine grained, bivalves, brachiopods, crinoids, forams, phylloid algae, phylloid algal fragments, sponge spicules, possible burrows at 6694 ft, styolites, interparticle, moldic, and fracture porosity, 5%.
6695.0	3.5	Limestone. Brown to dark gray, automicrite, well sorted, fine grained, highly micritic, bivalves, brachipods, crinoids, forams, phylloid algae, phylloid algal fragments, sponge spicules, little to no porosity, highly micritized.
6698.5	1.5	Limestone. Gray, grainstone, moderate to good sorting, skeletal and non skeletal grains (peloids and clasts), brachiopods, crinoids, forams, fusulinids phylloid algae, low porosity.
6700.0	2.1	Limestone. Light brown to gray, automicrite, well sorted, fine grained with the exception of large brachiopod shells, non skeletal grains (peloids or intraclasts), bivalves, brachiopods, crinoids abundant, forams, possible trilobite shell, approximately 3% porosity.
6702.1	0.9	Absent.
6703.0	1.2	Limestone. Light tan to gray, automicrite, poor sorting, bivalves, brachiopods, crinoids, forams, fusulinids, phylloid algae, sponge spicules, 10-12% porosity.

Core Description
Parallel Petroleum
Emerald #1 (cont.)
Diamond M Field
Scurry County, Texas
Core Interval 6704.2'- 6718.9'

Depth (ft.)	Thickness (ft.)	Description
6704.2	2.0	Limestone. Brown, mudstone/wackestone, well sorted, fine grained, highly micritic, bivalves, brachiopods, crinoids, forams, fusulinids, sponge spicules, no porosity.
6706.2	2.9	Limestone. Light brown to gray, automicrite, moderately sorted, mottled, bivalves, brachiopods, crinoids, forams, fusulinids, phylloid algae, sponge spicules, 1-3% porosity.
6709.1	1.9	Limestone. Brown, wackestone/packstone, moderately sorted, fine grained with with exception of fusulinids, bivalves, brachiopods, forams, fusulinids, phylloid algae, sponge spicules, massive, low porosity.
6711.0	3.5	Limestone. Brown, packstone, moderate to well sorted, medium to coarse grained, skeletal and non-skeletal grains (peloids), bivalves, brachiopods, crinoids, forams, fusulinids, phylloid algal fragments, sponge spicules, transitions into a grainstone at approximately 6713.5 ft., zero porosity.
6714.5	4.5	Limestone. Tan, grainstone, moderate to well sorted, skeletal and non-skeletal grains (peloids), sorting decreases after 6718.2 ft., as well as abundance of grains, transitions into packstone, bivalves, brachiopods, forams, fusulinids, phylloid algal fragments, sponge spicules, parallel present from 6714.5 to 6718.2, porosity ranges from 5-10%.

Core Description
Parallel Petroleum
Emerald #1 (cont.)
Diamond M Field
Scurry County, Texas
Core Interval 6718.9'- 6739.1'

Depth (ft.)	Thickness (ft.)	Description
6718.9	4.1	Limestone. Brown, mudstone, well sorted, fine grained, bivalves, brachiopods, crinoids, forams, phylloid algal voids, sponge spicules, highly micritic, styolites present, 1% porosity, only in small fractures.
6723.0	13.0	Limestone. Gray, automicrite, poor to moderate sorting, skeletal and non-skeletal grains (peloids), bivalves, brachiopods, crinoids, forams, fusulinids, phylloid algae and phylloid algal fragments, sponge spicules, micritic clasts, styolites common throughout, rock darkens to dark gray at 6733.0 ft, 1-3% porosity.
6736.0	1.9	Limestone. Gray, grainstone/packstone at top, interbedded with automicritic bands from 6737.0 ft. and down, poorly sorted, skeletal and non-skeletal grains (peloids), bivalves, brachiopods, crinoids, forams, fusulinids, phylloid algae and phylloid algal fragments, sponge spicules, micritic clasts, styolites, 10-15 % porosity.
6737.9	0.6	Preserved.
6738.5	0.6	Limestone. Gray, automicrite, moderately sorted, fine to coarse grained, skeletal and non-skeletal grains (peloids), bivalves, brachiopods, crinoids, forams, fusulinids, phylloid algae mainly dissolved, sponge spicules, micrite clasts, styolites, abundant porosity, 70%, large dissolution vug.

Core Description
Parallel Petroleum
Emerald #1 (cont.)
Diamond M Field
Scurry County, Texas
Core Interval 6739.1'- 6763.0'

Depth (ft.)	Thickness (ft.)	Description
6739.1	0.4	Preserved.
6739.5	0.8	Limestone. Gray, automicrite, moderately sorted, fine to coarse grained, skeletal and non-skeletal grains (peloids), bivalves, brachiopods, crinoids, forams, fusulinids, phylloid algae (often dissolved), sponge spicules, micritic clasts, styolites, approximately 15% porosity.
6740.3	0.3	Preserved.
6740.6	2.4	Limestone. Gray, automicrite, moderately sorted, fine to coarse grained, skeletal and non-skeletal grains (peloids), bivalves, brachiopods, crinoids, forams, fusulinids, phylloid algae (often dissolved), sponge spicules, micritic clasts, styolites, approximately 15% porosity, end of small vugs until bottom of core.
6743.0	20.0	Limestone. Gray, automicrite, moderately sorted, fine to coarse grained, skeletal and non-skeletal grains (peloids), micritic clasts, bivalves, brachiopods, crinoids, forams, fusulinids, phylloid algae (often dissolved), styolites, 10% porosity possible, often located below styolites in association with oil staining.
6763.0	0.0	End of core.
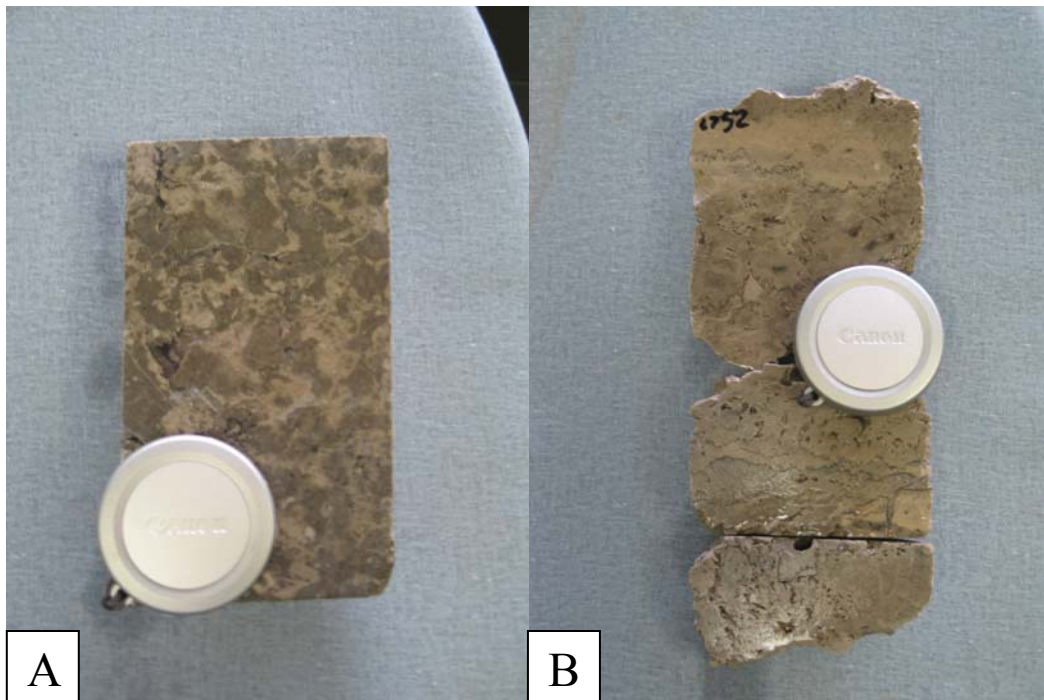
Figure A-1. A) Core photo taken from Jade # 1 @ 6,848' representing Reef Facies 1. B) Core photo taken from Topaz # 1 @ 6,752' representing Reef Facies 2 as well as abundant vuggy porosity.
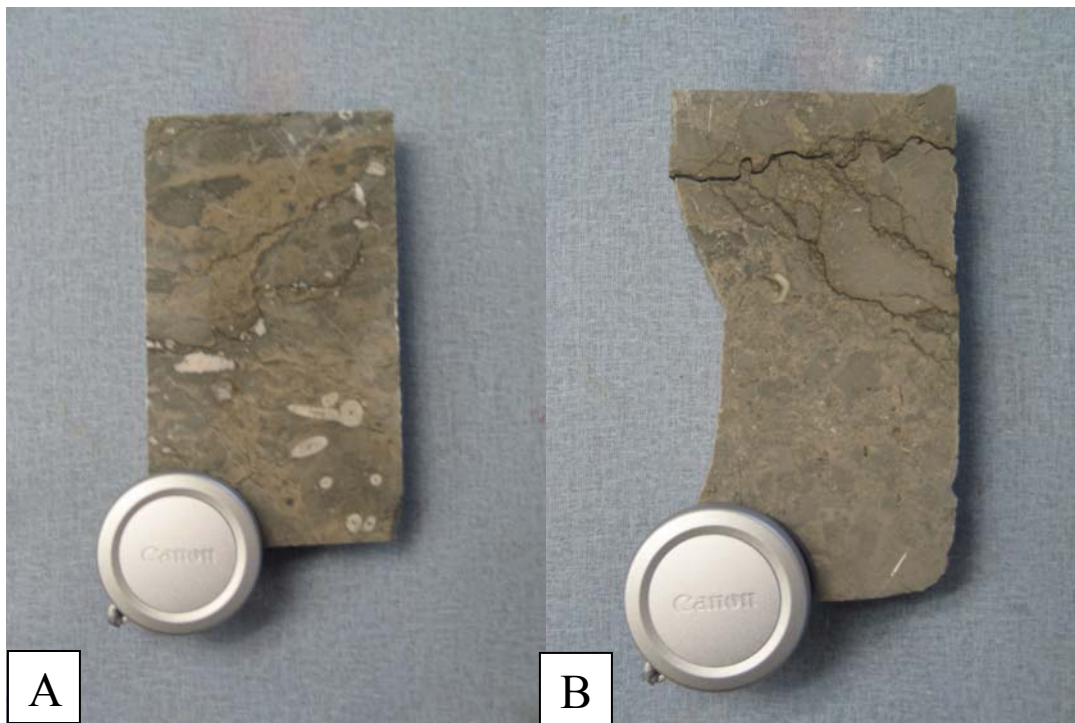
Figure A-2. A) Core photo taken from Jade # 1 @ 6,853' representing reef facies 2. B) Core photo taken from Jade # 1 @ 6,819' representing erosional debris at top of reef facies 1.
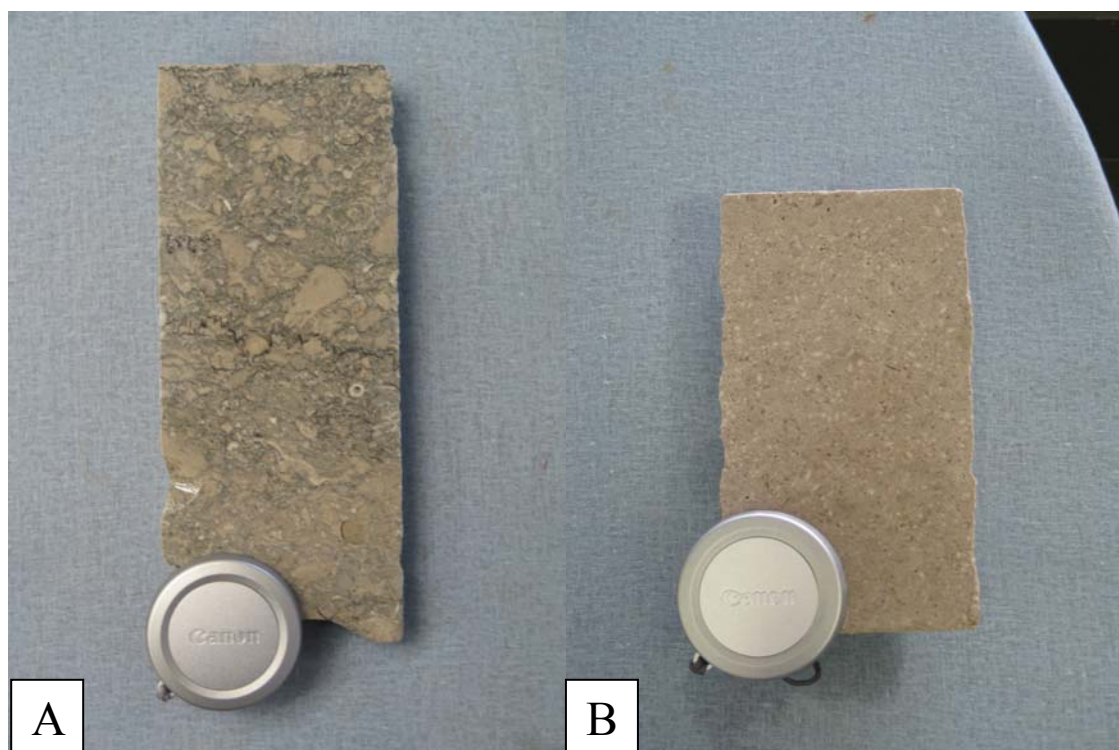
Figure A-3. A) Core photo taken from Jade # 1 @ 6,868' representing Debris Facies. B) Core photo taken from Topaz # 1 @ 6,710' representing the Grainstone/Packstone Facies.

APPENDIX B

THIN SECTION DESCRIPTIONS AND PHOTOMICROGRAPHS

Thin Section Description
Parallel Petroleum
Topaz #1
Diamond M Field
Scurry County, Texas

Depth (ft.)	Description

6707.1   Limestone. Brown, grainstone, well sorted, well rounded grains, majority of grains < 1mm, dominated by forams, less common phylloid algal fragments, crinoids (often dolomitized by saddle dolomite), bivalves, brachiopods, and sponge spicules (dissolved), estimated 20-25% porosity.

                 Abundant solution enhanced intramatrix, vuggy, moldic, and intraparticle porosity (in order of abundance). Three or more stages of diagenesis possible. 1. Micritization of grains and shells. 2. At least two stages of cementation by calcite cement and dissolution. 3. Saddle dolomite replacing calcified fossils and possible filling of pores, followed by abundant dissolution.

6707.7   Limestone. Tan to brown, grainstone, well sorted, sub to well rounded grains, parallel bedding present by micritized and calcite cemented layers with calcite cemented layers being highly fossiliferous. Majority of grains < 1mm, dominated by forams, less common phylloid algal fragments, brachiopods, crinoids, sponge spicules (dissolved), estimated 25% porosity.

                 Abundant solution enhanced moldic, intramatrix, and intraparticle porosity (in order of abundance). Three or more stages of diagenesis possible. 1. Micritization of grains and shells. 2. Two or more stages of cementation by calcite cement and dissolution. Different stages of calcification represented by stages of pore filling growth from sparry calcite to large blocky calcite. 3. Styolites, saddle dolomite replacing calcified fossils and filling of pores (dominant form), followed by abundant dissolution.

6712.9   Limestone. Gray/Tan, packstone, moderate to poor sorting, round to angular grains, fine to coarse grained, composed of bivalves, brachiopods, crinoids, forams, fusulinids, phylloid algal fragments, sponge spicules. Crinoids and brachiopods most abundant. 70% micrite to 30% calcite matrix, estimated 20% porosity.

                 Solution enhanced intergranular, moldic, vuggy, and intraparticle porosity (in order of abundance). Two or more stages of diagenesis possible. 1.

Micritization of grains and shells. 2. Two or more stages of cementation by calcite cement with possible dissolution between stages. Calcite overgrowths of shells and grains common as well as pore filling calcite. Prismatic calcite visible. Dissolution is dominant final stage of dissolution.

6713.9   Limestone. Tan, packstone/wackestone, poorly sorted, round to angular grains, fine to coarse grained, composed of crinoids (abundant), brachiopods, bivalves, forams, fusulinids, phylloid algae, sponge spicules, estimated 20% porosity.

Solution enhanced vuggy, moldic, intramatrix, and intraparticle porosity (in order of abundance). Two or more stages of diagenesis possible. 1. Abundant micritization of grains, shells, and matrix. 2. Two or more stages of cementation by calcite cement with possible dissolution between stages. Sparry calcite appears to be first stage followed by blocky calcite. No accessory replacement by saddle dolomite, anhydrite, or silica. Appears dissolution was dominant final stage creating large vugs which contain most porosity.

6716.5   Limestone. Light gray, automicrite, well sorted, well rounded grains, dominated by micritic matrix (80%), remaining 20% composed of bivalves, brachiopods, crinoids, forams, one fusulinid, possible phylloid algae, sponge spicules, trilobite shells, estimated 15-17% porosity.

Solution enhanced vuggy, moldic, intramatrix, and intraparticle porosity (in order of abundance). Two or more stages of diagenesis possible. 1. Abundand micritization of grains, shells, and matrix. 2. One stage at least of calcite cementation of grains or shells. However, most calcite cement has been dissolved, remnants of spar and blocky calcite visible. Mainly vuggy porosity.

6751.7   Limestone. Light gray to brown, automicrite, moderately sorted, round to angular grains, 50% micritic matrix. Grains dominated by forams, bivalves, brachiopods, crinoids, phylloid algal fragments, sponge spicules constitute 30% of grains, estimated 20-25% porosity.

Solution enhanced vuggy to cavernous, moldic, intramatrix, intraparticle porosities (in order of abundance). Two or more stages of diagenesis possible. 1. Abundant micritization of grains and shells. 2. At least two stages of cementation by calcite. First by sparry calcite, second by blocky calcite. May be a stage of micritization in between two calcite cementation stages. Dissolution is final stage, dissolving most of the

calcite cement as well as some micritized shells. Styolite also present, most likely final stage of diagenesis.

6752.9   Limestone. Light gray to brown, automicrite, reef facies, moderately sorted, round to sub-angular grains, 80% micrite matrix, 20% grains, dominated by forams and fusulinids, bivalves, brachiopods, crinoids, phylloid algae, sponge spicules, estimated 20-25% porosity.

Solution enhanced vuggy to cavernous, moldic, intramatrix, intraparticle porosities (in order of abundance). Two or more stages of diagenesis recognizable. 1. Abundant micritization of grains and shells. 2. At least two stages of cementation by calcite with possible dissolution in between cementation of sparry to blocky cement. Styolites present and may represent third stage along with abundant dissolution of calcite cement. Styolites shelter rock from dissolution at bottom of slide.

6755.2   Limestone. Light gray, automicrite, with packstone pockets, well sorted, fine to medium well rounded grains, forams most common, bivalves, brachiopods, crinoids, fusulinids, phylloid algal fragments, sponge spicules, estimated 10-12% porosity, mainly in packstone intervals.

Solutions enhanced intramatrix and moldic porosity, as well as intraparticle and small amounts of vuggy porosity (in order of abundance). At least two stages of diagenesis. 1. Micritization of grains and shells. 2. Possibly two stages of calcite cementation present. Small blocky calcite cement most common with appearances of larger blocky calcite filling large pores. Late stage dissolution of calcite cement definitely dominate form of diagenesis.

6760.2   Limestone. Light gray to brown, wackestone, well sorted, fine grained, well rounded, majority of grains are small forams and sponge spicules of which many are dissolved. Bivalves, brachiopods, crinoids, possible phylloid algal fragments. Well defined zones of medium to low energy characterized by abundances of micrite and grains, estimated 5% porosity.

Moldic and intramatrix porosity dominate. Intraparticle porosity as well as fracture porosity present (in order of abundance). At least two stages of diagenesis. 1. Abundant micritization of grains and shells. 2. Cementation by sparry to small blocky calcite followed by dissolution of calcite. Dissolution of calcite results in porosity. Moldic porosity is mainly in sponge spicules and small forams.

6820.9   Limestone. Light brown to gray, automicrite, poor to moderately sorted, fine to coarse grained, round to sub-angular grains, approximately 50% grains/matrix, grains composed of bivalves, brachiopods, crinoids, forams, fusulinids, phylloid algal fragments, sponge spicules. Well defined medium to low energy zones defined by styolites and grain/micrite abundances, estimated 1% porosity.

Small amount of porosity present in fractures and styolites. At least two stages of diagenesis. 1. Abundant micritization of grains and shells. 2. Two visible stages of calcite cementation, small blocky calcite followed by large blocky calcite. May be a dissolution event in between. Appears to be some small scale dissolution of styolites which results in a small amount of porosity.

6828.8   Limestone. Brown, automicrite, well sorted, less than 10% grains, mainly small forams. Highly micritic with large phylloid algae, some bivalves, brachiopods, sponge spicules no porosity.

Two visible stages of diagenesis. 1. Abundant micritization of grains and shells. 2. Possible of dissolution of micrite followed by at least one stage of calcite cementation. Large blocky calcite seems to dominate with small amounts of small blocky calcite present. May be two stages of cementation with dissolution between. No porosity, dominated by cement.

6832.4   Limestone. Brown, automicrite, very grainy, 50-60% small rounded grains, possibly foram fragments and sponge spicules. Bivalves, brachiopods, crinoids, forams, fusulinids, phylloid algal fragments, sponge spicules, abundant micrite and calcite cement, estimated 1-2% porosity.

Two visible stages of diagenesis. 1. Abundant micritization of grains and shells. 2. At least one stage of calcite cementation. Blocky calcite seems to dominate with small amounts of small blocky calcite present. Little porosity, small fractures which hold porosity.

Thin Section Description
Parallel Petroleum
Emerald # 1
Diamond M Field
Scurry County, Texas

Depth (ft.)	Description

6614.3   Limestone. Tan, packestone, poorly to moderately sorted, fine to coarse grained, dominated by forams and crinoid fragments, bivalves, brachiopods, fusulinids, phylloid algal fragments, sponge spicules, highly micritic, estimated 3-5% porosity.

Solution enhanced intramatrix porosity dominates, intraparticle and moldic porosity present (in order of abundance). At least two stages of diagenesis possible. 1. Micritization of grains and shells. 2. One stage of cementation of grains followed by minor dissolution of calcite cement and micritic matrix. Small blocky calcite cement is dominant form of cementation. No large blocky calcite, dolomite, anhydrite, or chert.

6621.9   Limestone. Tan, wackestone/automicrite, moderately sorted, angular to round grains, abundant micrite, calcite cement common, 20-30% grains, dominated by forams and crinoid fragments, bivalves, brachiopods, fusulinids, gastropods, phylloid algae molds present, sponge spicules. Easily recognizable bedding surfaces. High energy, poorly sorted layers with abundant calcite cement and low energy micritic layers, estimated 7-10% porosity.

Solution enhanced intramatrix, moldic, and intraparticle porosity (in order of abundance). At least three stages of diagenesis possible. 1. Micritization of grains and shells. 2. At least two stages of cementation by calcite and dissolution. Many large shells and sponge spicules dissolved. Small pore filling blocky calcite cement present as well as replacement of fossils by large blocky calcite. 3. Styolites, saddle dolomite replacing calcified fossils and filling of pores (dominant form), followed by another stage of dissolution.

6626.4   Limestone. Tan to light brown, automicrite, poorly sorted, angular to round grains, approximately 30-40 % grains, highly micritic, appears that all fossils have been altered by diagenesis, either micritized or dissolved and replaced by calcite, crinoids, forams, and phylloid algae (dissolved and replaced by calcite) dominate slide, bivalves, brachiopods, bryozoans, fusulinids, gastropods, sponge spicules (abundant). Appears

to be low energy due to large amount of micrite, less than 1% porosity, located in small fractures.

Small amount of fracture porosity visible as well as minimal dissolution porosity along styolites. At least three stages of diagenesis possible. 1. Micritization of grains and shells. 2. Dissolution and cementation by small blocky calcite, followed by possible dissolution and cementation by large blocky calcite abundant in phylloid algal casts. 3. Styolites, as well as pore filling silica, first appearance in Emerald #1 well.

6631.8   Limestone. Brown, grainstone, well sorted, rounded grains, moderate amount of micrite composing encompassing grains, highly cemented, crinoids and phylloid algal fragments dominate, bivalves, brachiopods, bryozoans, and forams. Most likely intermound grainstone, pyrite present at bottom of slide, no porosity.

No porosity, completely cemented. At least two stages of diagenesis. 1. Abundant micritization of grains and shells. 2. Dissolution and cementation by small blocky calcite cement. Followed by a dissolution event and precipitation of pore and void filling large block calcite. 3. Pyrite evident at bottom of slide, final stage of diagenesis.

6637.8   Limestone. Light brown, grainstone/packstone (top/bottom), coarse grained, well sorted on top half of slide above styolite, dominated by crinoids, bivalves, brachipods, bryozoans, forams, fusulinids, phylloid algal fragments present. Bottom is fine to coarse grained, moderately sorted below styolite. Abundant micrite, dominated by forams and less crinoids, bivalves, brachiopods, bryozoans, fusulinids, phylloid algal fragments, sponge spicules. Pyrite abundant at bottom of slide, estimated 10% porosity.

Dominated by solution enhanced interparticle porosity. Small amounts of moldic and intraparticle porosity present. At least two stages of diagenesis visible, most likely three. 1. Abundant micritization of grains, shells, and matrix, especially in bottom half. 2. At least two stages of dissolution occurring before and after cementation of calcite, small blocky to medium grained cement. 3. Styolites and pyrite growth, possible silica on right side of slide.

6645.9   Limestone. Gray to tan, grainstone/packstone, difficult to determine due to amount of dissolution and cementation, moderate to good sorting, micritized grains and shells, possible non-skeletal grains (peloids), dominated by forams and phylloid algal fragments, bivalves, brachiopods, crinoids, fusulinids, sponge spicules, estimated 3-5% porosity.

Solution enhanced interparticle porosity, moldic, cement reduced moldic, and cement reduced fracture porosity (in order of abundance). At least two stages of porosity. 1. Micritization of grains and shells. 2. At least two stages of dissolution and cementation by calcite, first by small blocky calcite followed by large blocky calcite cementation. Followed by final dissolution stage creating present porosity.

6649.8   Limestone. Gray to tan, grainstone, moderate to poor sorting, well rounded to angular grains and shells, highly micritized, dominated by forams and fusulinids, bivalves, brachiopods, crinoids, phylloid algal fragments, sponge spicules. Possible non-skeletal grains (peloids). Definable boundary between leached porosity and no porosity near bottom of slide, no difference in fossils or sorting, estimated 15% porosity.

Solution enhanced interparticle and intraparticle porosity (in order of abundance). Unusual boundary near bottom which divides porous to non-porous zone. At least two stages of diagenesis. 1. Abundant micritization of grains, shells, and matrix. 2. Dissolution and cementation by small blocky calcite and large pore filling blocky calcite. Dissolution final stage of diagenesis resulting in dissolution of most calcite cement.

6654.6   Limestone. Light gray to light tan, packstone, poorly sorted, well rounded to angular grains and shells, micritized grains and shells, dominated by forams, bivalves, brachiopods, crinoids, fusulinids, phylloid algal fragments, sponge spicules all common to abundant. No porosity, same type of rock as 6649.8 ft.

No porosity, completely cemented. At least two stages of diagenesis. 1. Abundant micritization of grains and shells. 2. Cementation by small blocky calcite and larger blocky calcite. Appears that there may be a dissolution stage between the two stages of cementation.

6656.6   Limestone. Gray, light brown, automicrite, mottled, highly micritic, bivalves, brachiopods, bryozoans, crinoids, forams, fusulinids, phylloid algae, sponge spicules all present, estimated 3-5% porosity.

Solution enhanced intramatrix, intraparticle, and moldic porosity (in order of abundance). At least two stages of diagenesis. 1. Micritization of present grains and shells. 2. Dissolution of grains and shells and recrystalization by calcite cement. Difficult to identify more than one

type of calcite cement. Small amount of prismatic calcite cement in brachiopods.

6668.6   Limestone. Light brown, tan, gray, automicrite, dominated by micritic matrix, present shells and grains, composed of bivalves, brachiopods, other grains and fragments, dissolved crinoids, phylloid algae, and sponge spicules, estimated 15% porosity.

Solution enhanced moldic porosity forming into vugs, intramatrix porosity (in order of abundance). Two stages of diagenesis possible. 1. Difficult to see, however some grains have been micritized. 2. Abundant dissolution of shells and large grains and fragments. Small amount of calcite cement filling voids. Abundant micrite, almost all fossils dissolved.

6675.5   Limestone. Gray to light brown, automicrite, moderately sorted, fine grained, highly micritic, forams and bivalves abundant, brachiopods, crinoids, gastropods, bryozoans, phylloid algae and sponge spicules (often replaced or dissolved), estimated 20% porosity.

Solution enhanced vuggy to cavernous porosity, moldic, intramatrix (in order of abundance). At least two stages of diagenesis visible. 1. Micritization of grains and shells. 2. Dissolution of grains and shells and replacement and cementation by small blocky calcite. 3. Styolites and pyrite present along styolites as well as abundant dissolution of large and small shells, probably dissolved calcite which had filled voids.

6676.6   Limestone. Light gray, brown, automicrite, moderately sorted, fine grained with exception of coral and fusulinids, highly micritic, bivalves, brachiopods, bryozoans, crinoids, forams, fusulinids, phylloid algae, sponge spicules, estimated 3-5% porosity.

Solution enhanced intramatrix, moldic, and intraparticle porosity (in order of abundance). At least two stages of diagenesis visible. 1. Micritization of grains and shells. 2. Dissolution and cementation by small blocky calcite followed by possible dissolution and cementation by large blocky calcite. Dissolution is responsible for porosity.

6679.3   Limestone. Tan, gray, packstone, 50/50 micritic matrix/shells and grains. Well sorted, medium sized grains dominate, bivalves, brachiopods, crinoids, corals, forams, phylloid algal fragments, sponge spicules, estimated 3-4% porosity.

Solution enhanced intraparticle, intramatrix, and moldic porosity (in order of abundance). Appears to be two stages of diagenesis. 1. Micritization of matrix and possibly grains, however it is not common. 2. Replacement of grains and shells by calcite. Dissolution and precipitation of small blocky calcite cement visible in places.

6684.4 Limestone. Gray, brown, automicrite, well sorted, sub-angular to rounded grains 10-15%, forams and crinoids most abundant, bivalves, brachiopods, gastropods, possible dissolved phylloid algae, sponge spicules (dissolved). Highly micritic, estimated 17% porosity.

Solution enhanced moldic to vuggy porosity and intramatrix porosity (in order of abundance). Appears to be at least two stages of diagenesis. 1. Micritization of matrix and grains, however most grains are now dissolved. 2. Possible selective replacement of grains by calcite cement followed by abundant dissolution and minor amounts of pore filling cement by blocky calcite. Solution enhanced moldic pores turning to vugs prominent.

6694.7 Limestone. Light tan to gray, automicrite, moderate sorting, angular to round grains, 15-20% grains, bivalves, brachiopods, crinoids, forams, phylloid algae (dissolved or replaced), sponge spicules (dissolved or replaced). Highly micritic, with vertical fractures that have been partially filled by calcite cement, estimated 5% porosity.

Solution enhanced intramatrix, moldic to vuggy in places, and fracture porosity (in order of abundance). Appears to be at least two stages of diagenesis. 1. Micritization of selective grains and shells as well as matrix. 2. Dissolution and replacement of selective grains and shells by calcite cement followed by large dissolution event resulting in many shells dissolved. Pore filling large blocky calcite cement abundant in pores and fractures.

6699.4 Limestone. Gray, grainstone, well sorted, coarse grained, inner mound fill grainstone. Composed of skeletal and possible non-skeletal grains (peloids and clasts), dominated by phylloid algal fragments and forams, brachiopods, crinoids, and fusulinids common. Highly cemented, more porosity near top of slide, estimated 5-7% porosity.

Solution enhanced interparticle and rare intraparticle. Appears to be at least two stages of diagenesis. 1. Abundant micritization of grains and shells. 2. Abundant dissolution and replacement by small blocky calcite cement. Second phase of dissolution (large scale) and pore filling as well

as replacing large blocky calcite. Top of slide contains more interparticle porosity than bottom, most likely due to fresh water leaching.

6700.5   Limestone. Dark gray to brown, stained, automicrite, moderate to well sorted, fine grained with exception of large brachiopods shells, skeletal and possible non-skeletal grains (peloids), highly micritic, bivalves, brachiopods, bryozoans, crinoids, forams, phylloid algae, sponge spicules (dissolved or replaced), and trilobite shells, estimated 3% porosity.

Solution enhanced intramatrix, moldic, and fracture porosity (in order of abundance). At least three stages of diagenesis. 1. Selective micritization of grains and shells. 2. Dissolution and replacement by small blocky calcite cement followed by possible dissolution and growth of large blocky calcite cement which filled pores and fractures. 3. Pressure dissolution and formation of styolites (not dissolved) with leaching of cement. Small amounts of porosity associated with styolites.

6703.6   Limestone. Gray to tan, automicrite, poorly sorted, bivalves, brachiopods, crinoids, echnoids, forams, fusulinids, phylloid algae, and sponge spicules all common to abundant. Pyrite and saddle dolomite common, estimated 10-12 % porosity.

Solution enhanced intramatrix and moldic porosity, both turning to vuggy porosity commonly. At least three stages of diagenesis. 1. Selective micritization of grains and shells. 2. Dissolution and replacement of grains and shells by small blocky calcite cement. Followed by dissolution and replacement by large blocky calcite cement. 3. Styolites, pyrite, and saddle dolomite become present. Pyrite and saddle dolomite common to abundant. Saddle dolomite seems to be filling open pores and possibly replacing large calcite crystals.

6712.2   Limestone. Brown to dark gray, packstone to grainstone, moderate to well sorted, medium to coarse grained, skeletal and possible non-skeletal grains (peloids), abundant phylloid algae and forams, bivalves, brachiopods, crinoids, fusulinids, sponge spicules common to abundant. Appears to be a possible thalli or phylloid algal cup that is holding a foram rich grainstone matrix with noticeable differences in micritic matrix. Above and below cup the thin section becomes moderately sorted with a higher micritic matrix content, no porosity

No porosity. Appears to be at least two stages of diagenesis. 1. Selective micritization of grains and shells. 2. Dissolution and replacement of grains and shells by calcite cement as well as pore filling

small blocky calcite cement. Second stage of possible dissolution and filling of pores by large blocky calcite cement.

6717.4 Limestone. Tan, grainstone, well sorted, sub-rounded, fine to medium grained, composed of skeletal and possible non-skeletal grains (peloids), similar to very fine grained highly micritized forams. Grains are 90% forams, bivalves, brachiopods, fusulinids, phylloid algal fragments, and sponge spicules all common. Possible bedding which houses large fusulinids and phylloid algal fragments near top of slide, estimated 5-7% porosity, mainly on top half of slide.

Solution enhanced interparticle, moldic, and intraparticle (in order of abundance, interparticle dominates). Appears to be at least three stages of diagenesis. 1. Selective micritization of grains and shells. 2. At least one stage of dissolution and replacement of grains and shells as well as pores by small blocky calcite. Possible second stage which precipitated larger blocky calcite. 3. Leaching and small amount of saddle dolomite being precipitated in open pore spaces.

6718.5 Limestone. Tan, grainstone to packstone, well sorted, fine to medium grained, skeletal and possible non-skeletal grains (peloids). Dominated (80-90%) by forams, bivalves, brachiopods, fusulinids, phylloid algal fragments, and sponge spicules all common. No bedding present, less porosity than 6717.4, estimated 1-2% porosity.

Small amount of interparticle porosity. Appears to be 2 stages of diagenesis. 1. Selective abundant micritization of grains, shells, and possibly matrix. 2. At least on stage of dissolution and replacement by small blocky calcite. No large dissolution pores as in 6717.4 ft. or saddle dolomite.

6726.8 Limestone. Dark gray, automicrite, moderate to poor sorting, highly micritic, most grains and shells have been dissolved and replaced by calcite cement. Bivalves, brachiopods, crinoids, forams, phylloid algae (dissolved), sponge spicules. Different type of phylloid algae. Noted. No porosity.

No porosity. Appears to be at least two stages of diagenesis. 1. Selective micritization of grains, shells, and possibly matrix. 2. Dissolution and cementation by small blocky calcite cement, followed by possible dissolution and cementation by large blocky calcite cement. May be small pyrite crystals.

6736.8   Limestone. Gray, automicrite, poorly sorted, angular to round grains, fine to coarse grained, highly micritic, abundant diagenesis. Bivalves, brachiopods, crinoids, forams, fusulinids, phylloid algae, sponge spicules, and possible peloids, estimated 10-15% porosity. Poorly sorted, conglomeritic.

                Solution enhanced intramatrix and moldic porosity, both types commonly vuggy throughout slide (in order of abundance). Appears to be at least three stages of diagenesis. 1. Abundant selective micritization of grains, shells, and matrix throughout slide. 2. At least two stages of dissolution and cementation by small and large blocky calcite cement. 3. Styolites present, as well as saddle dolomite, pyrite, and silica present. Porosity is a result of final stage of dissolution. Porosity is associated with styolites.

6742.7   Limestone. Gray, automicrite, moderately sorted, fine to coarse grained, skeletal and non-skeletal grains (peloids). Bivalves, brachiopods, crinoids, forams, fusulinids, phylloid algae, and sponge spicules. Highly micritic. No accessory minerals such as those from 6736.8 ft. Compartmentalized, estimated 20-25% porosity.

                Solution enhanced intramatrix and moldic porosity, both types commonly vuggy throughout slide (in order of abundance). Appears to be at least two stages of diagenesis. 1. Selective abundant micritization of grains, shells, and possibly matrix. 2. At least one stage of dissolution and recrystalization by calcite cement. No saddle dolomite, silica, pyrite or styolites. However, final stage of dissolution has created a large amount of porosity.

6758.4   Limestone. Gray to light tan, automicrite, poorly sorted, fine to coarse grained, skeletal and non-skeletal grains (peloids and clasts). Bivalves, brachiopods, crinoids, forams, fusulinids, phylloid algae, and sponge spicules, estimated 15-20% porosity.

                Solution enhanced intramatrix and moldic porosity, both commonly vuggy throughout slide (in order of abundance). Appears to be at least three stages of diagenesis. 1. Abundant selective micritization of grains, shells, and possibly matrix. 2. At least two stages of dissolution and cementation by small and large blocky calcite cement. 3. Abundant dissolution and saddle dolomite growth. Appears to be pore filling as well as replacing large calcite crystals.

Thin Section Description
Parallel Petroleum
Jade #1
Diamond M Field
Scurry County, Texas

Depth (ft.)	Description

6747.6   Limestone. Gray, dark gray, brown, automicrite, poorly sorted, fine to coarse grained, bivalves, brachiopods, crinoids, forams, fusulinids, gastropods, phylloid algae (dissolved and replaced), and sponge spicules, highly micritic, estimated 5-7% porosity.

                Solution enhanced intramatrix and moldic porosity (in order of abundance). Appears to be at least three stages of diagenesis. 1. Abundant selective micritization of grains, shells, and matrix. 2. Two stages of dissolution and cementation by small and large blocky calcite cement respectively. 3. Styolites accompanied by the growth of pore filling and replacing saddle dolomite as well as silica. Small amount of porosity associated with styolites.

6767.5   Limestone. Tan to light brown, grainstone/automicritic layers. Top and bottom of slide contain a well sorted, medium grained foram rich grainstone. Middle of slide is composed of a moderately sorted fossiliferous automicrite. Bivalves, brachiopods, crinoids, forams, phylloid algae (dissolved), and sponge spicules are all present below top grainstone layer. Appears to be an erosional surface between top grainstone and automicrite. A large styolite forms the boundary between the automicrite and the lower grainstone. Automicrite may be a large clast that was shed during a erosional event. Entire slide is highly micritized, estimated 15-25% porosity.

                Solution enhanced interparticle and intramatrix, moldic, and intraparticle porosity (in order of abundance). Some interparticle and moldic porosity transforming into vuggy porosity. At least three stages of diagenesis. 1. Abundant selective micritization of shells, grains, and matrix. 2. At least two episodes of dissolution and precipitation of small and large blocky calcite cement respectively. 3. Styolites and formation of abundant pore filling and calcite replacing saddle dolomite. Linear dissolution porosity associated within styolites.

6769.3   Limestone. Tan, grainstone, well sorted, fine grained, dominated by forams, bivalves, brachiopods, crinoids, phylloid algal fragments

(dissolved), sponge spicules, possible non-skeletal peloids, less than 1% porosity.

Small amount of interparticle and intraparticle porosity. Appears to be at least two stages of diagenesis. 1. Abundant micritization of grains and shells. 2. Two stages of dissolution and cementation, first by small blocky calcite, second, by large pore filling blocky calcite.

6771.9   Limestone. Tan, wackestone/automicrite, poorly sorted, fine to coarse grained, skeletal and non-skeletal grains (peloids) present, highly micritic, bivalves, brachiopods, crinoids, forams, gastropods, phylloid algae (dissolved and replaced), and sponge spicules, estimated 10-12% porosity.

Solution enhanced intramatrix and moldic porosity (in order of abundance), both turning to vuggy porosity commonly. At least three stages of diagenesis. 1. Abundant selective micritization of grains, shells, and possibly matrix. 2. At least two stages of dissolution and cementation, first by small blocky calcite, second, by large pore filling blocky calcite. 3. Precipitation of pore filling as well as calcite replacing saddle dolomite.

6784.4   Limestone. Light tan to light gray, automicrite, moderately sorted, highly micritic. Bivalves, brachiopods, bryozoans, crinoids, forams, fusulinids, gastropods, phylloid algal fragments (dissolved), and sponge spicules. Estimated 7 % porosity.

Solution enhanced intramatrix, moldic, and fracture porosity (in order of abundance). Interparticle and moldic porosity transforming to vuggy in places. At least three stages of diagenesis. 1. Abundant selective micritization of grains, shells, and possibly matrix. 2. At least two stages of dissolution and cementation, first by small blocky calcite, second, by large pore filling blocky calcite. 3. Styolites and precipitation of pore filling as well as calcite replacing saddle dolomite.

6785.5   Limestone. Tan, packestone, moderate to well sorted, composed of skeletal and non-skeletal grains (peloids). Bivalves, brachiopods, crinoids, echnoids, forams, phylloid algal fragments (dissolved), and sponge spicules. Interpreted as inner mound fill, estimated 15% porosity.

Solution enhanced moldic and intramatrix porosity dominate. Intraparticle porosity present. At least three stages of diagenesis. 1. Abundant selective micritization of grains, shells, and possibly matrix. 2. At least two stages of dissolution and cementation, first by small blocky

calcite, second, by large pore filling blocky calcite. 3. Precipitation of calcite replacing saddle dolomite.

6795.2   Limestone. Tan, packstone, moderately sorted, composed of skeletal grains and non-skeletal grains (peloids). Bivalves, brachiopods, crinoids, echnoids, forams, phylloid algal fragments (dissolved), and sponge spicules. Inner mound fill packstone, estimated 5-7% porosity.

Solution enhanced intramatrix and moldic porosity. Appears to be three stages of diagenesis. 1. Abundant selective micritization of grains, shells, and possibly matrix. 2. At least two stages of dissolution and cementation, first by small blocky calcite, second, by large pore filling blocky calcite. 3. Possible precipitation of calcite replacing saddle dolomite.

6799.9   Limestone. Tan, grainstone, well sorted, coarse grained, phylloid algal fragments. Occasional forams and gastropods. Well cemented, possible oil staining, estimated 10-15% porosity.

Solution enhanced interparticle, intercrystalline, and moldic porosity (in order of abundance). Interparticle and intercrystalline turning to vuggy often. At least three stages of diagenesis. 1. Abundant micritization of shells, grains, and phylloid algae rims. 2. At least two stages of dissolution and cementation, first by small blocky calcite, second, by large pore filling blocky calcite. Second stage dominates, most likely occurred after erosion and shedding of algal fragments. 3. Saddle dolomite replacement of selective large calcite grains.

6805.9   Limestone. Tan to light gray, grainstone/packstone, moderate sorting, dominated by forams and phylloid algae (dissolved and replaced). Highly micritized grains and shells. Some non-skeletal grains (peloids). Bivalves, brachiopods, crinoids, forams, phylloid algal fragments, and sponge spicules, estimated 7% porosity.

Solution enhanced interparticle and moldic porosity as well as vuggy porosity. Appears to be at least two stages of diagenesis. 1. Abundant micritization of shells and grains. 2. At least two stages of dissolution and cementation, first by small blocky calcite, second, by large pore or void filling calcite cement. Does not appear to be any major saddle dolomite, however some small grains exhibit sweeping extinction.

6811.5   Limestone. Tan, grainstone, well to moderate sorting, dominated by forams (75%), bivalves, brachiopods, crinoids, gastropods, phylloid algal

fragments, and sponge spicules common. Grains and shells micritized, estimated 3-5% porosity.

Solution enhanced moldic and interparticle porosity. Appears to be at least two stages of diagenesis. 1. Abundant micritization of shells and grains. 2. At least two stages of dissolution and cementation, first by small blocky calcite, followed by a small amount of remaining large pore or void filling calcite cement. Does not appear to be any major saddle dolomite, however some small grains exhibit sweeping extinction.

6817.9   Limestone. Gray to brown, automicrite, poorly sorted, round to angular grains, highly micritic, 15-20% grains. Bivalves, brachiopods, crinoids, forams, phylloid algae (replaced), and sponge spicules, no porosity.

No porosity. Appears to be at least two stages of diagenesis. 1. Abundant micritization of shells, grains and possibly matrix. 2. At least two stages of dissolution and cementation, first by small blocky calcite, second, by large pore or void filling calcite cement. Evident in many phylloid algal filled molds.

6822.8   Limestone. Gray to light gray, automicrite but may be a higher energy wackestone to packstone. Poorly sorted, round to angular grains. Bivalves, brachiopods, bryozoans, crinoids, forams, phylloid algae (replaced), and sponge spicules. Abundant micrite, estimated 3-5% porosity.

Solution enhanced moldic and intergranular porosity with occasional vugs. Appears to be at least three stages of diagenesis. 1. Abundant micritization of shells, grains and possibly matrix. 2. At least two stages of dissolution and cementation, first by small blocky calcite, second, by large pore or void filling calcite cement. Evident in many phylloid algal filled molds. 3. Formation of saddle dolomite, both pore filling and replacing. Abundant bubble inclusions.

6823.8   Limestone. Gray, grainstone to automicrite. Appears to be micritic debris surrounded by a foram and phylloid algal rich medium to coarse grained grainstone. Abundant leaching. Poorly sorted, bivalves, brachiopods, crinoids, forams, phylloid algae, and sponge spicules. Highly micritc, estimated 7% porosity.

Solution enhanced intergranular and intramatrix, moldic, and fracture porosity. Appears to be at least three stages of diagenesis. 1. Abundant micritization of shells, grains and possibly matrix. 2. At least two stages of dissolution and cementation, first by small blocky calcite, second, by

large pore or void filling calcite cement. Evident in many phylloid algal filled molds. 3. Formation of saddle dolomite, both pore filling and replacing. Abundant bubble inclusions. Abundant styolites with large amounts of dissolution porosity associated.

6829.9   Limestone. Gray, automicrite, poorly sorted, abundant grains and shells, bivalves, brachiopods, bryozoans, crinoids, forams, fusulinids, gastropods, phylloid algae (replaced), sponge spicules, highly micritic, estimated 20-25% porosity.

Solution enhanced intramatrix, vuggy, and moldic porosity (in order of abundance). Appears to be at least three stages of diagenesis. 1. Abundant micritization of shells, grains and possibly matrix. 2. At least two stages of dissolution and cementation, first by small blocky calcite, second, by large pore or void filling calcite cement. Evident in many phylloid algal filled molds. 3. Formation of pore filling saddle dolomite crystal in middle of slide.

6843.6   Limestone. Gray, automicrite, well sorted, dominated by fine grained forams. Bivalves, brachiopods, crinoids, forams, phylloid algae (dissolved), and sponge spicules. Grains highly micritized, estimated 1-3% porosity.

Minor amounts of solution enhanced moldic and intramatrix porosity. Appears to be two stages of diagenesis. 1. Abundant micritization of grains, shells, and possibly matrix. 2. At least two stages of dissolution and cementation, first by small blocky calcite, second, by large pore or void filling calcite cement. Evident in many phylloid algal filled molds.

6865.5   Limestone. Gray, light gray, light brown, automicritic debris, poorly sorted, clasts, grains, algae, abundant forams, bivalves, brachiopods, bryozoans, crinoids, fusulinids, phylloid algal fragments, and sponge spicules. Abundant micrite, estimated 5-10% porosity.

Solution enhanced intramatrix, vuggy, moldic, and fracture porosity (in order of abundance). Appears to be at least three stages of diagenesis. 1. Abundant micritization of shells, grains and possibly matrix. 2. At least two stages of dissolution and cementation, first by small blocky calcite, second, by large pore or void filling calcite cement. Evident in many phylloid algal filled molds. 3. Formation of saddle dolomite, both pore filling and replacing. Styolites with small amounts of dissolution porosity associated.

6869.9   Limestone. Gray and tan, automicritic debris, poorly sorted, clasts, grains, algae, bivalves, brachiopods, bryozoans, crinoids, forams, phylloid algal fragments, sponge spicules, and abundant saddle dolomite. Estimated 5-7 % porosity.

Solution enhanced intramatrix, moldic, intercrystalline, and fracture porosity (in order of abundance). Appears to be at least three stages of diagenesis. 1. Abundant micritization of shells, grains and possibly matrix. 2. At least two stages of dissolution and cementation, first by small blocky calcite, second, by large pore or void filling calcite cement. Evident in many phylloid algal filled molds. 3. Formation of abundant saddle dolomite, both pore filling and replacing.

THIN SECTION PHOTOS
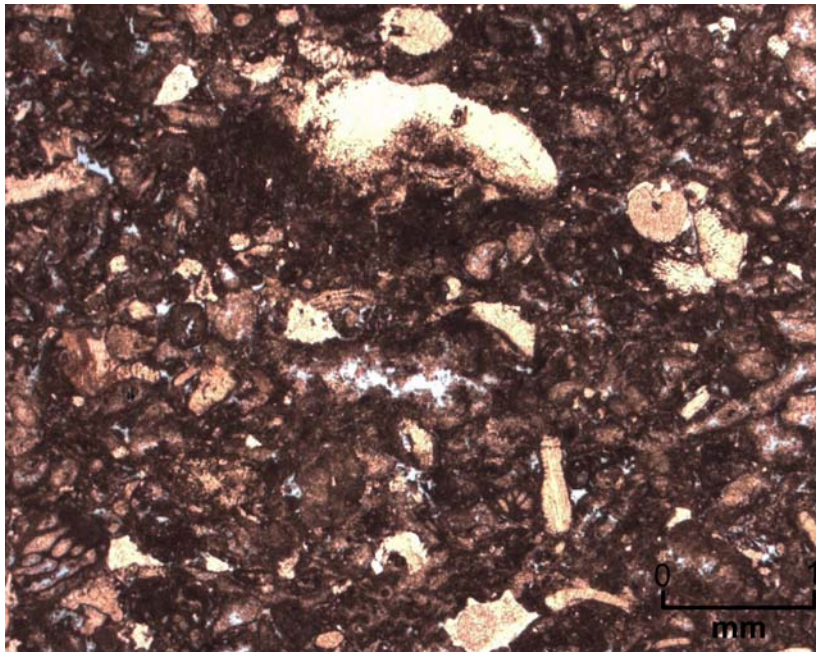
**Figure B-1. Thin section photo from Emerald #1 @ 6,614'
Pore types SEIM and M**
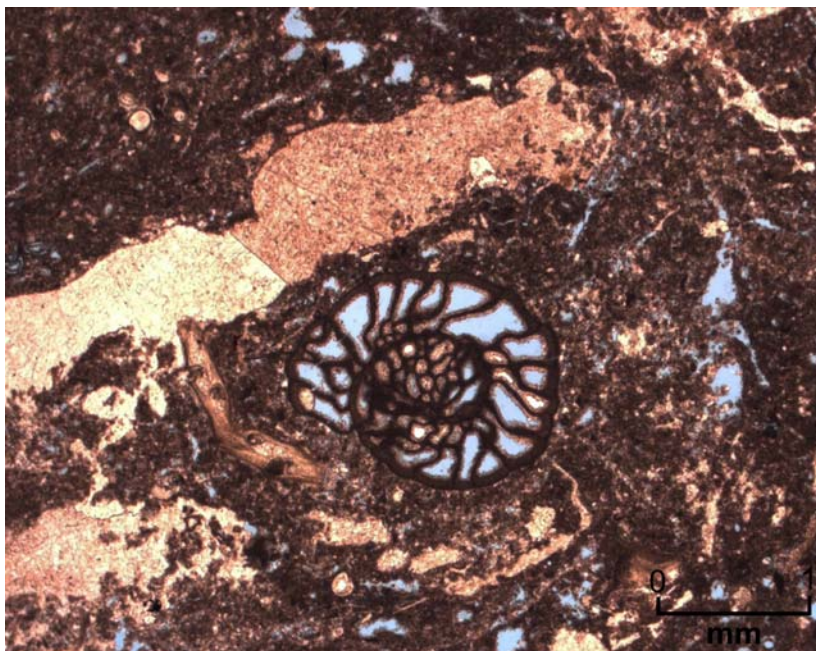
**Figure B-2. Thin section photo from Emerald #1 @ 6,621'
Pore types SEIM, SEIP, and M**
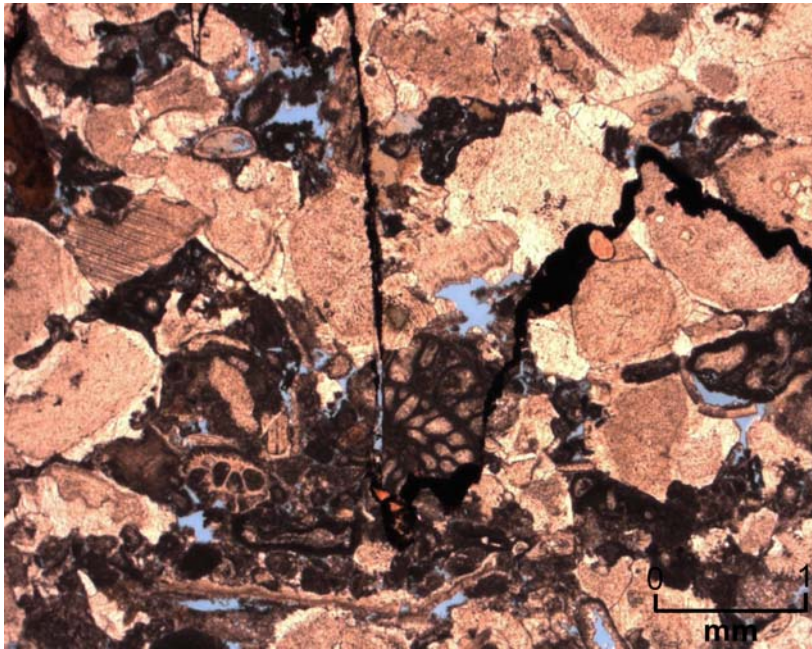
Figure B-3. Thin section photo from Emerald #1 @ 6,637'
Pore types M and SEIM
Crinoid Fragments

Figure B-4. Thin section photo from Emerald #1 @ 6,649'
Pore types M, SEIP, and SEIM
Large Fusulinids
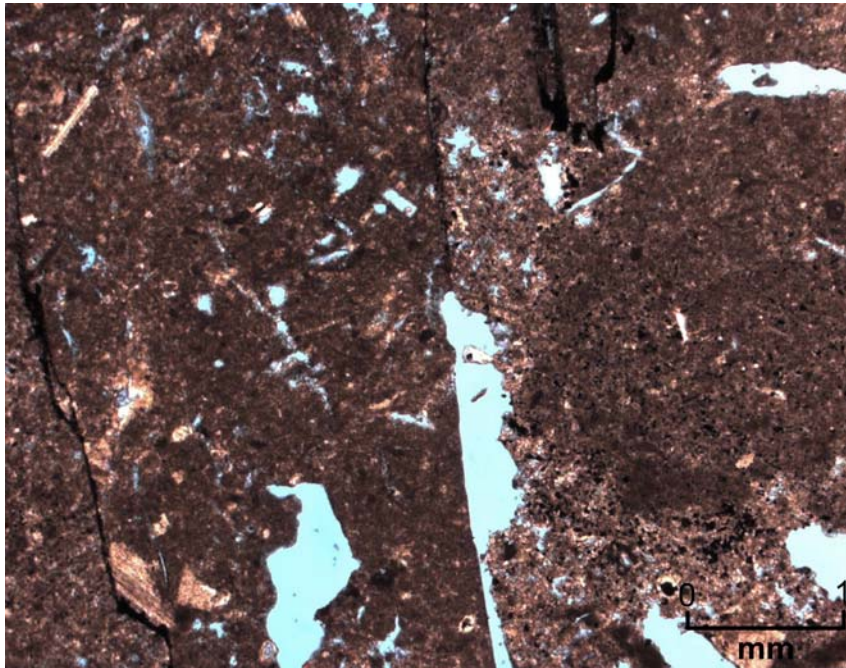
Figure B-5. Thin section photo from Emerald #1 @ 6,675'
Pore types S and M

Figure B-6. Thin section photo from Jade #1 @ 6,799'
Pore types CRIC, M, and SEIP
Phylloid Algal Fragments
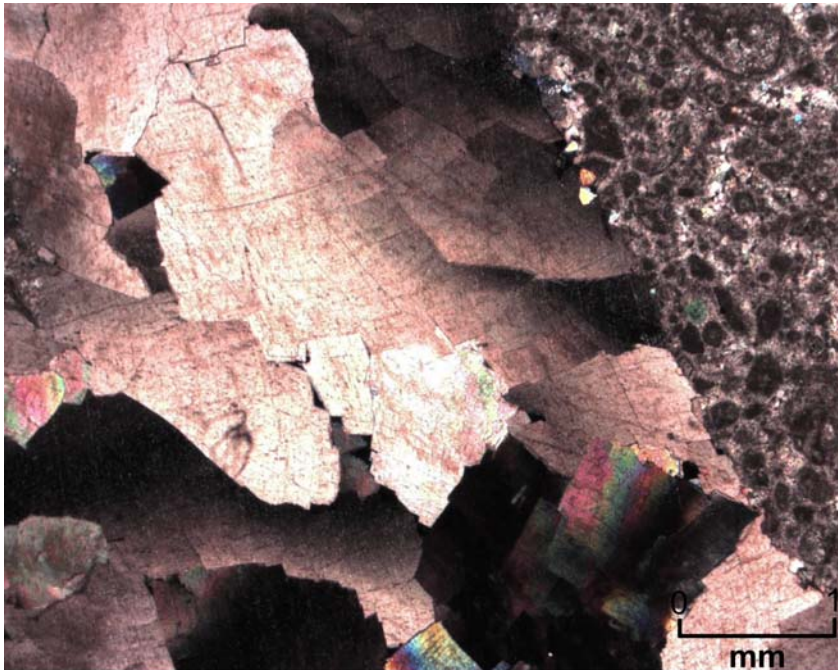
Figure B-7. Thin section photo from Jade #1 @ 6,869'
Saddle Dolomite (Crossed Polars)
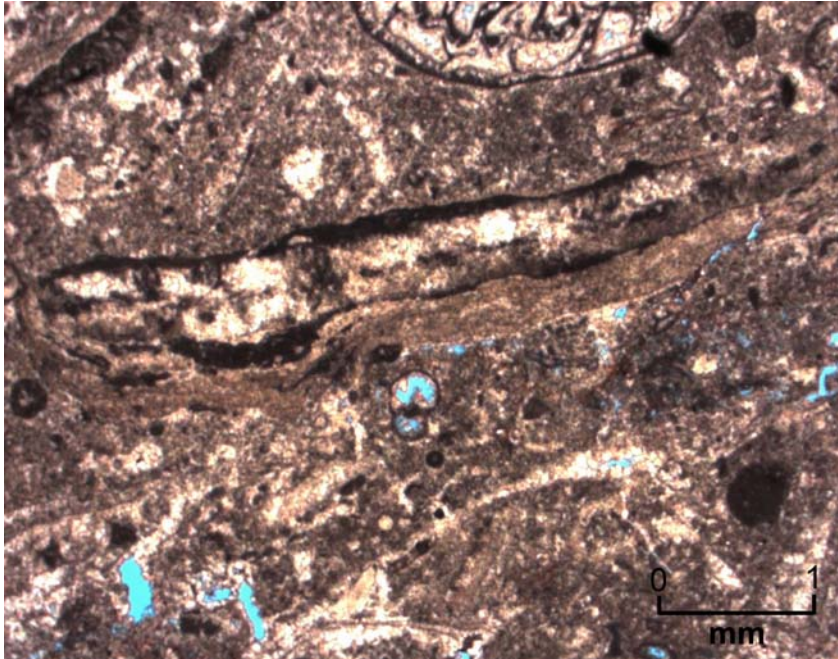
Figure B-8. Thin section photo from Topaz #1 @ 6,713'
Pore types M, SEIM, and SEIP
Phylloid Algal Fragment
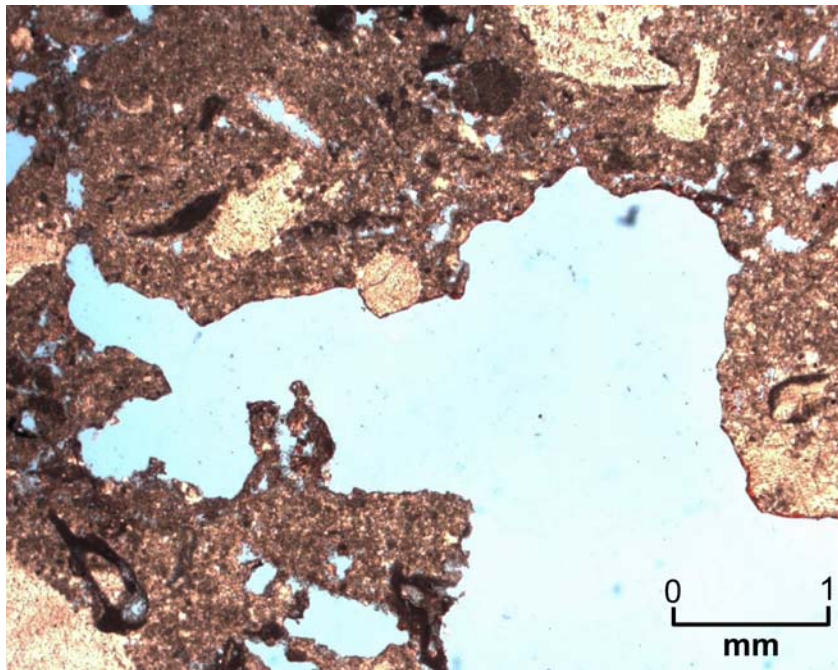
Figure B-9. Thin section photo from Topaz #1 @ 6,713'
Pore types V, M, and SEIM
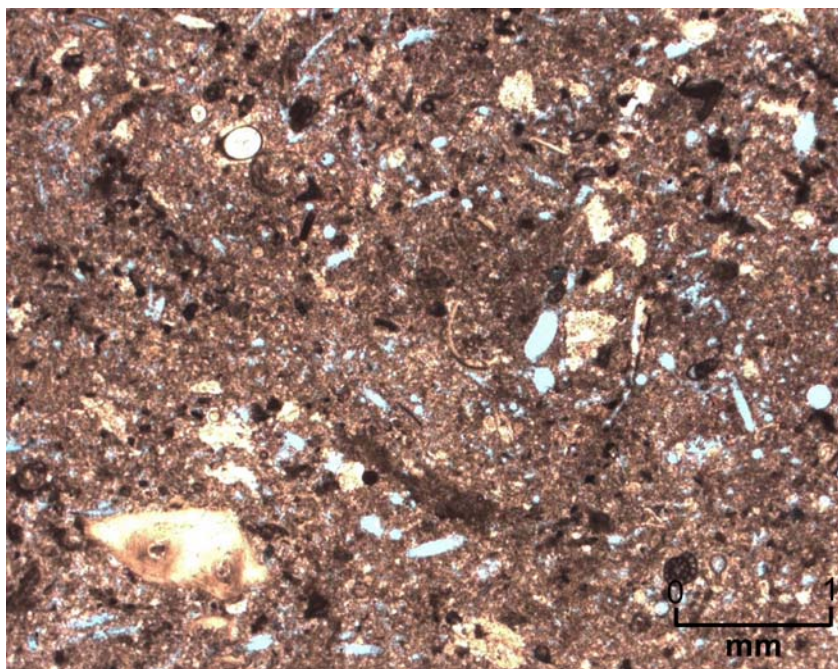
Figure B-10. Thin section photo from Topaz #1 @ 6,751'
Pore types M
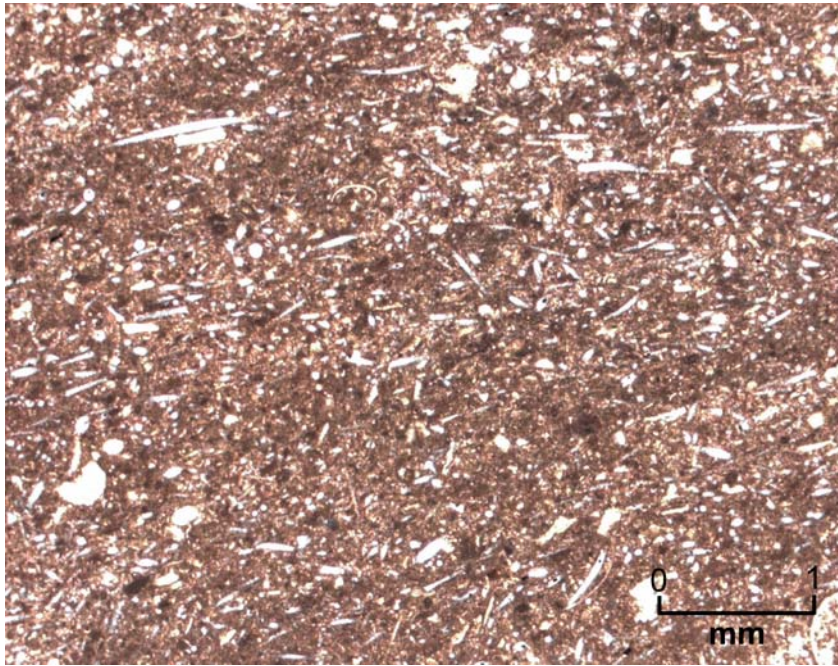
**Figure B-11. Thin section photo from Topaz #1 @ 6,760'
Pore type M**

**Figure B-12. Thin section photo from Topaz #1 @ 6,820'
Large Brachiopod Shell**
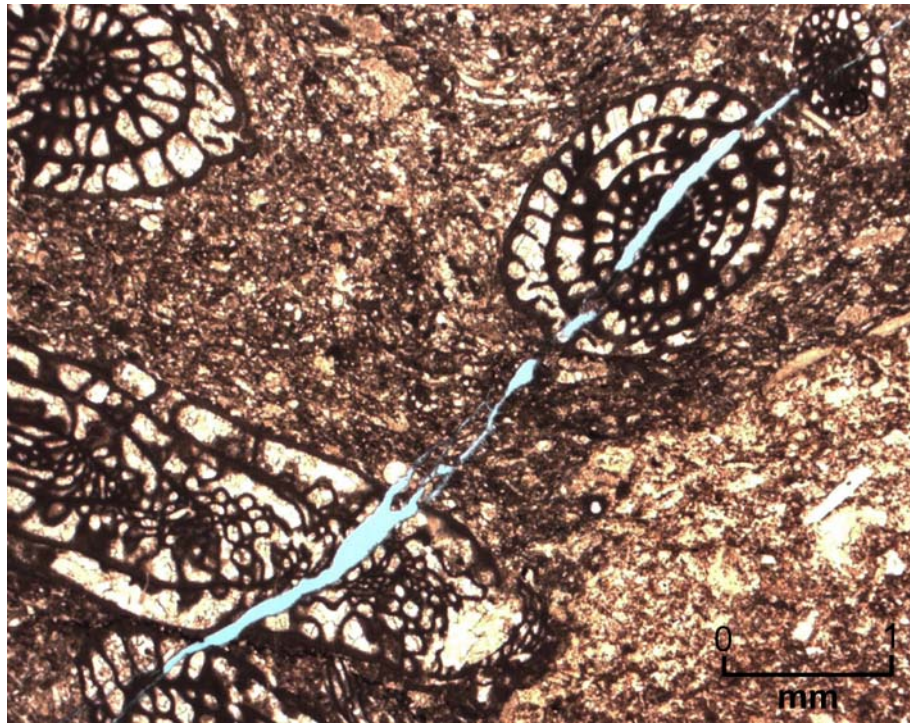
Figure B-13. Thin section photo from Topaz #1 @ 6,832'

APPENDIX C

STRUCTURE, POROSITY, PERMEABILITY AND FLOW UNIT MAPS
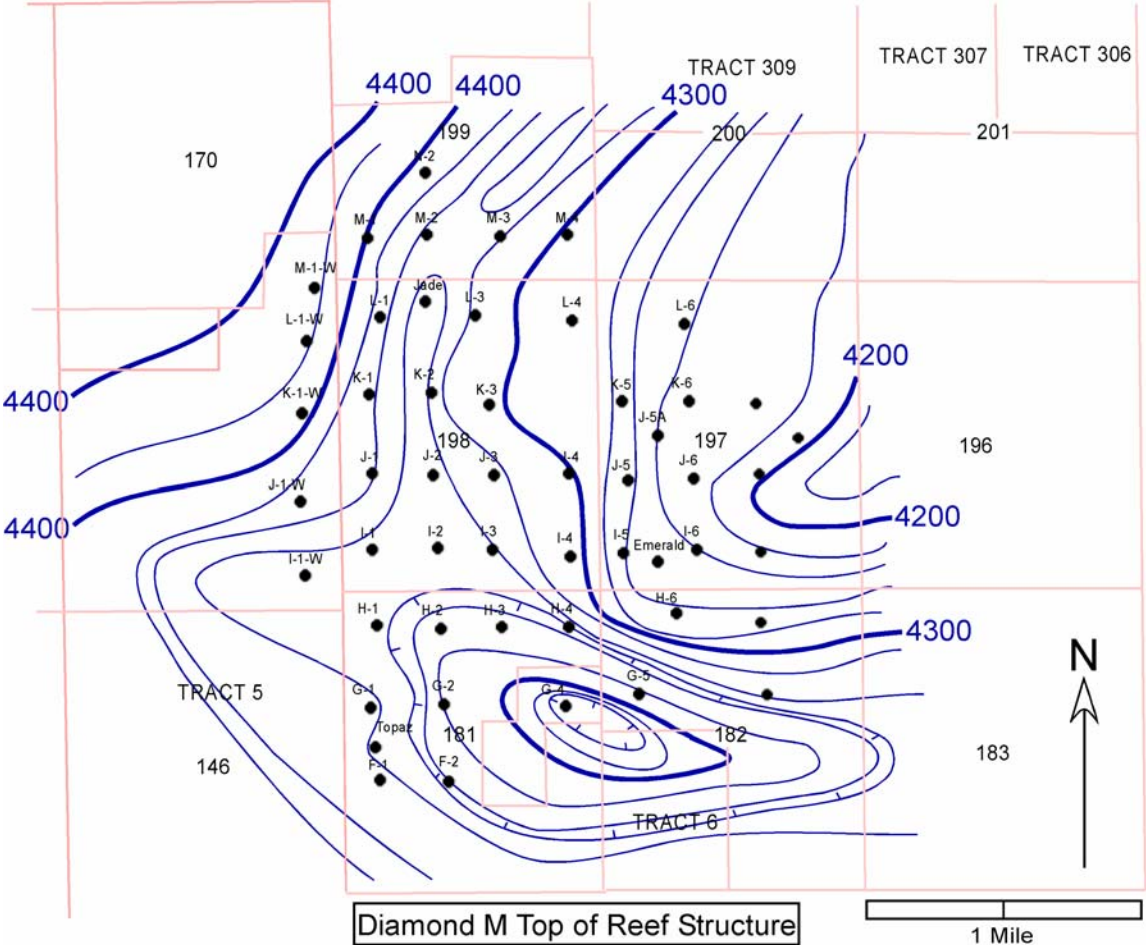
Figure C-1. Diamond M Top of Reef Stucture Map
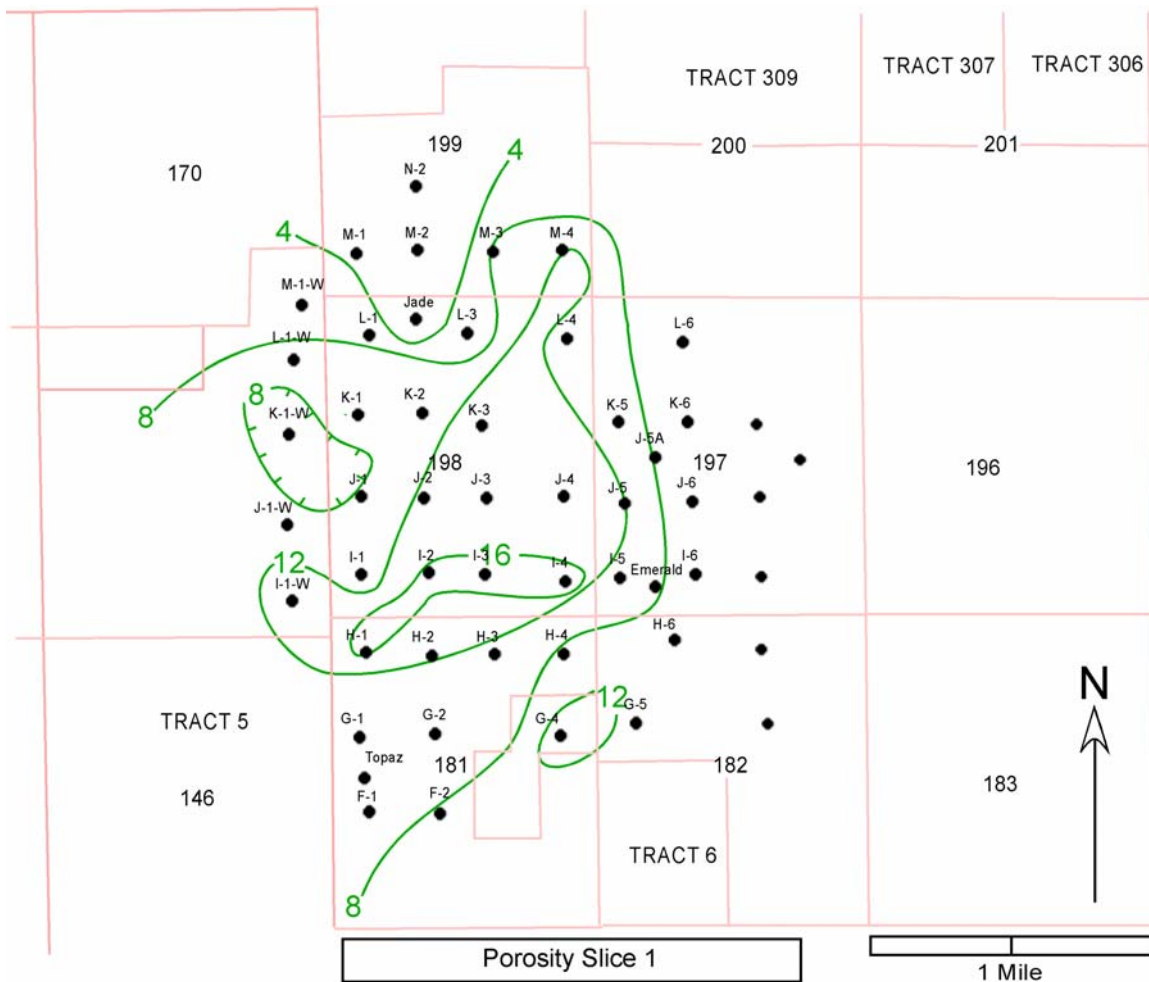
Figure C-2. Diamond M Porosity Slice Map 0 to 10 ft below Top of Reef
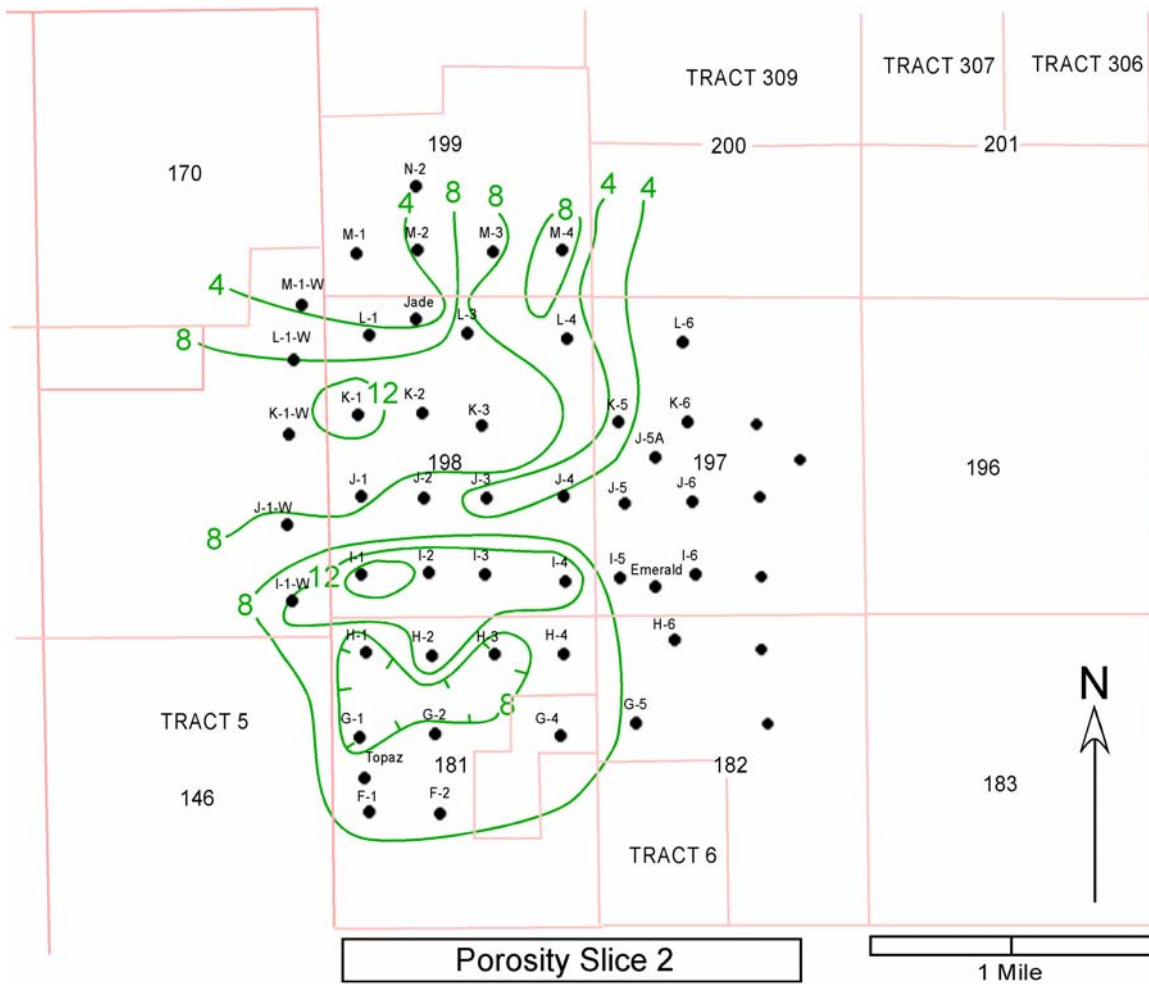
Figure C-3. Diamond M Porosity Slice Map 10 to 20 ft below Top of Reef
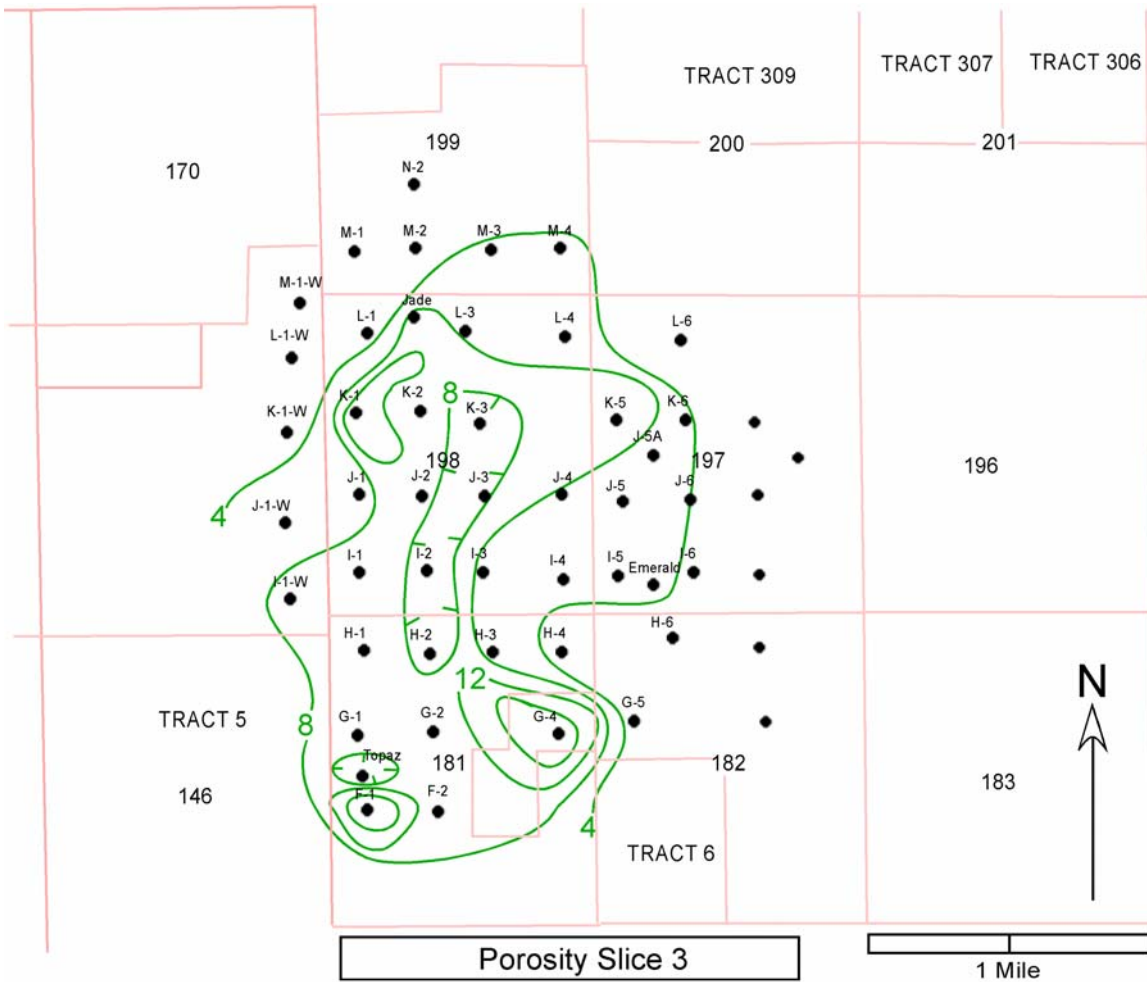
Figure C-4. Diamond M Porosity Slice Map 20 to 30 ft below Top of Reef
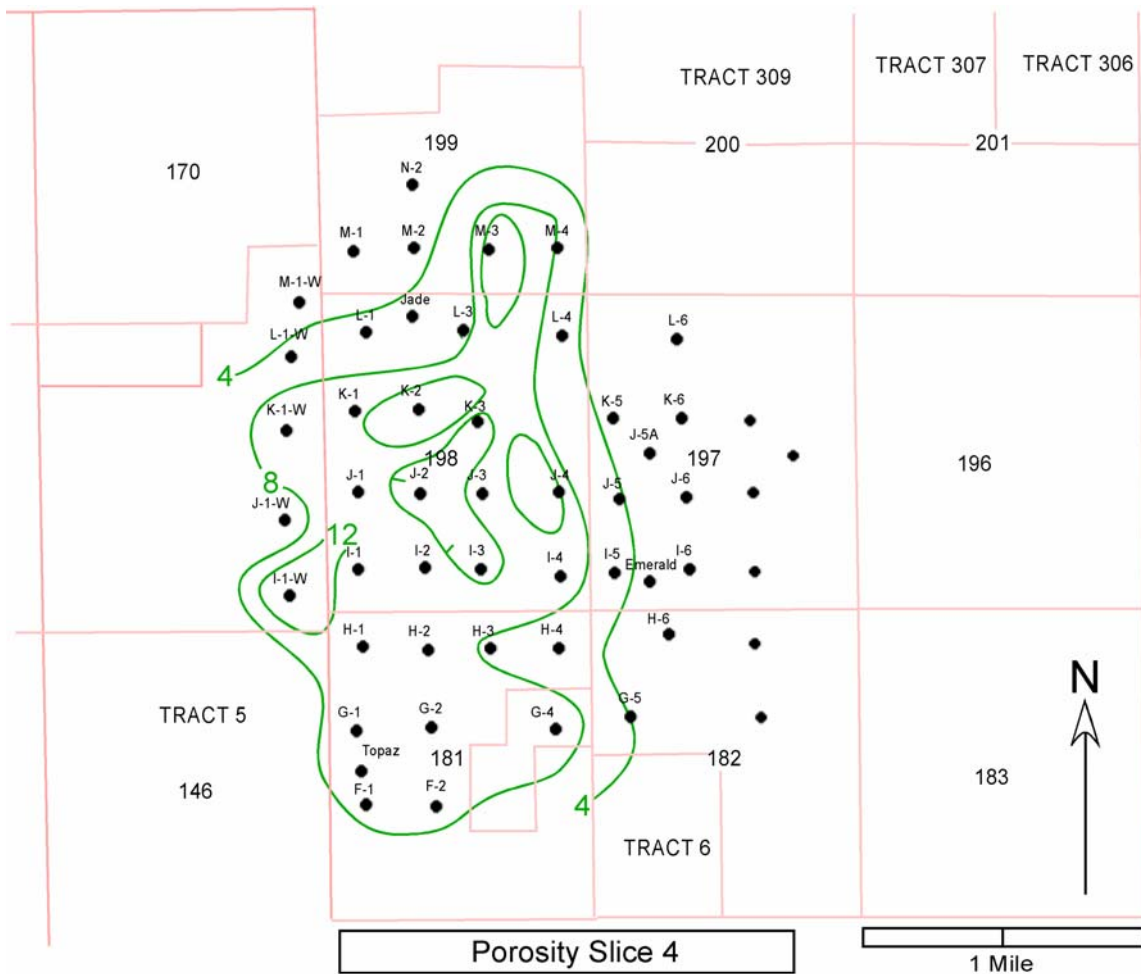
Figure C-5. Diamond M Porosity Slice Map 30 to 40 ft below Top of Reef
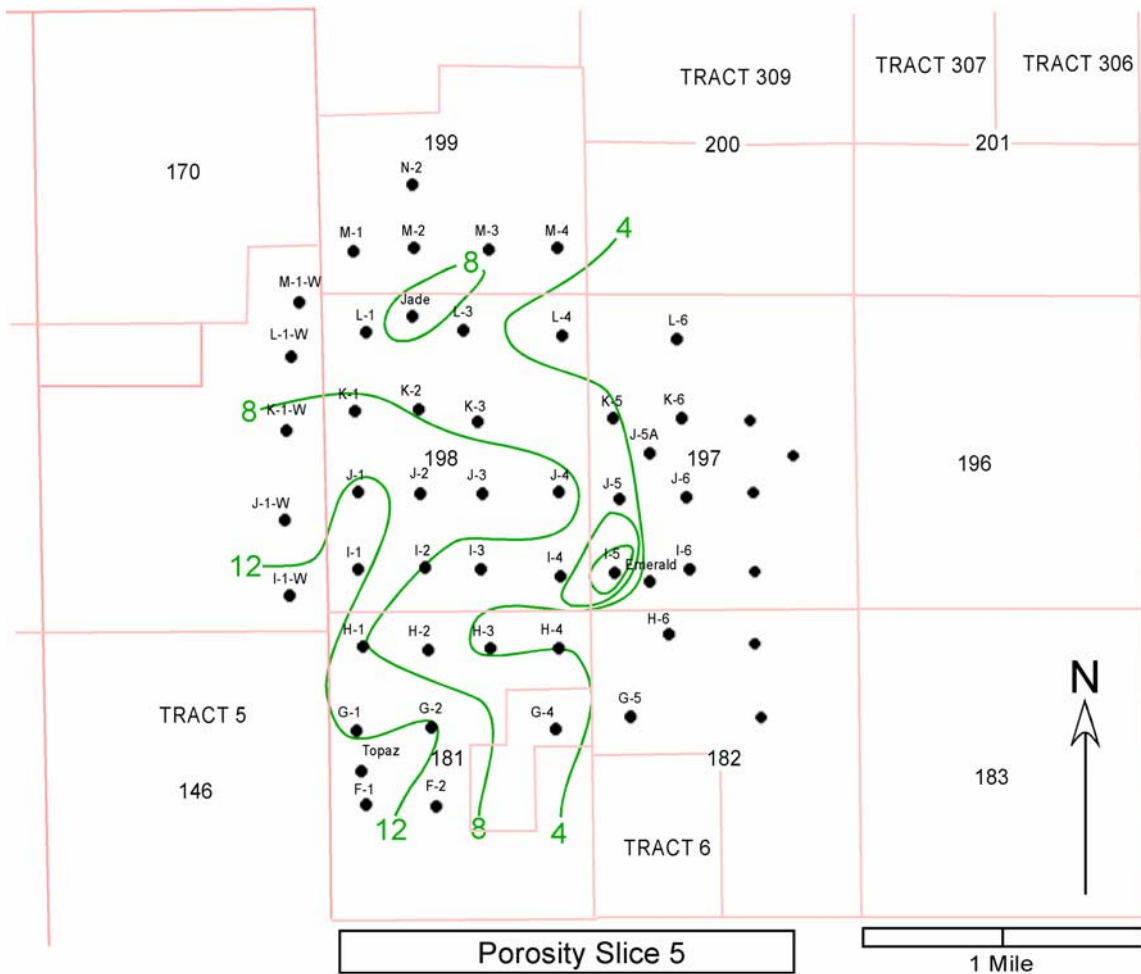
Figure C-6. Diamond M Porosity Slice Map 40 to 50 ft below Top of Reef
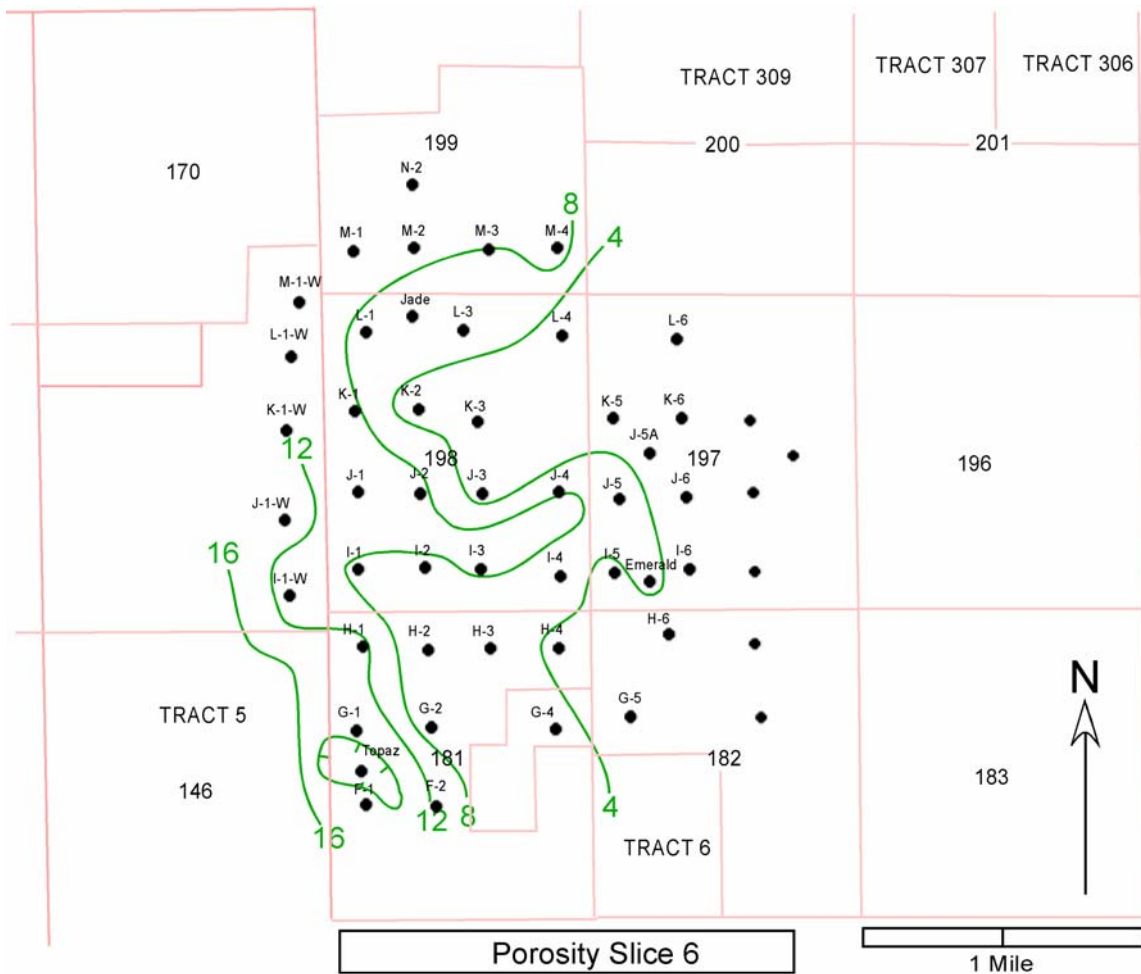
Figure C-7. Diamond M Porosity Slice Map 50 to 60 ft below Top of Reef
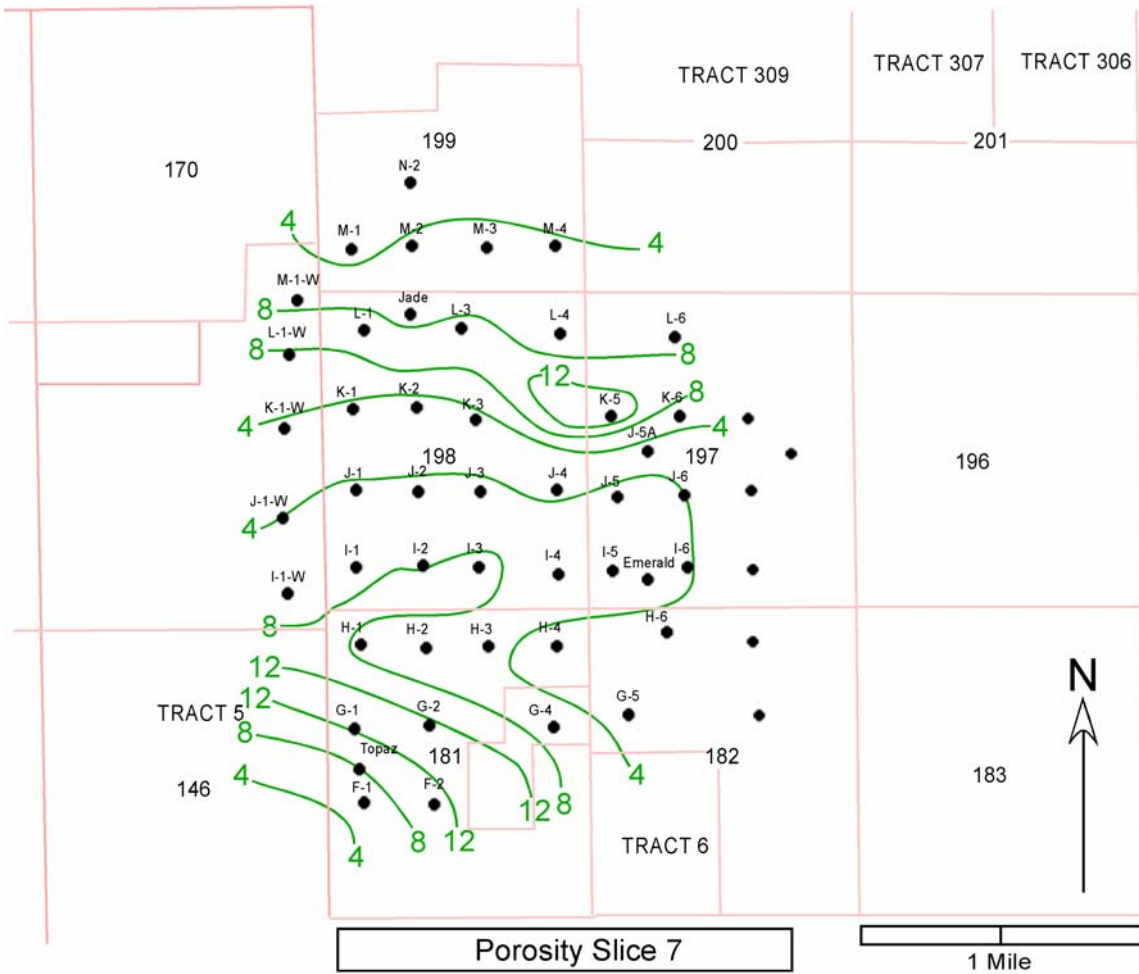
Figure C-8. Diamond M Porosity Slice Map 60 to 70 ft below Top of Reef
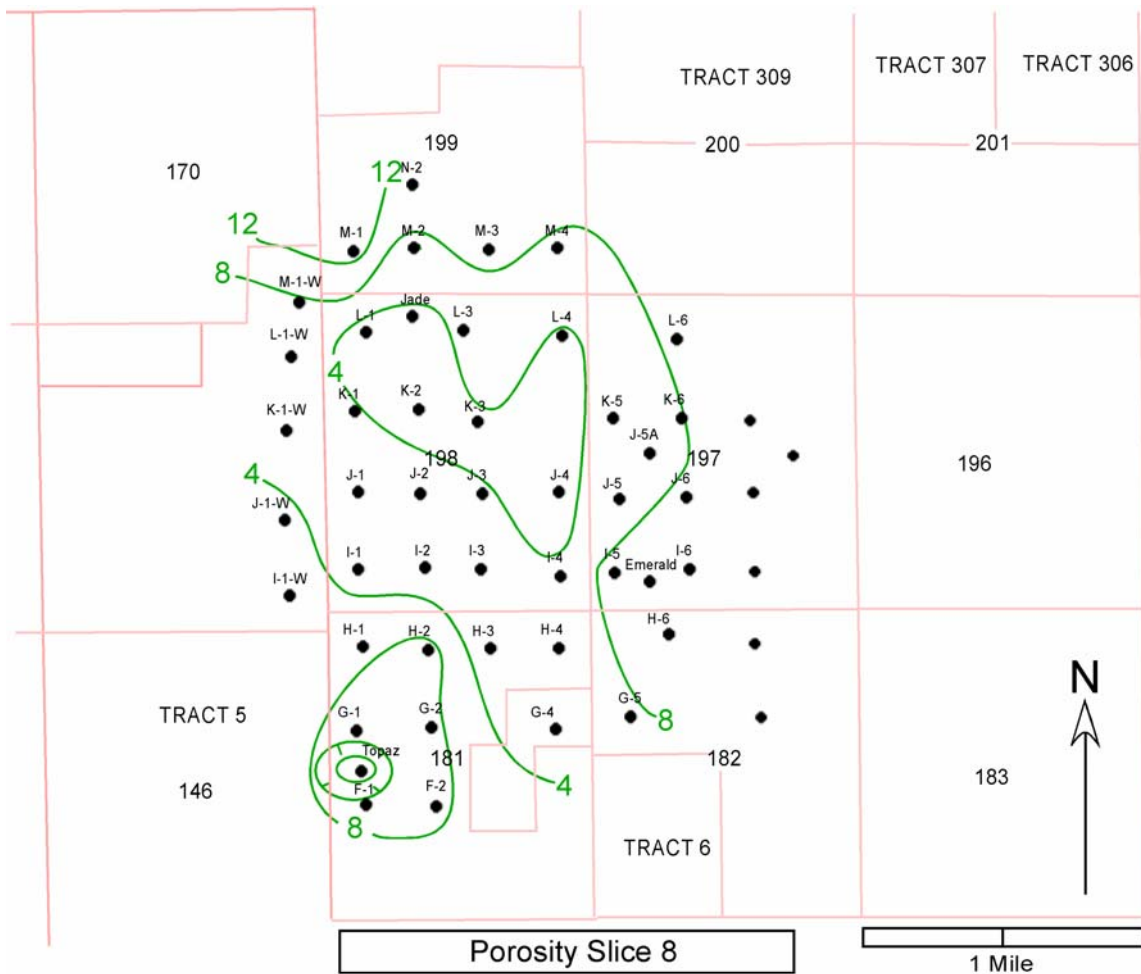
Figure C-9. Diamond M Porosity Slice Map 70 to 80 ft below Top of Reef
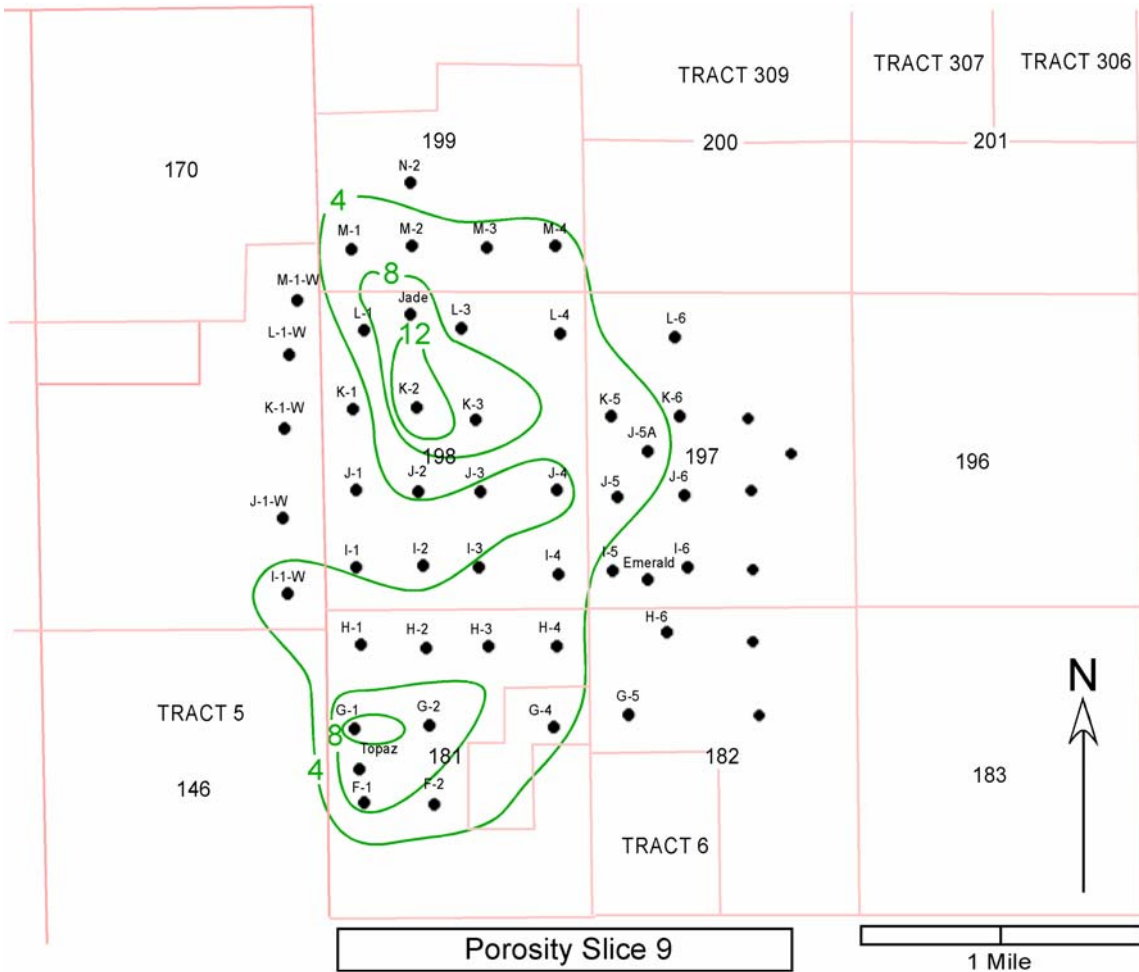
Figure C-10. Diamond M Porosity Slice Map 80 to 90 ft below Top of Reef
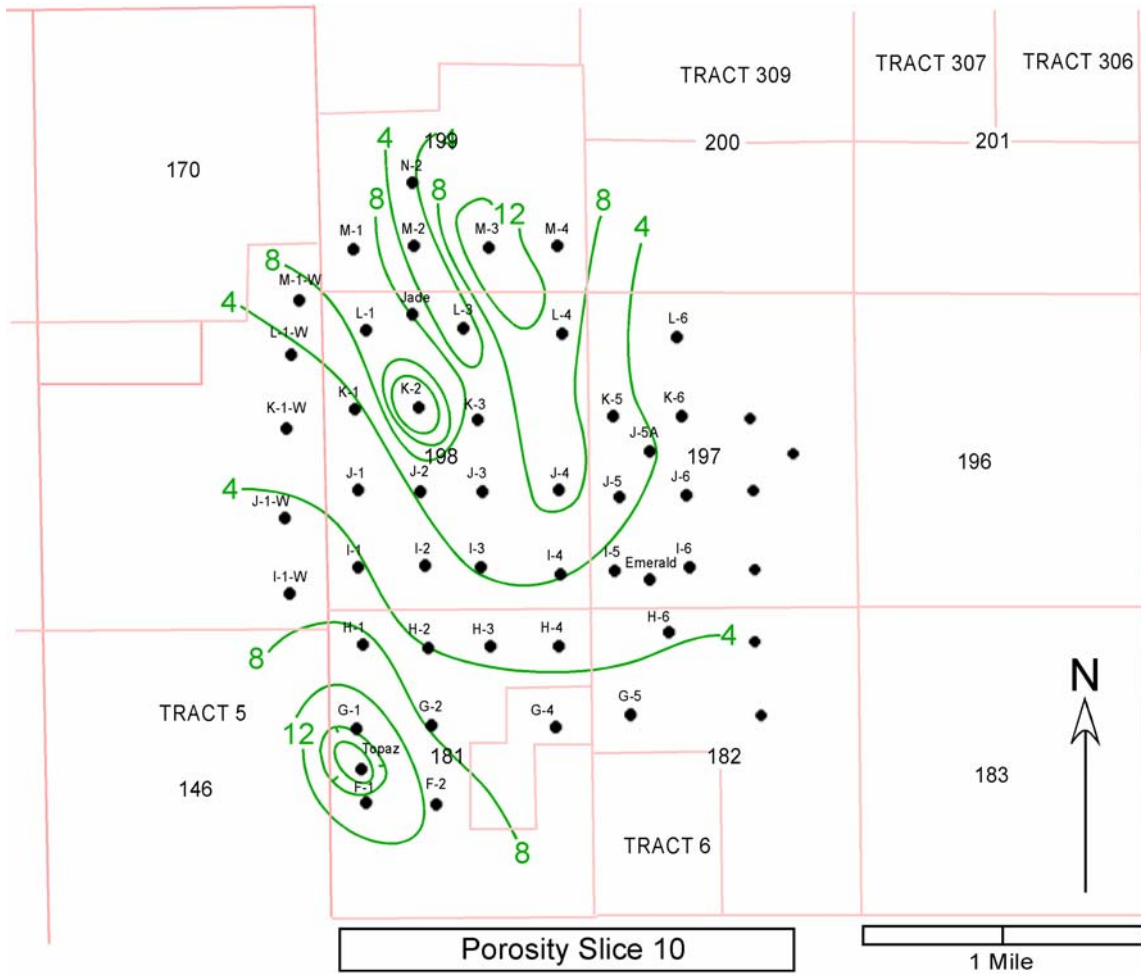
Figure C-11. Diamond M Porosity Slice Map 90 to 100 ft below Top of Reef
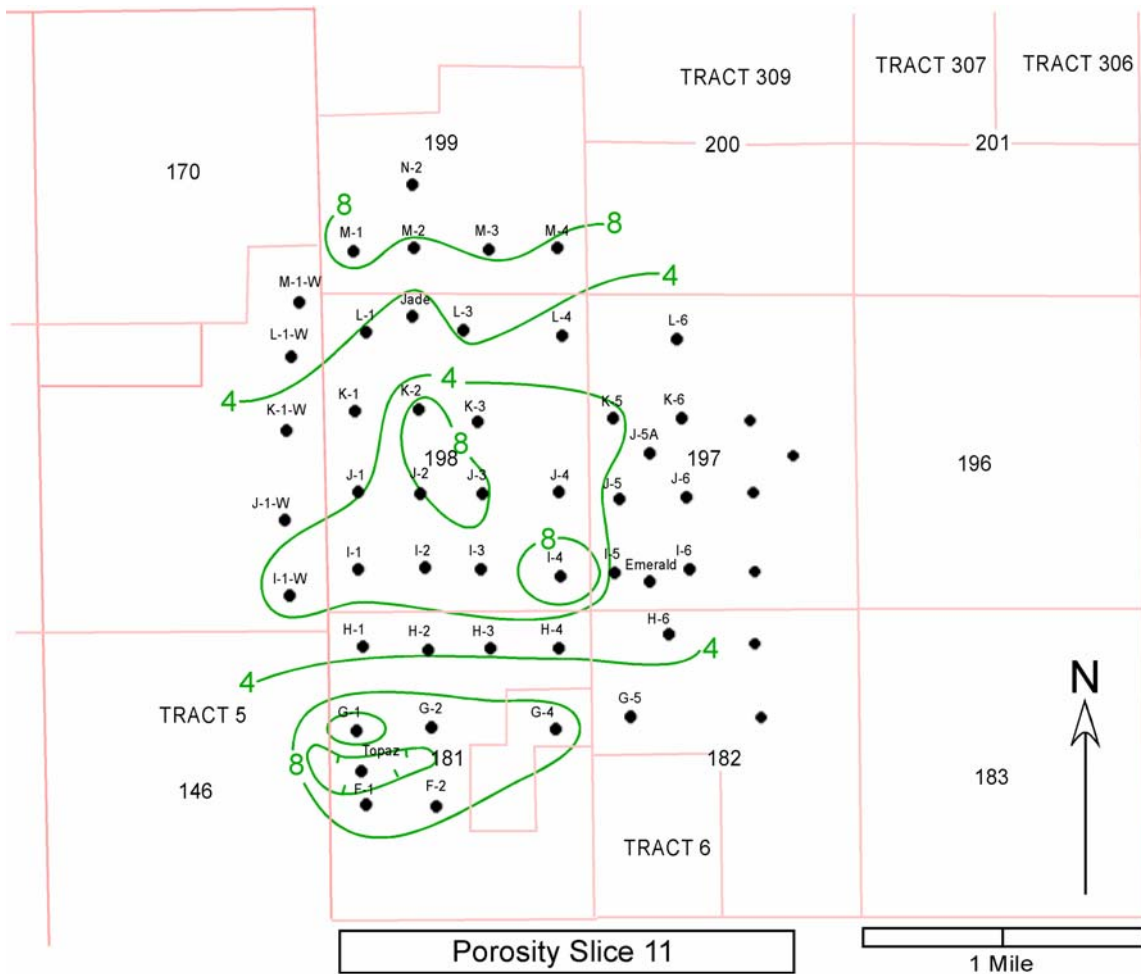
Figure C-12. Diamond M Porosity Slice Map 100 to 110 ft below Top of Reef
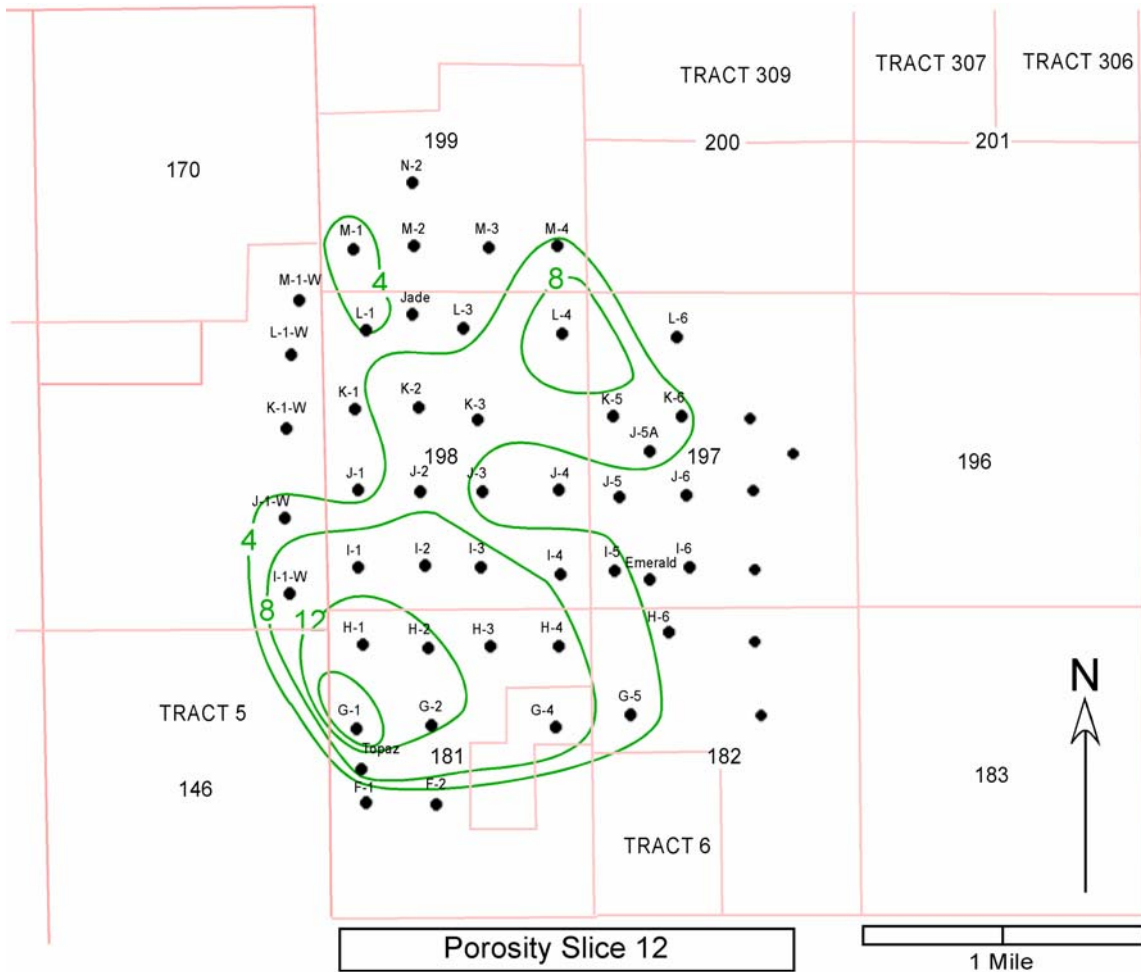
Figure C-13. Diamond M Porosity Slice Map 110 to 120 ft below Top of Reef
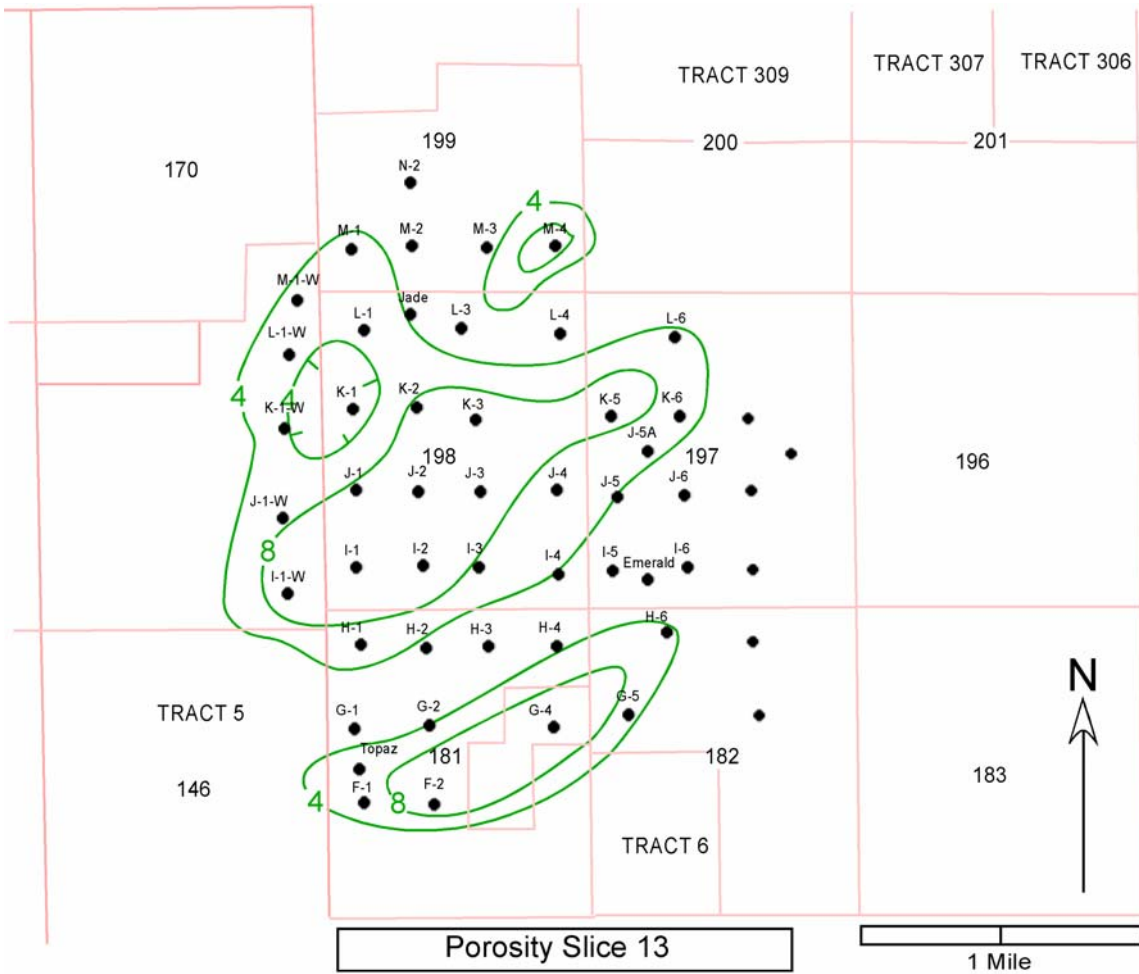
Figure C-14. Diamond M Porosity Slice Map 120 to 130 ft below Top of Reef
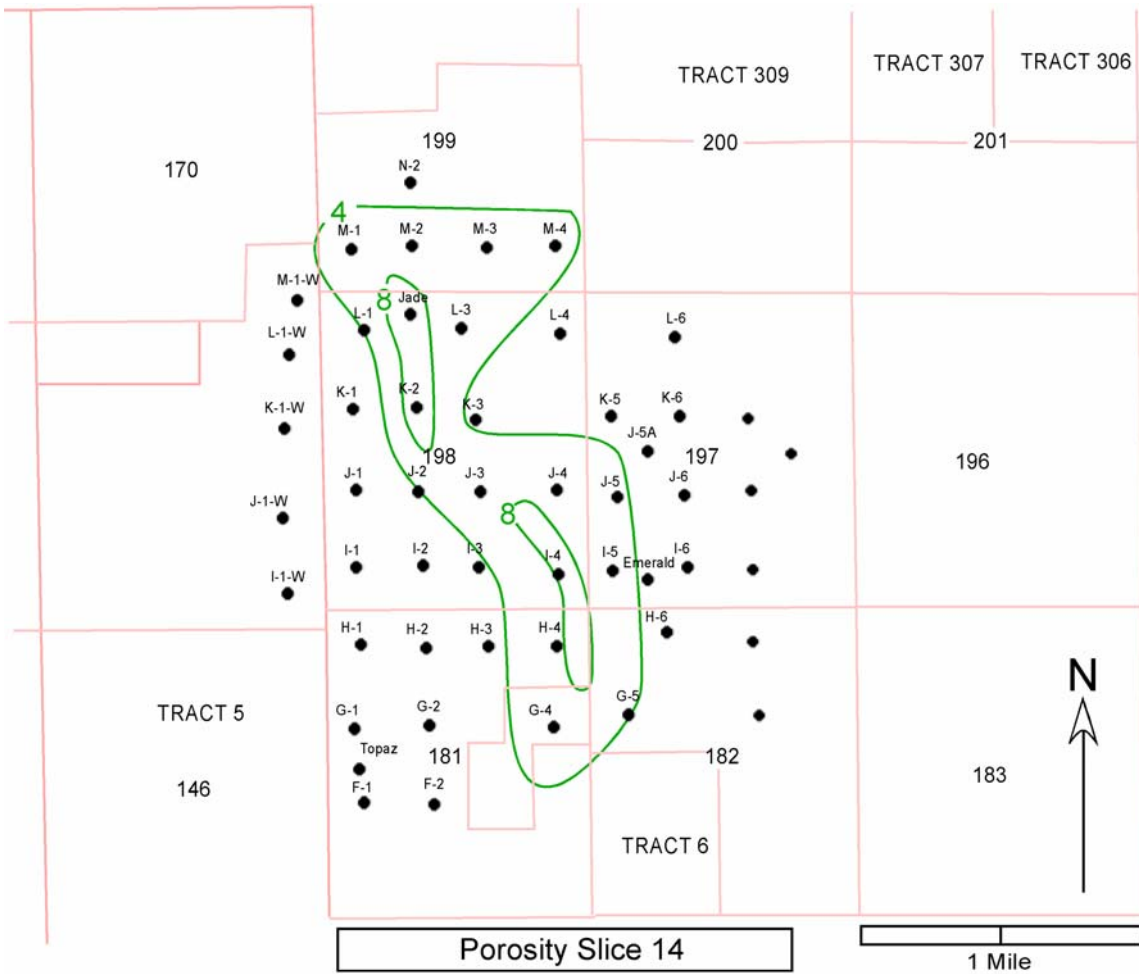
Figure C-15. Diamond M Porosity Slice Map 130 to 140 ft below Top of Reef
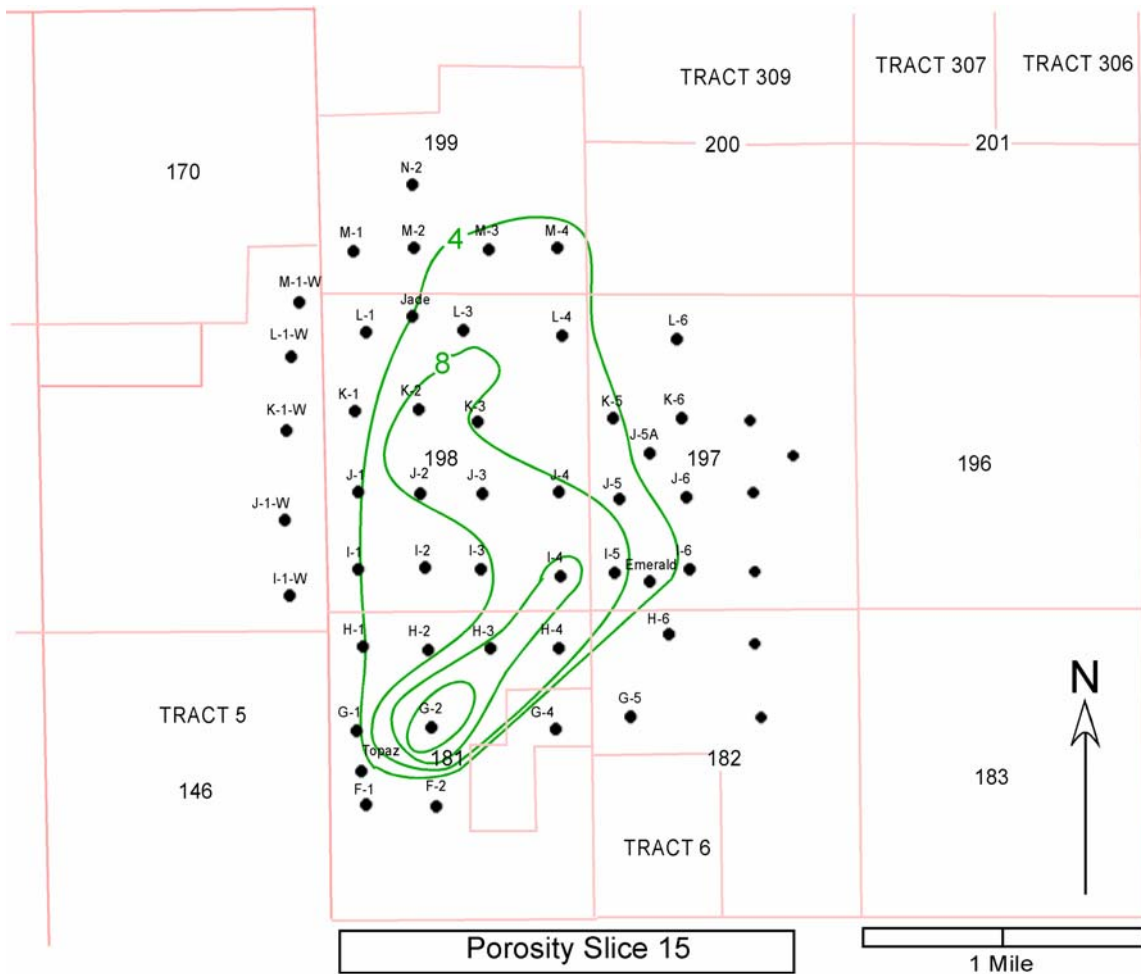
Figure C-16. Diamond M Porosity Slice Map 140 to 150 ft below Top of Reef
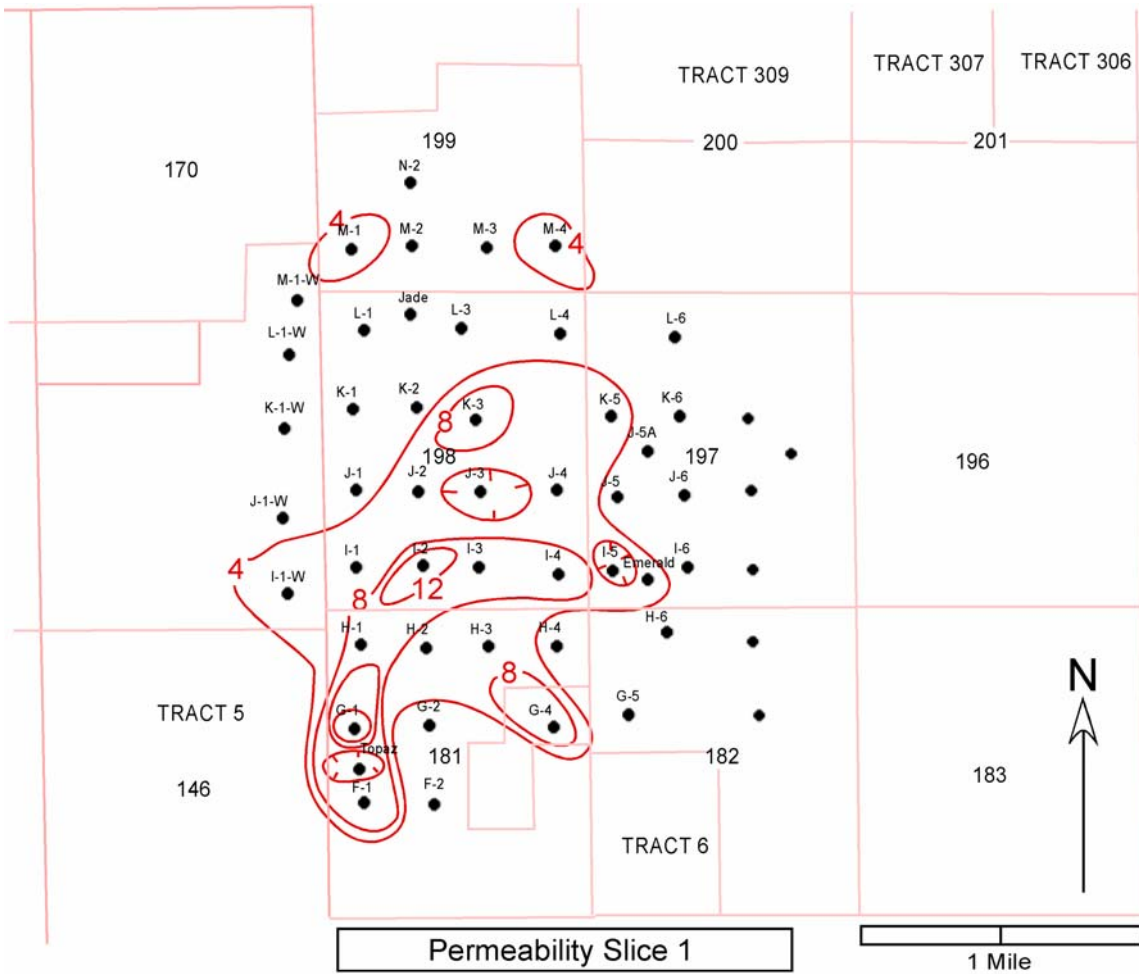
Figure C-17. Diamond M Permeability Slice Map 0 to 10 ft below Top of Reef
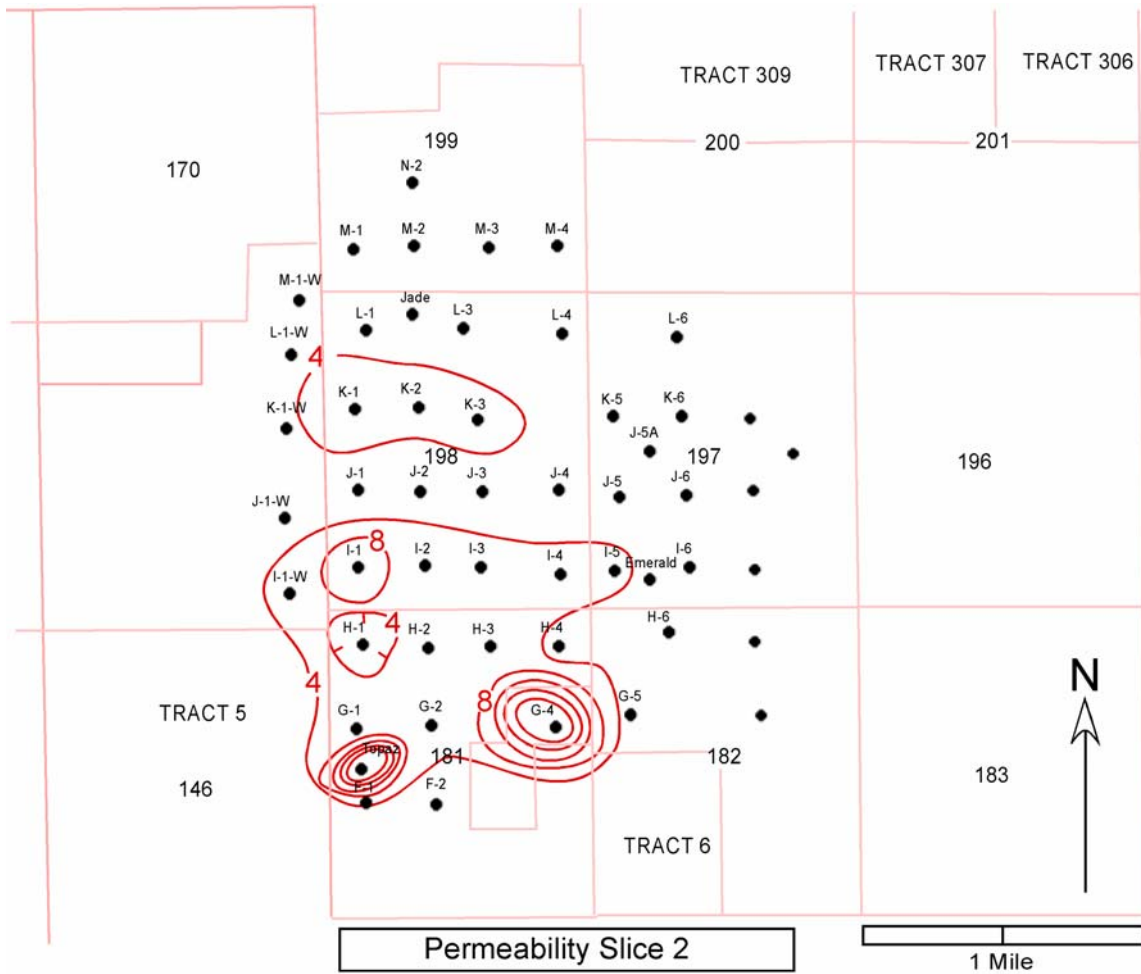
Figure C-18. Diamond M Permeability Slice Map 10 to 20 ft below Top of Reef
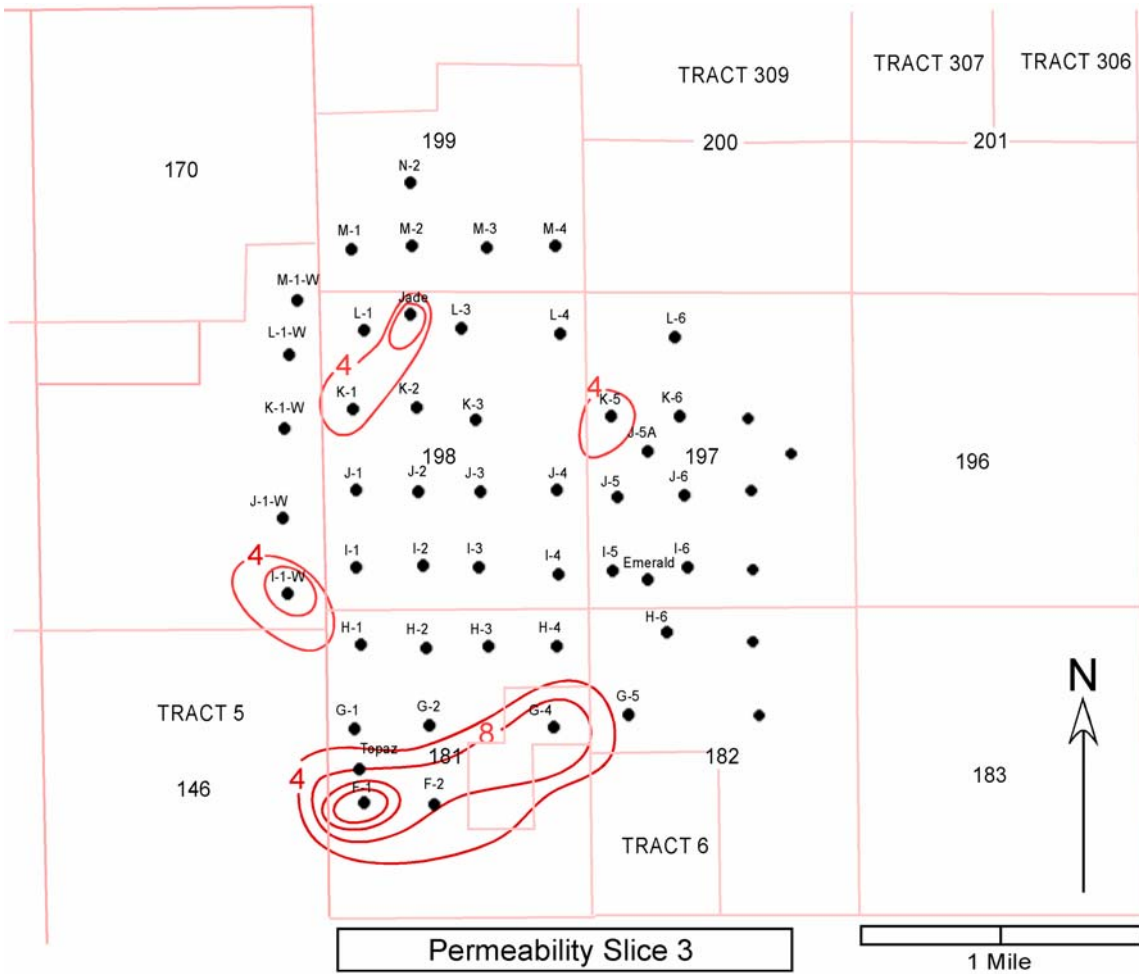
Figure C-19. Diamond M Permeability Slice Map 20 to 30 ft below Top of Reef
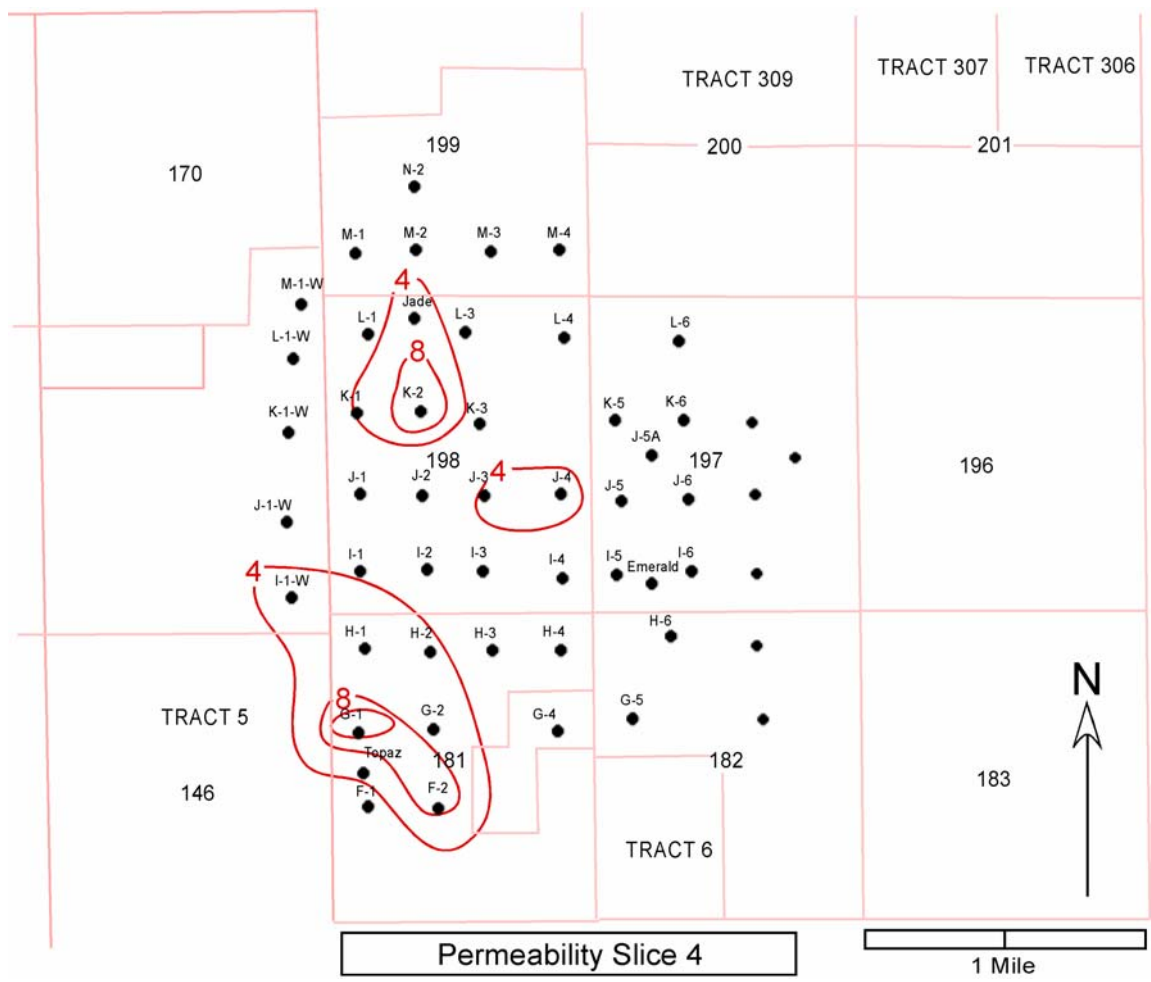
Figure C-20. Diamond M Permeability Slice Map 30 to 40 ft below Top of Reef
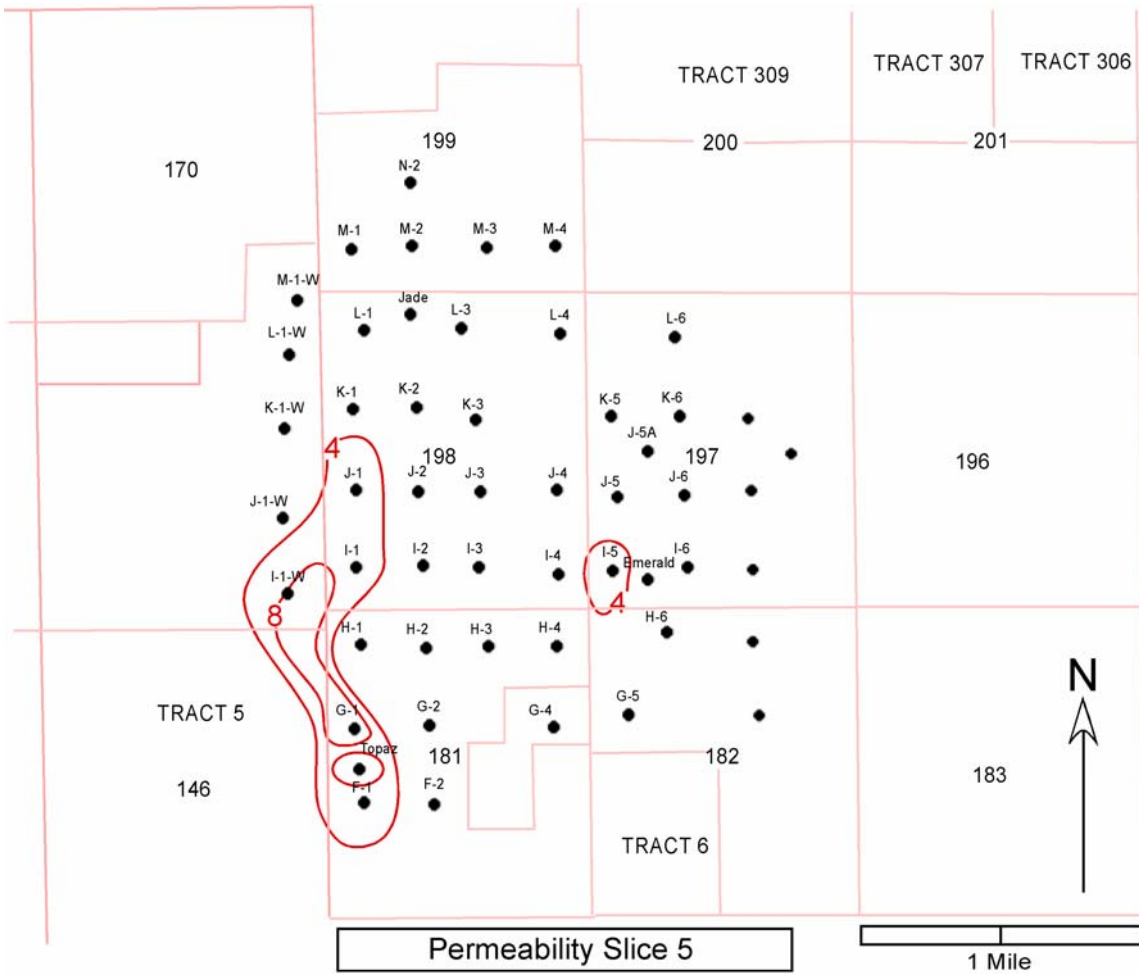
Figure C-21. Diamond M Permeability Slice Map 40 to 50 ft below Top of Reef
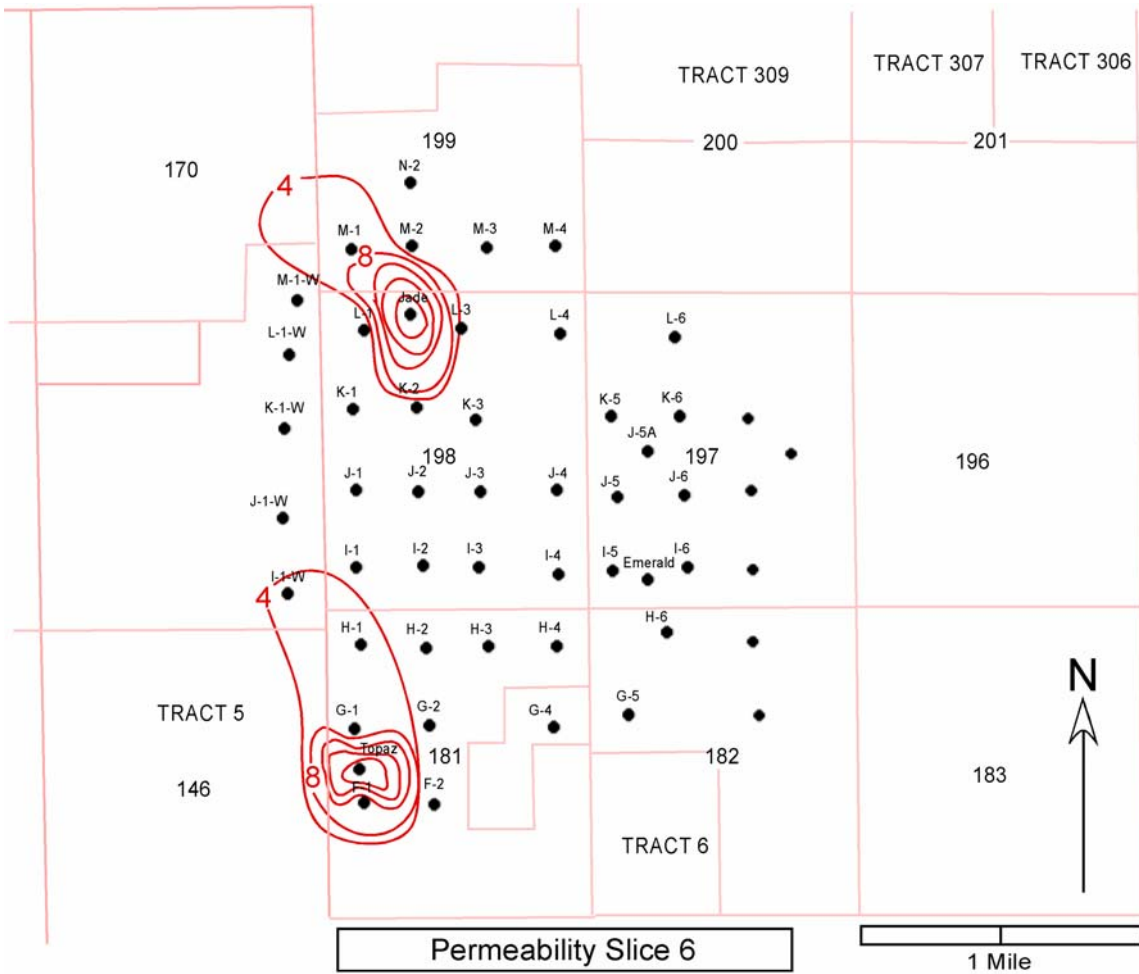
Figure C-22. Diamond M Permeability Slice Map 50 to 60 ft below Top of Reef
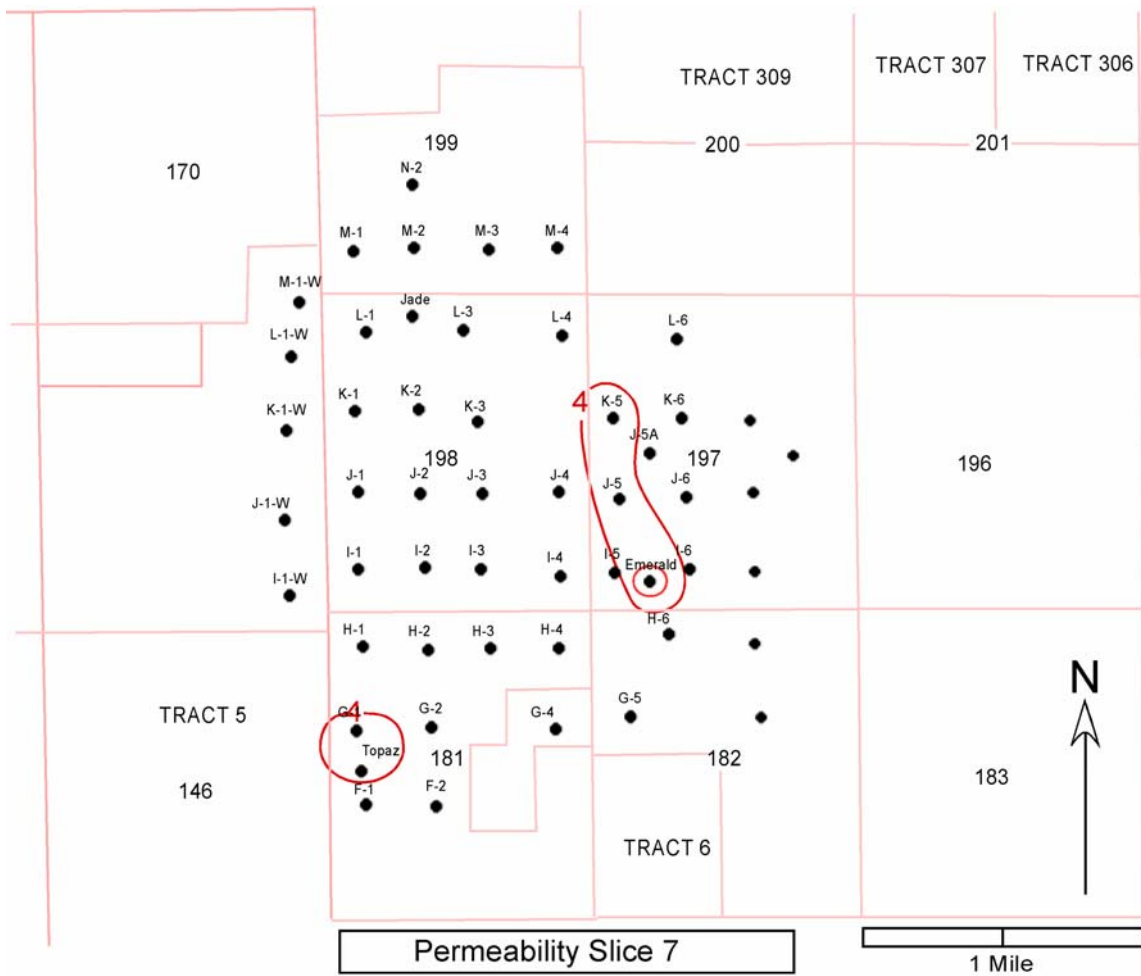
Figure C-23. Diamond M Permeability Slice Map 60 to 70 ft below Top of Reef
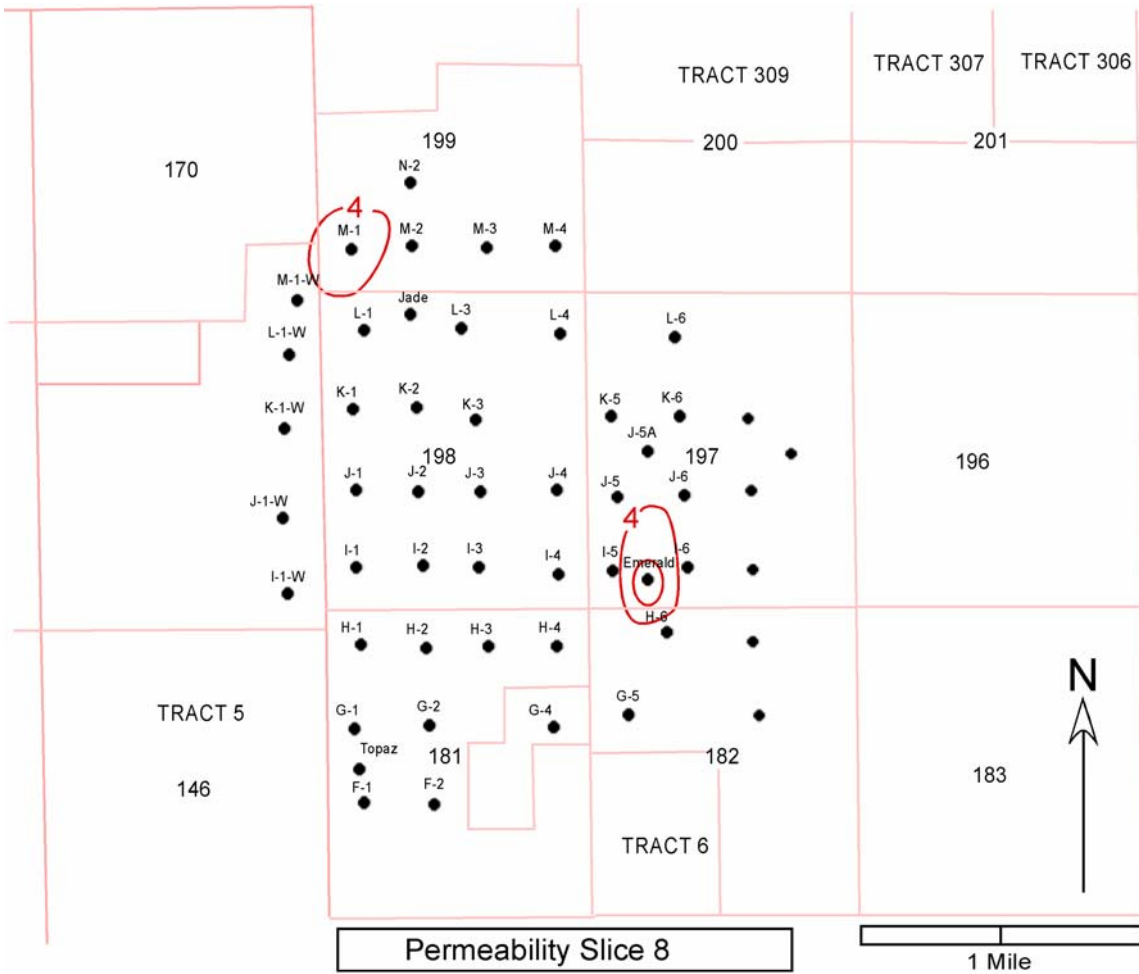
Figure C-24. Diamond M Permeability Slice Map 70 to 80 ft below Top of Reef
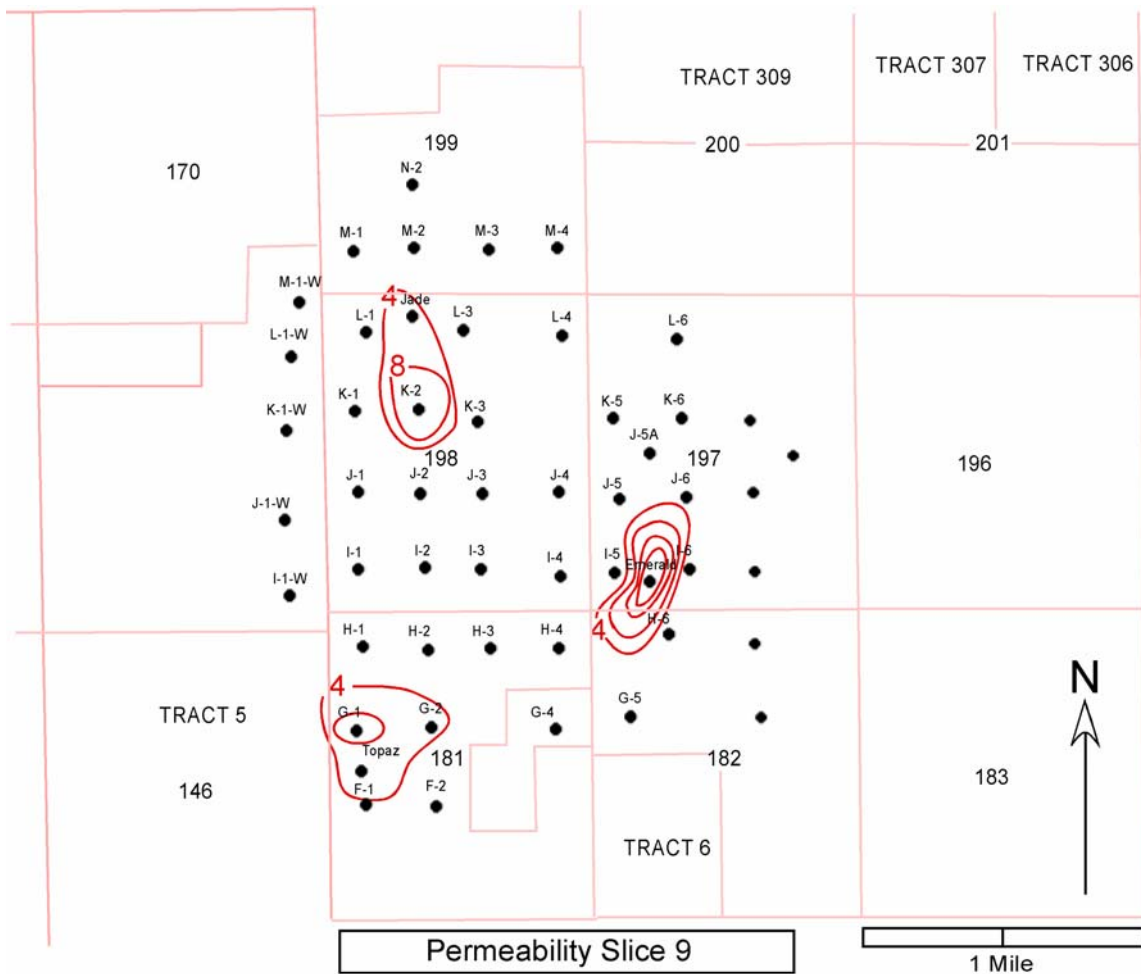
Figure C-25. Diamond M Permeability Slice Map 80 to 90 ft below Top of Reef
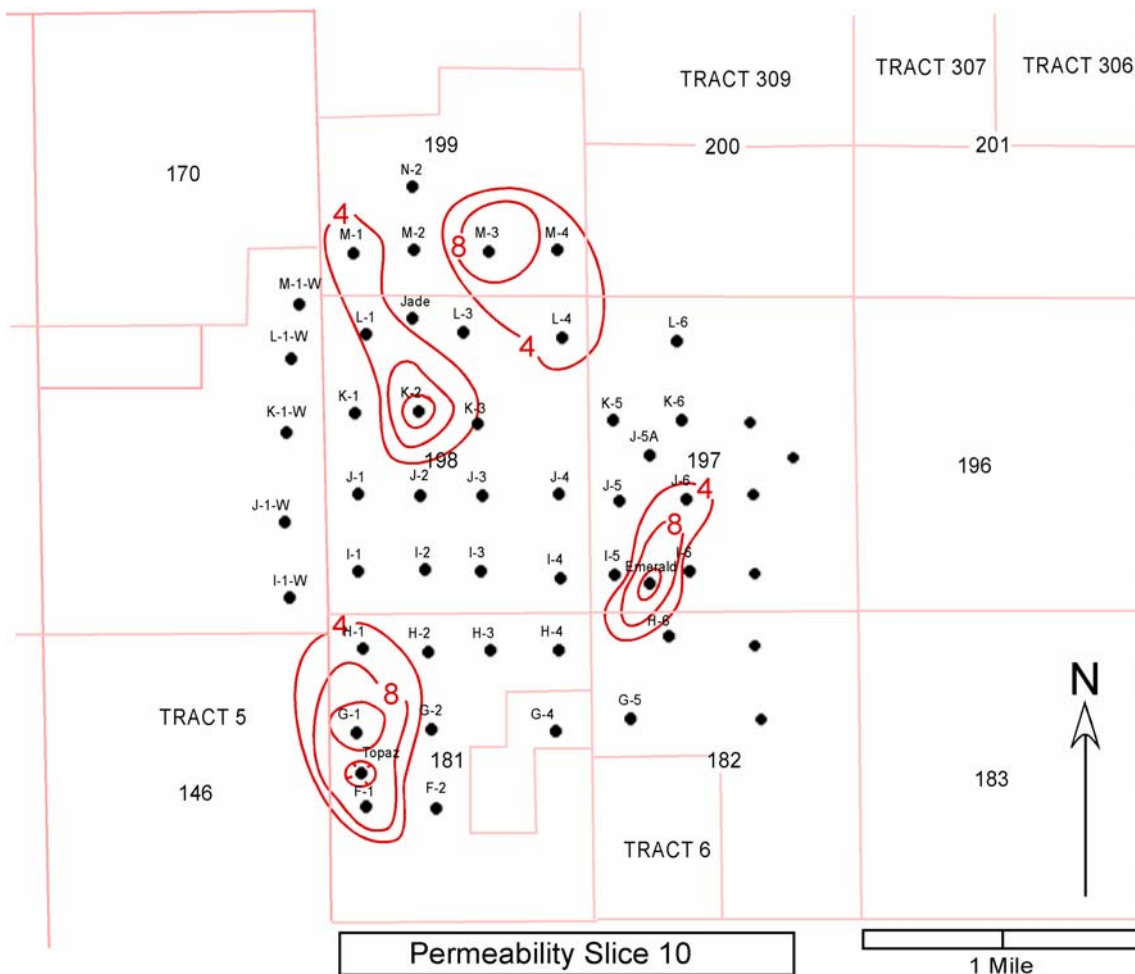
Figure C-26. Diamond M Permeability Slice Map 90 to 100 ft below Top of Reef
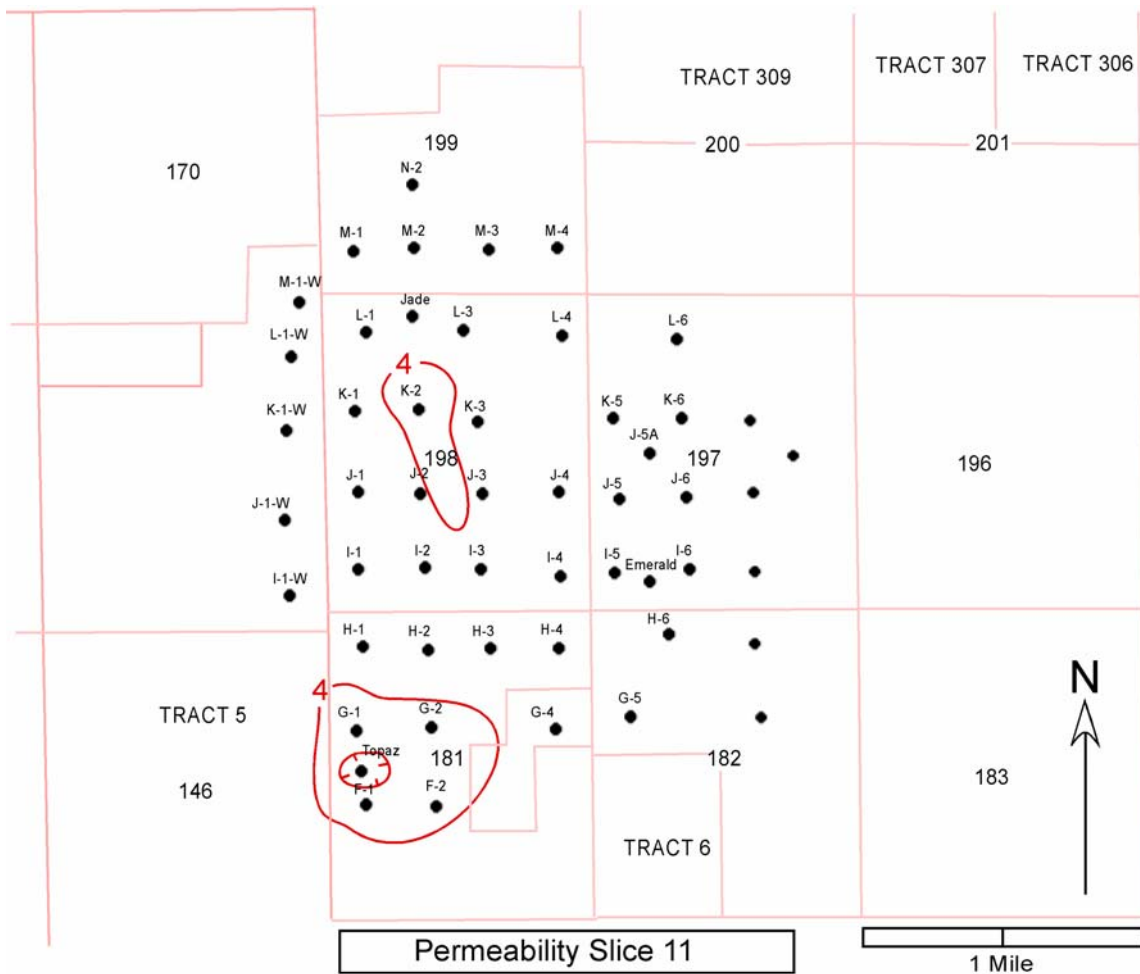
Figure C-27. Diamond M Permeability Slice Map 100 to 110 ft below Top of Reef
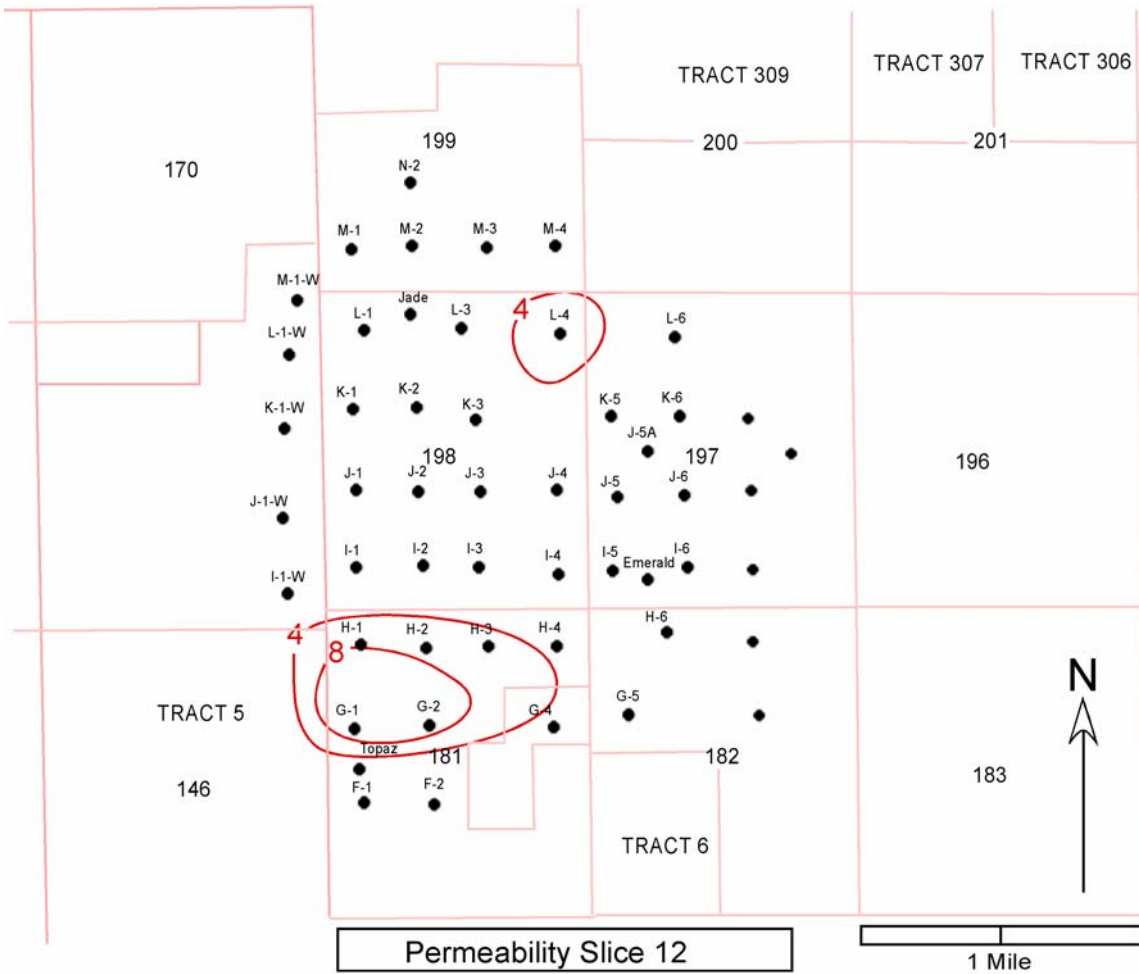
Figure C-28. Diamond M Permeability Slice Map 110 to 120 ft below Top of Reef
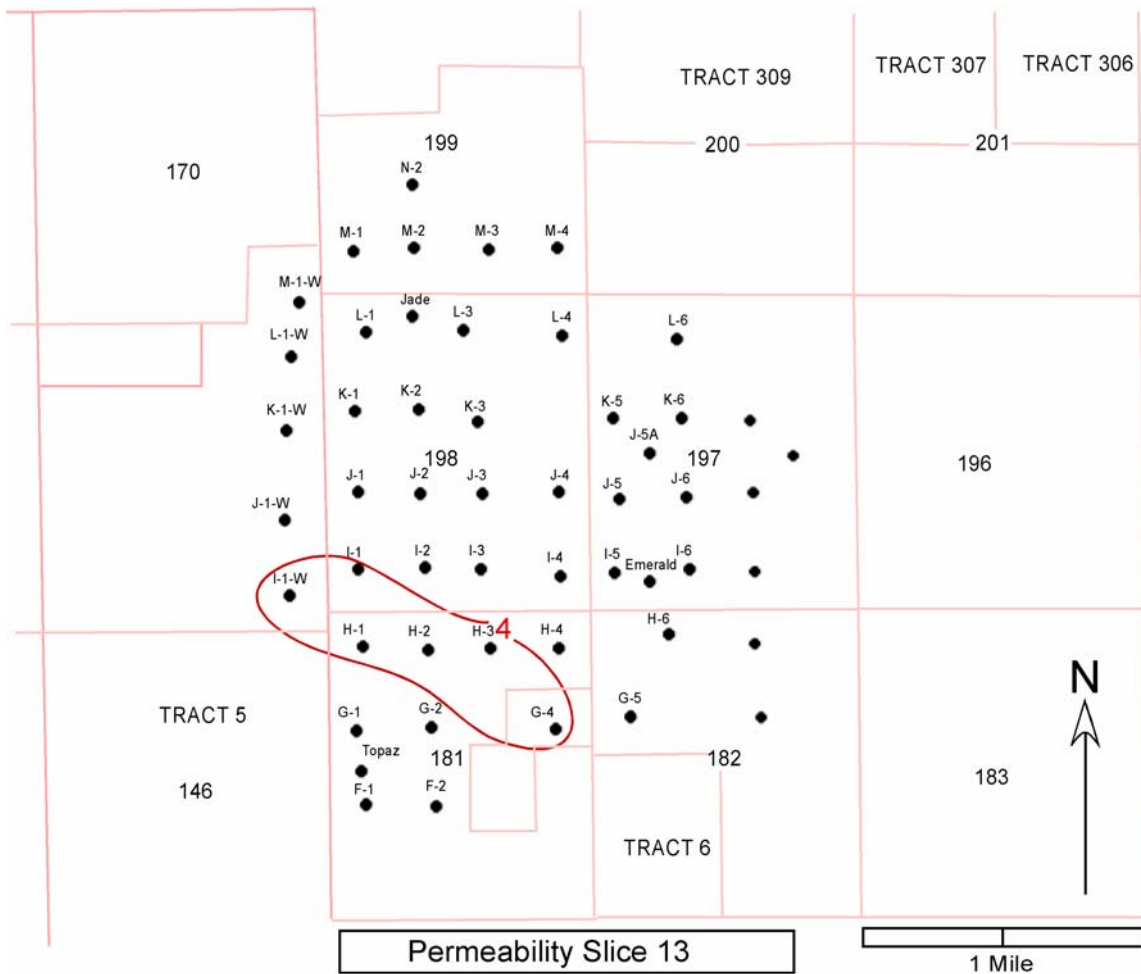
Figure C-29. Diamond M Permeability Slice Map 120 to 130 ft below Top of Reef
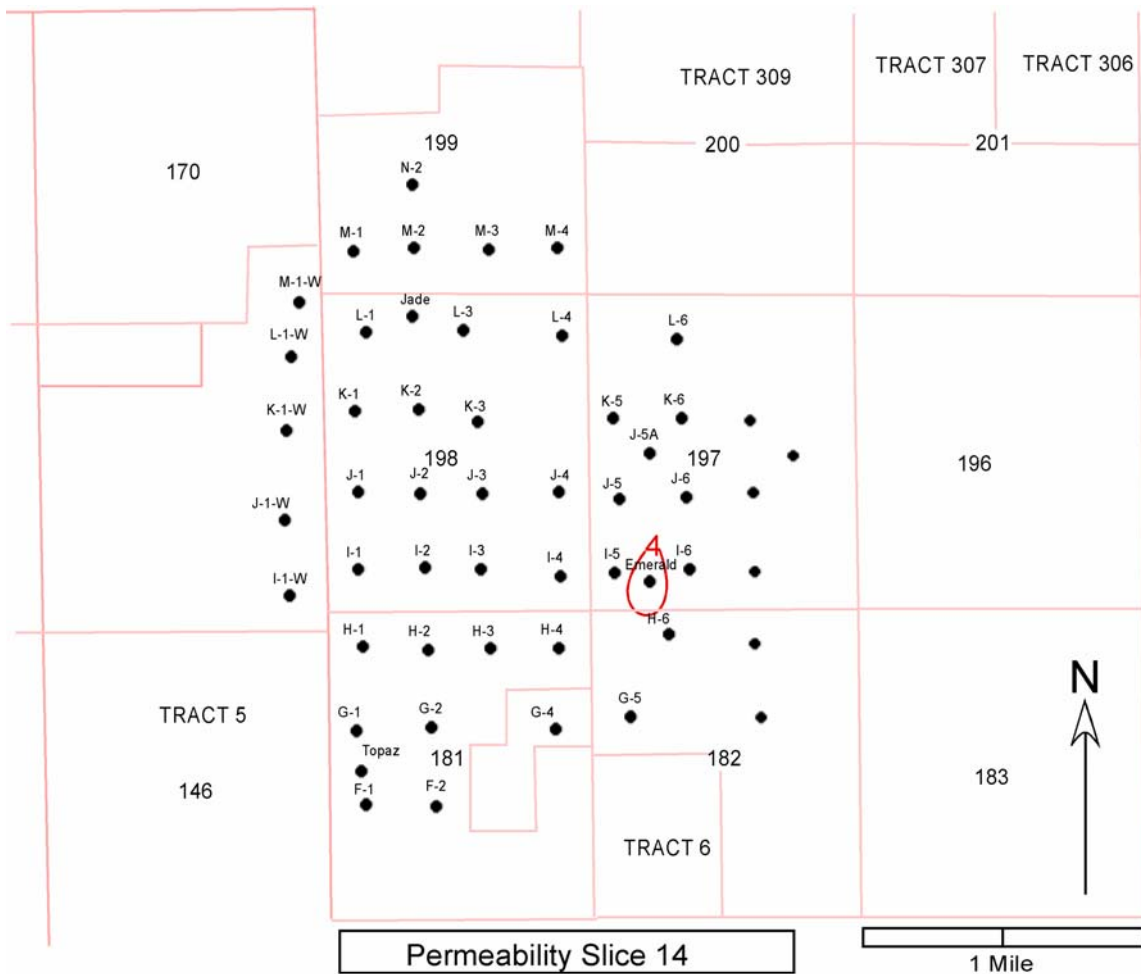
Figure C-30. Diamond M Permeability Slice Map 130 to 140 ft below Top of Reef
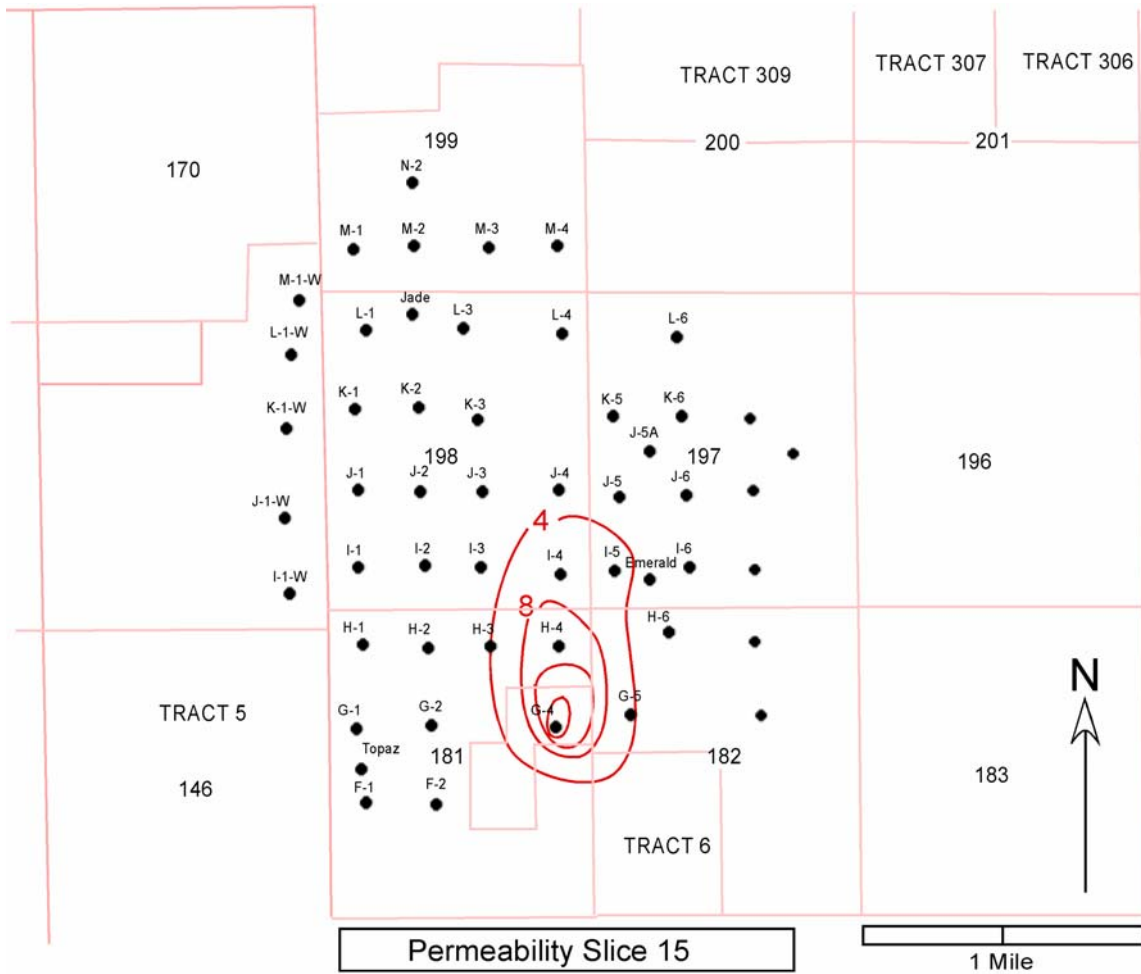
Figure C-31. Diamond M Permeability Slice Map 140 to 150 ft below Top of Reef

Porosity (%)
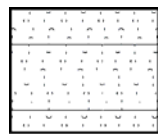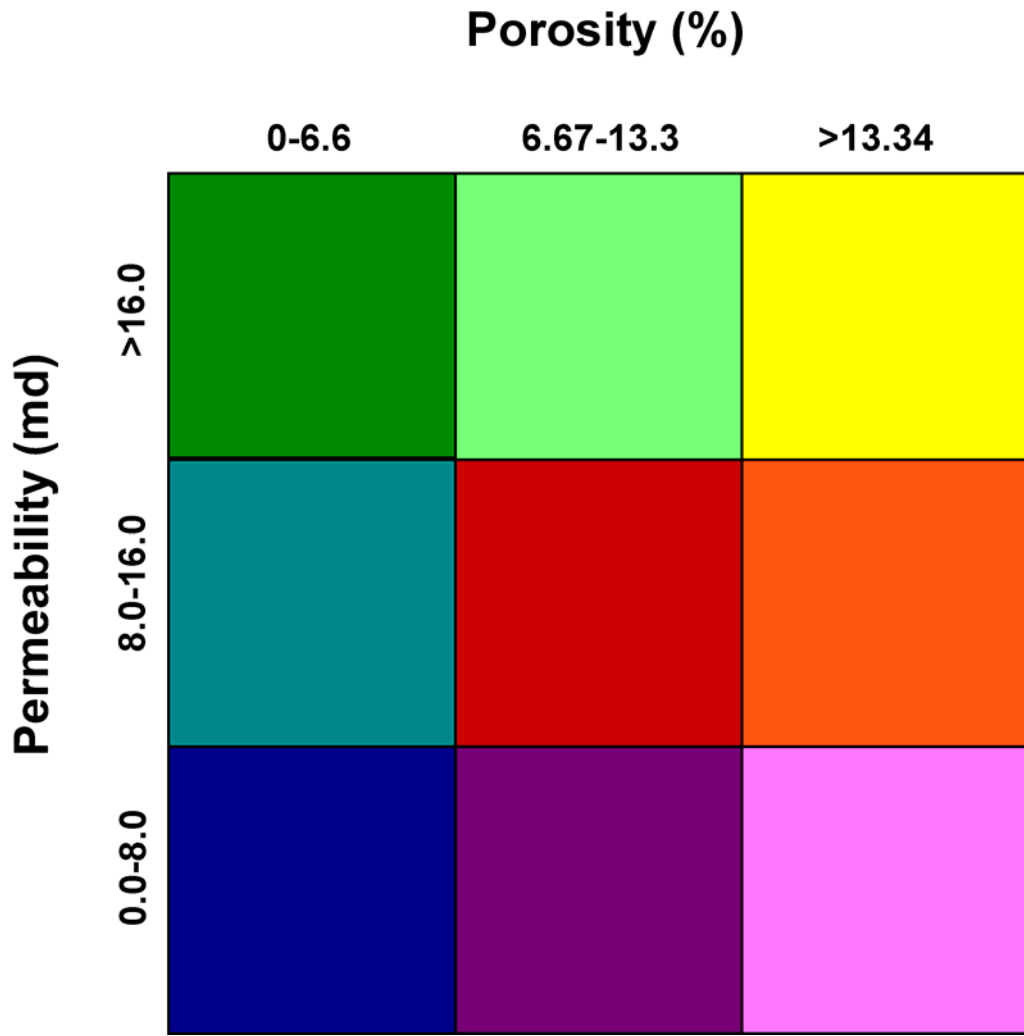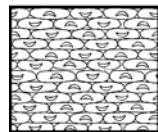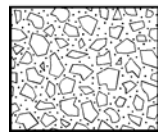
Figure C-32. Diamond M Reservoir Quality Map Key
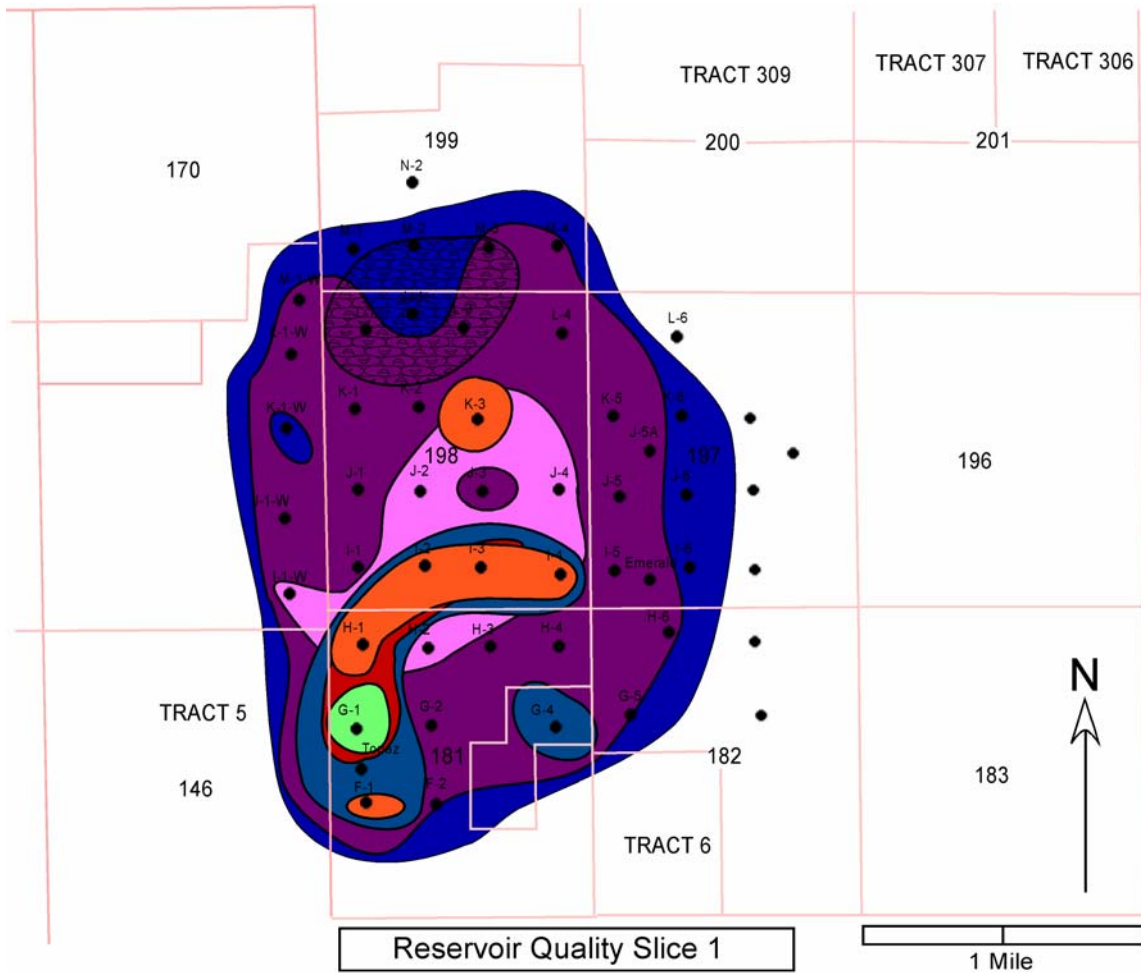
Figure C-33. Diamond M Flow Unit Map 0 to 10 ft Below Top of Reef
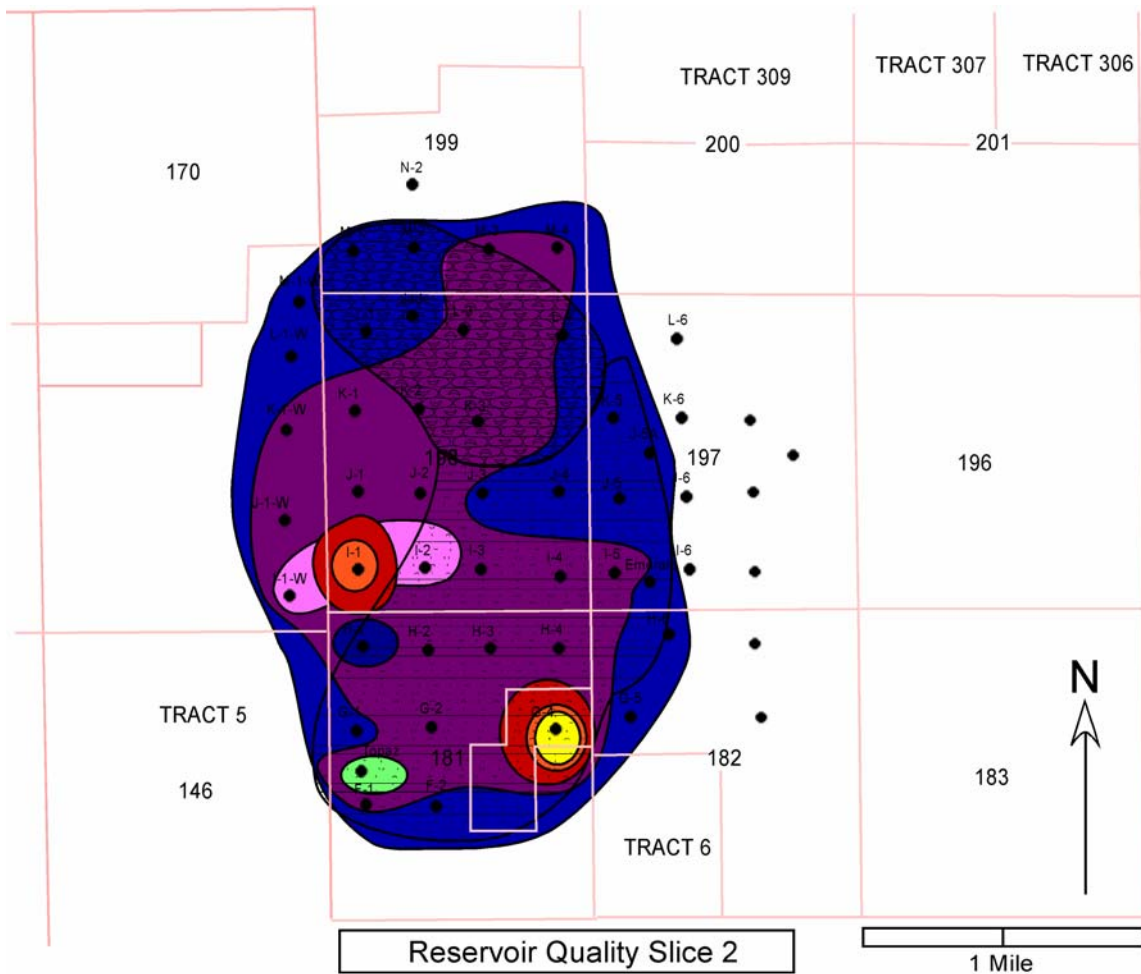
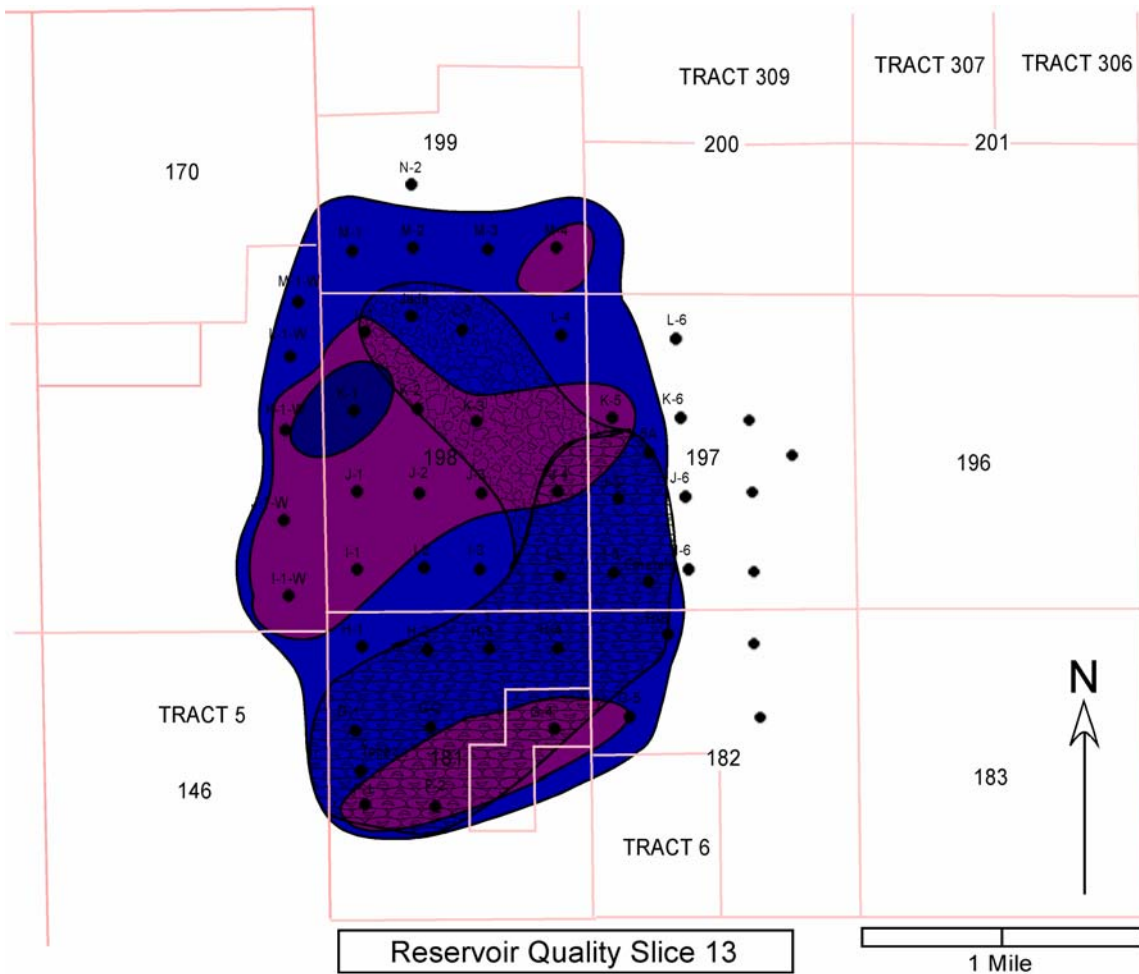**Figure C-34. Diamond M Flow Unit Map 10 to 20 ft Below Top of Reef**
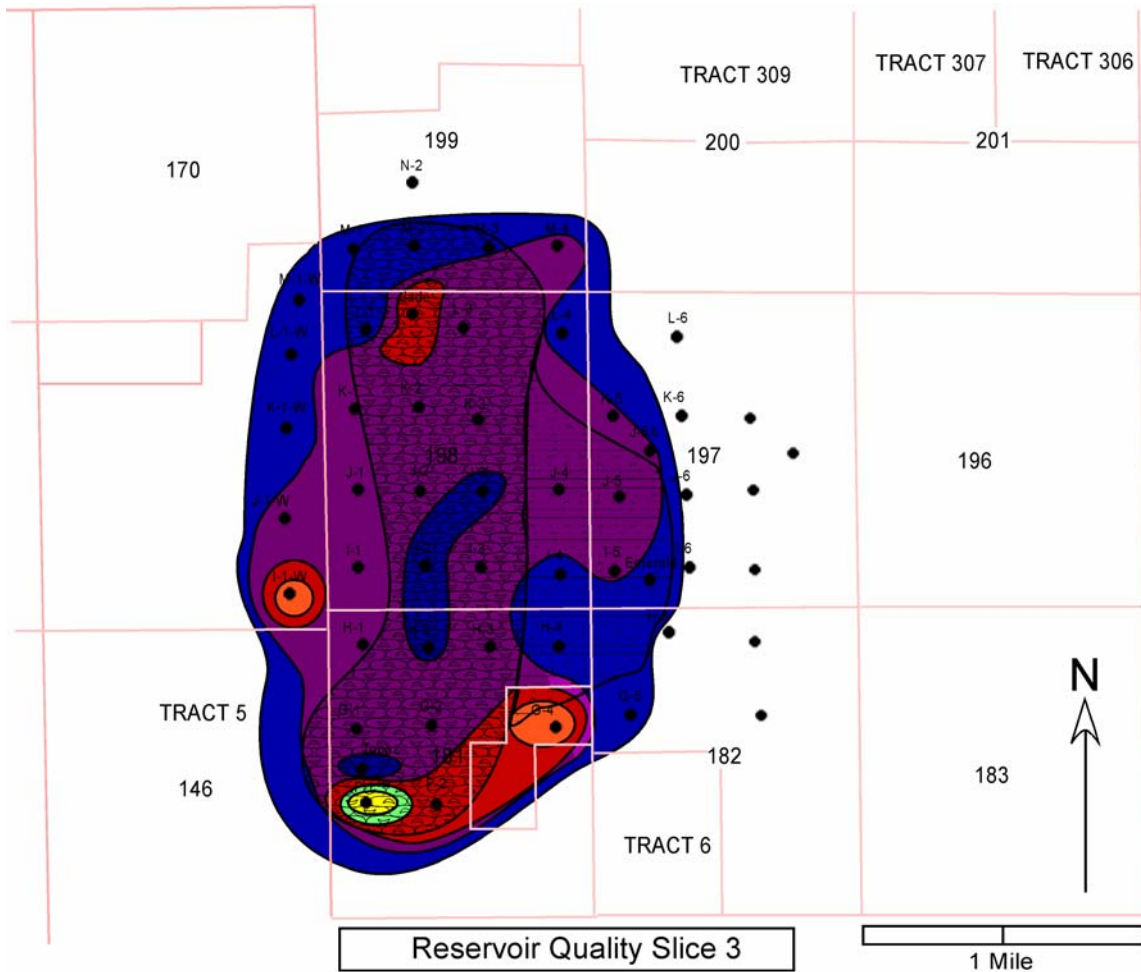
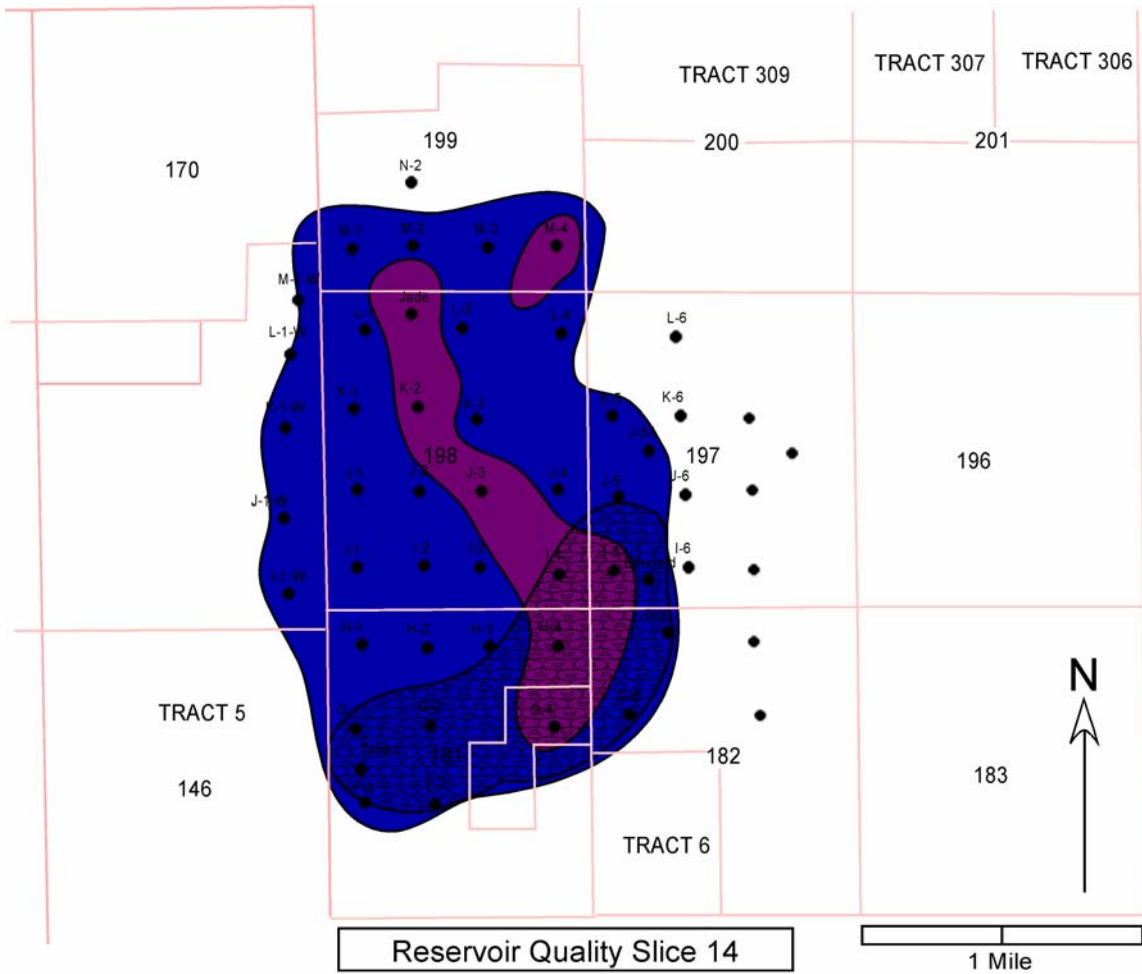**Figure C-35. Diamond M Flow Unit Map 20 to 30 ft Below Top of Reef**
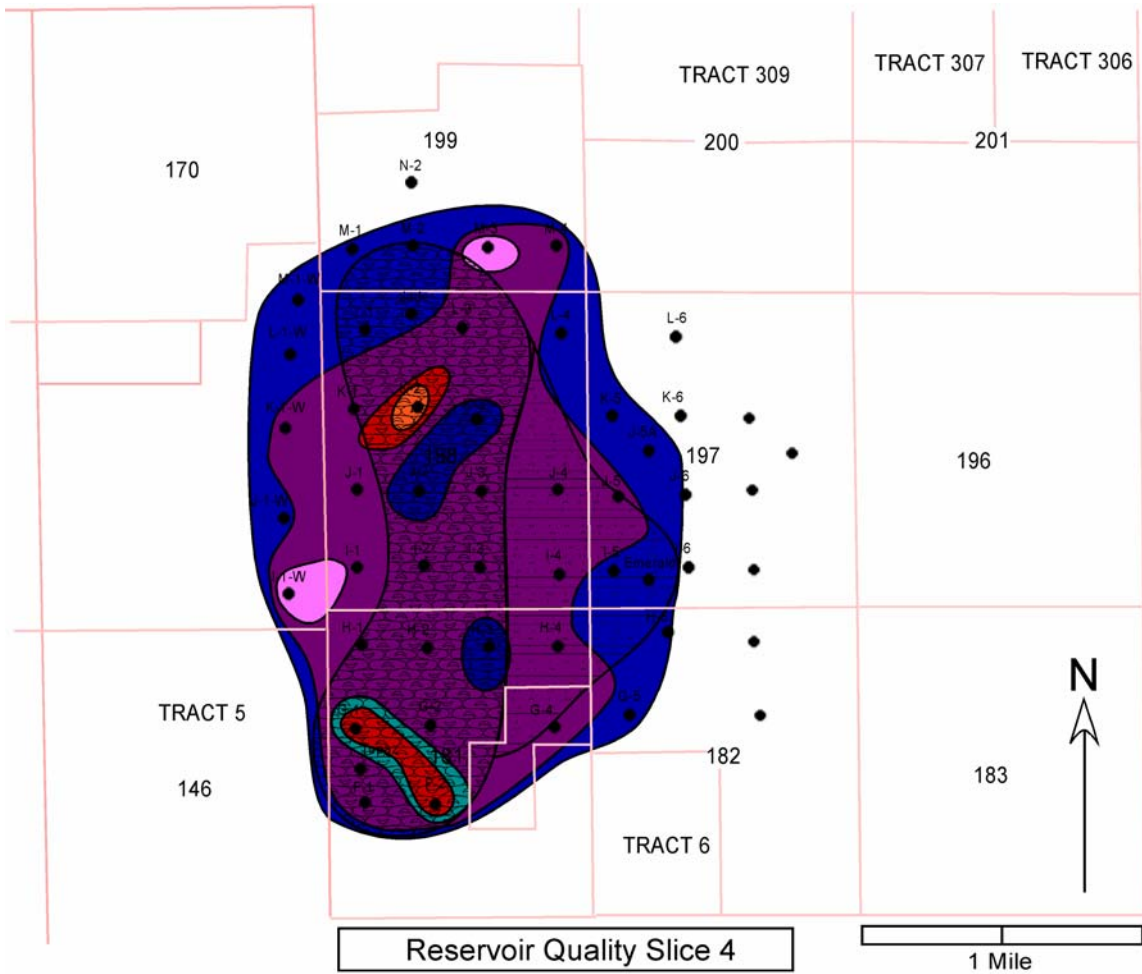
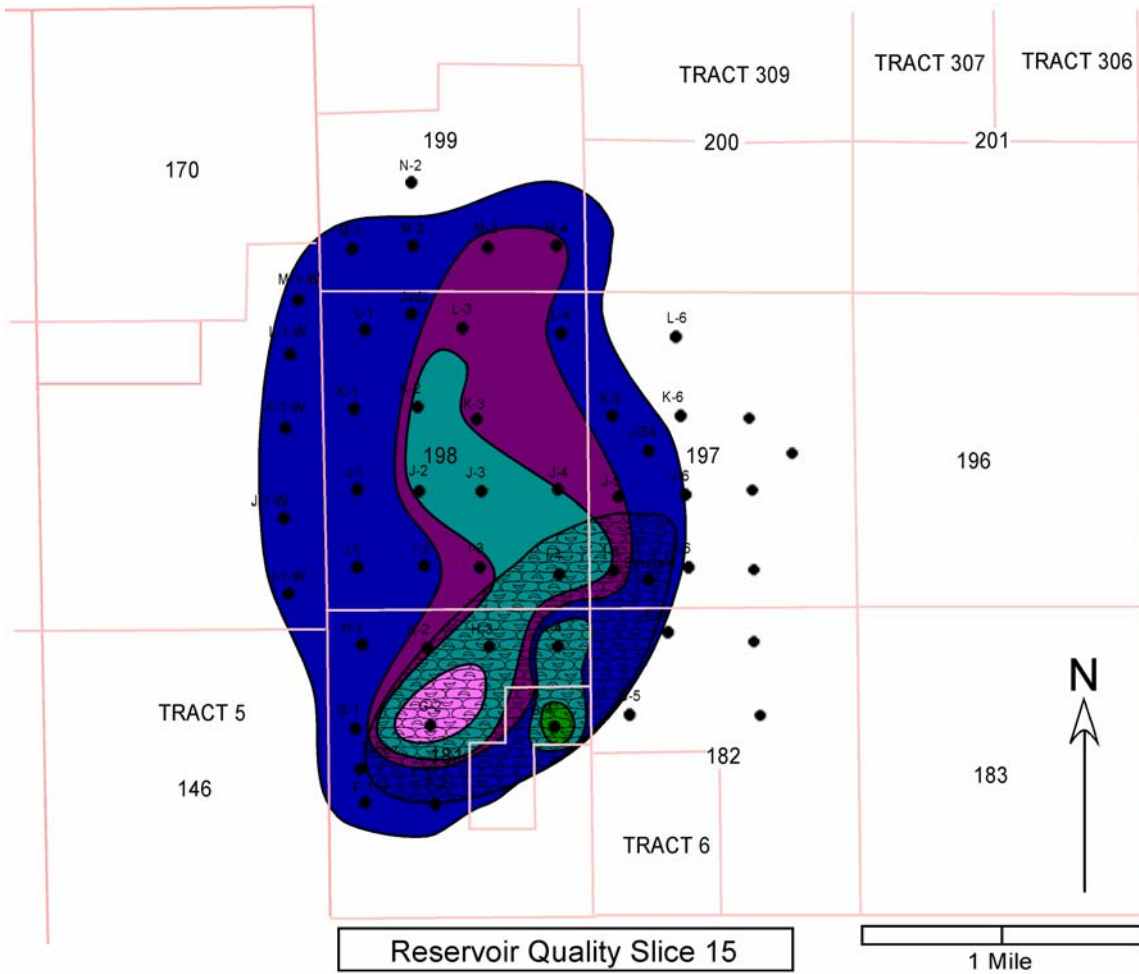**Figure C-36. Diamond M Flow Unit Map 30 to 40 ft Below Top of Reef**
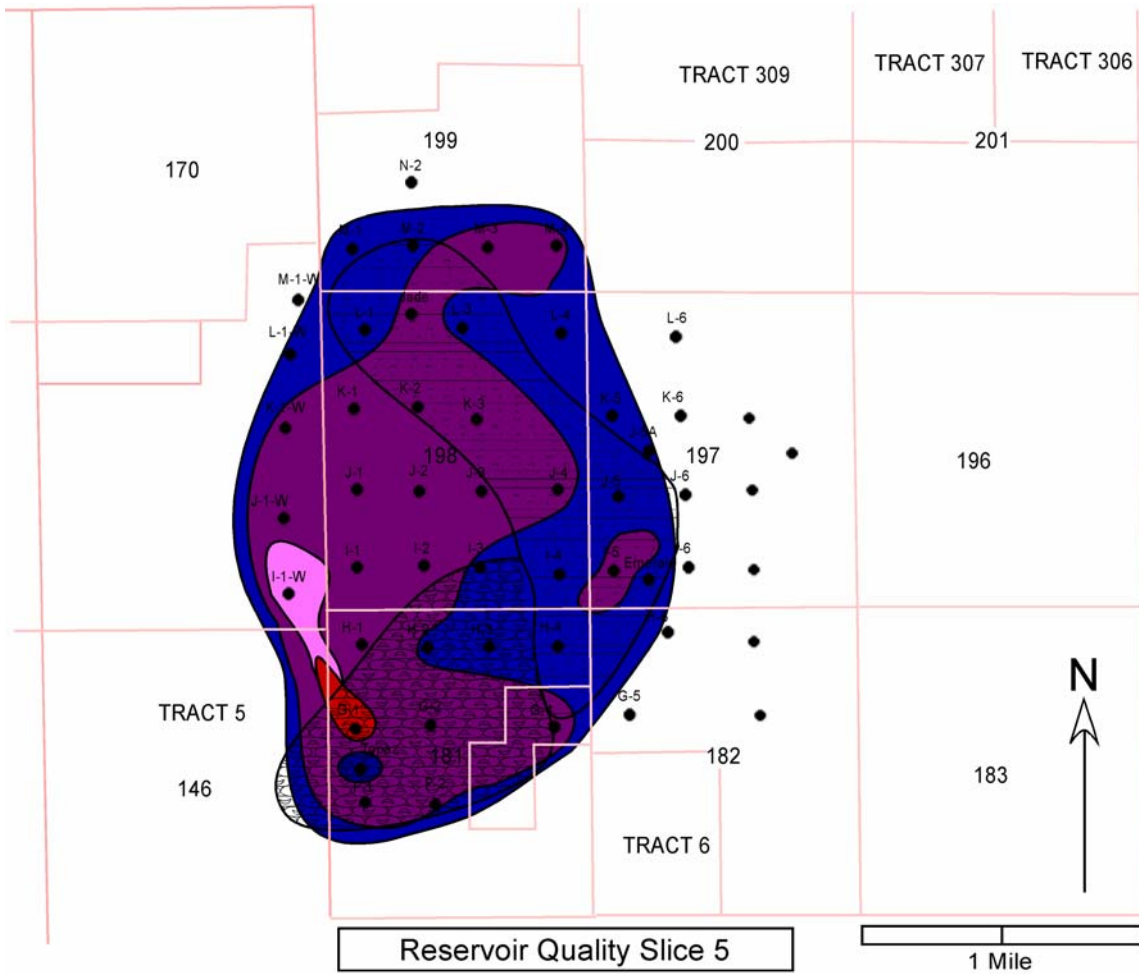
Figure C-37. Diamond M Flow Unit Map 40 to 50 ft Below Top of Reef
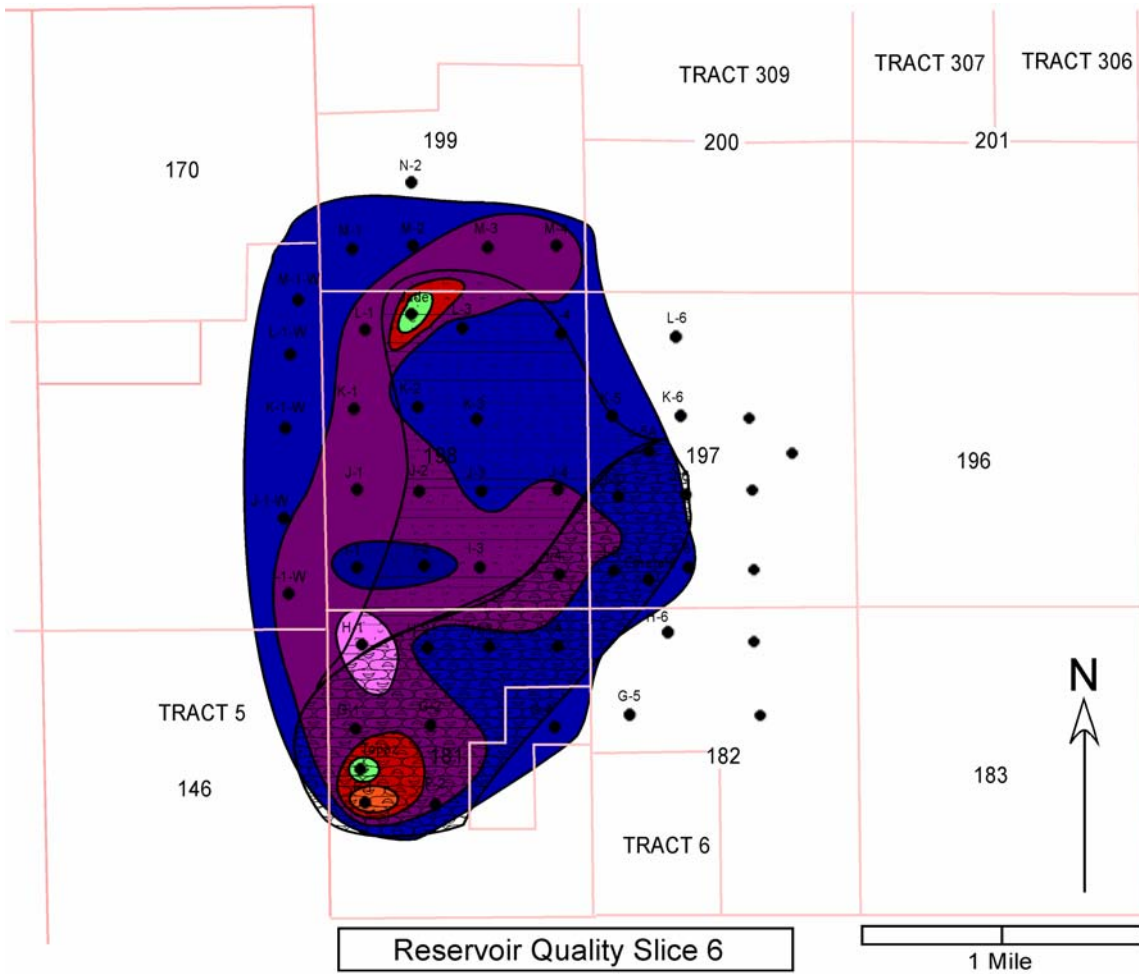
Figure C-38. Diamond M Flow Unit Map 50 to 60 ft Below Top of Reef
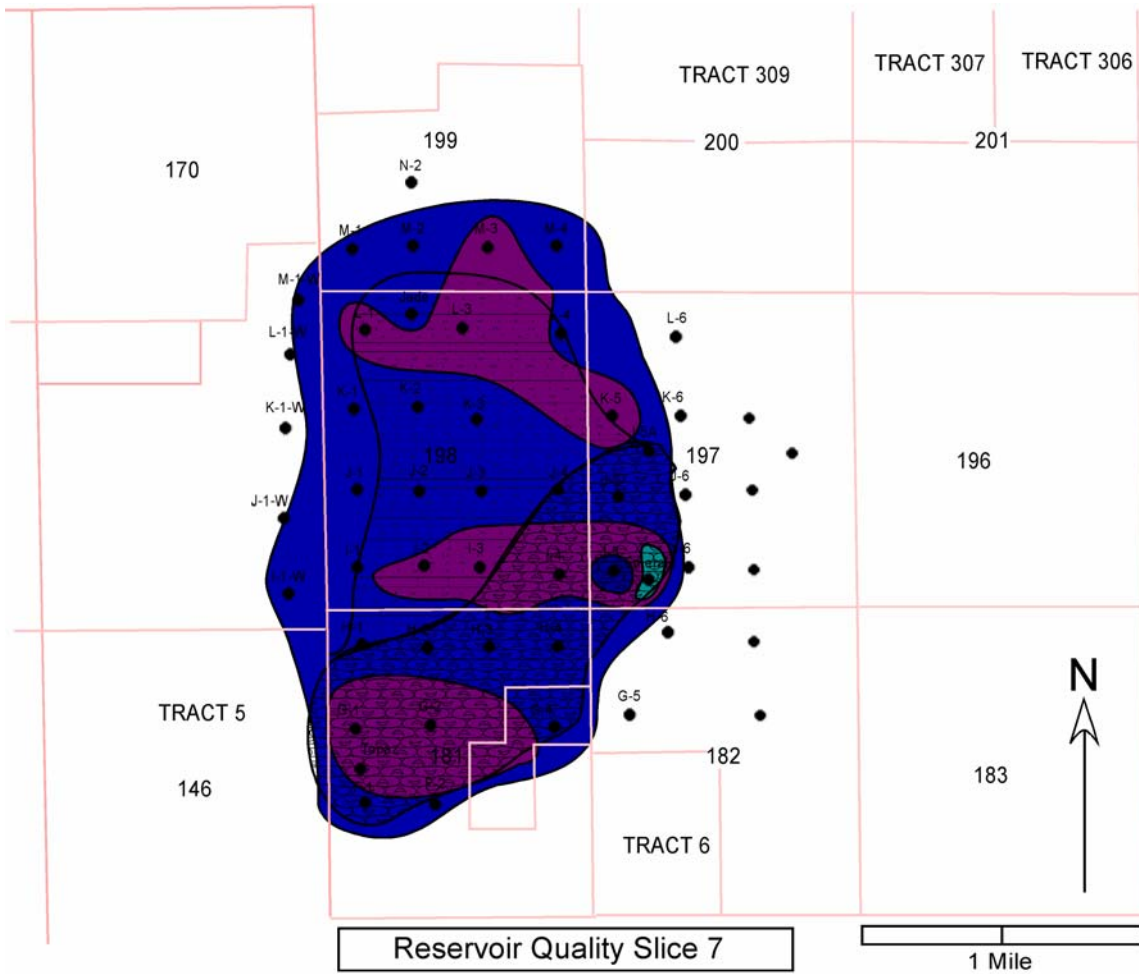
Figure C-39. Diamond M Flow Unit Map 60 to 70 ft Below Top of Reef
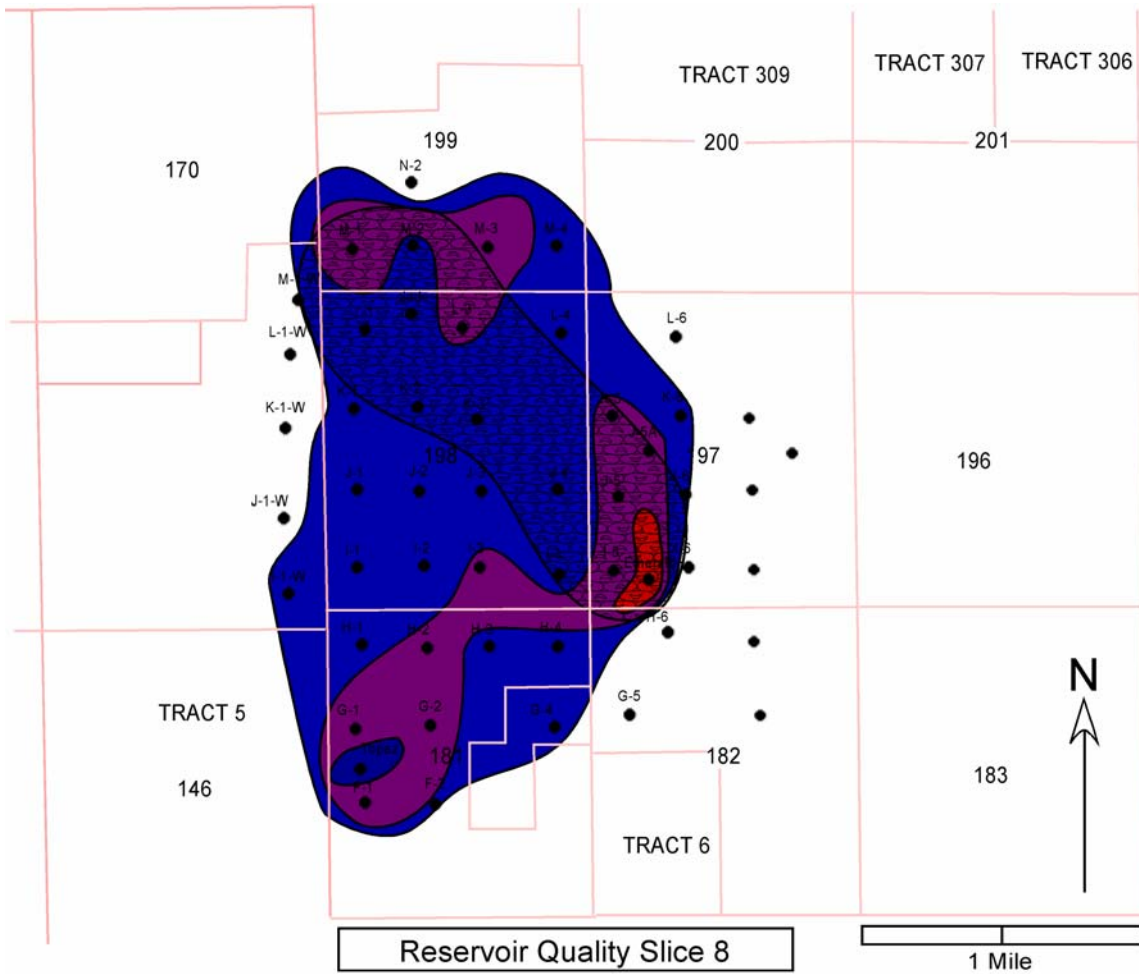
Figure C-40. Diamond M Flow Unit Map 70 to 80 ft Below Top of Reef
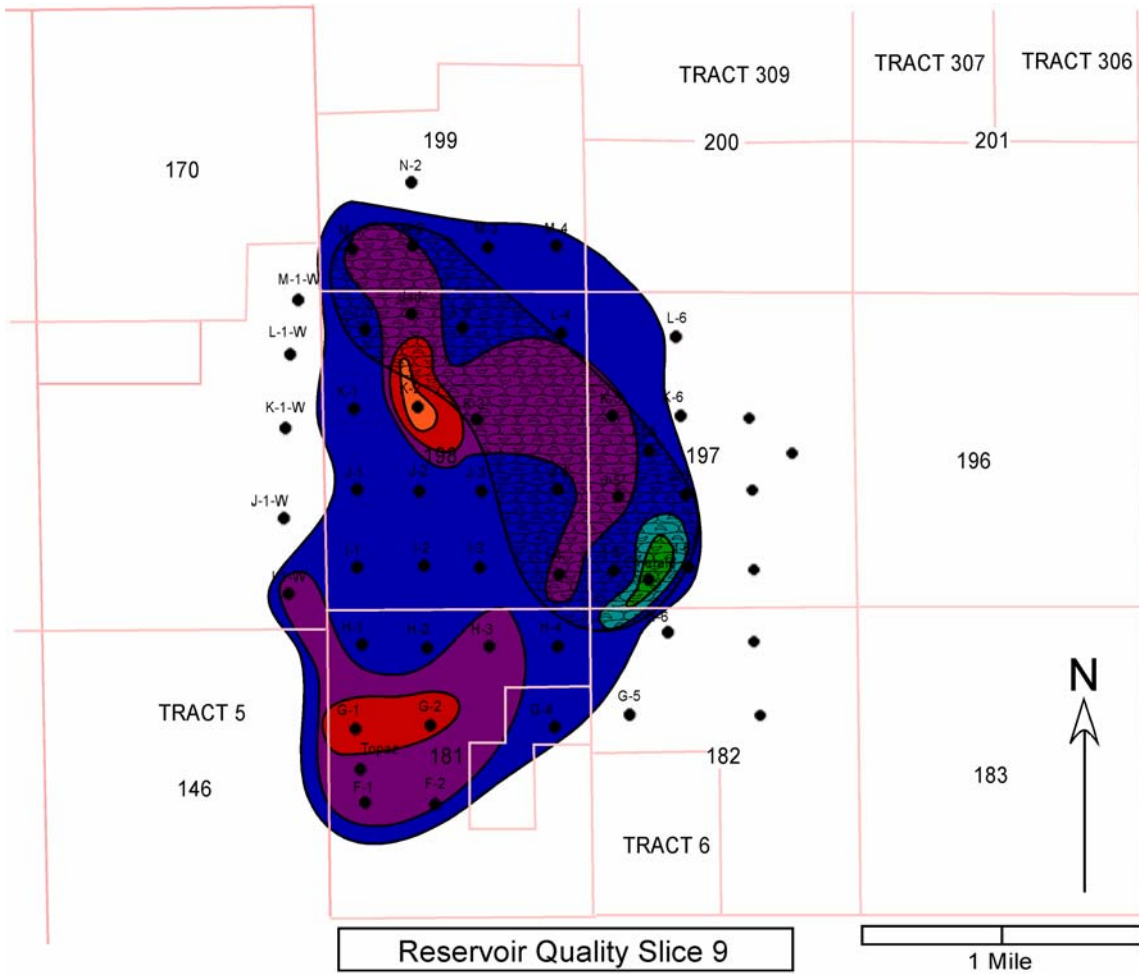
Figure C-41. Diamond M Flow Unit Map 80 to 90 ft Below Top of Reef
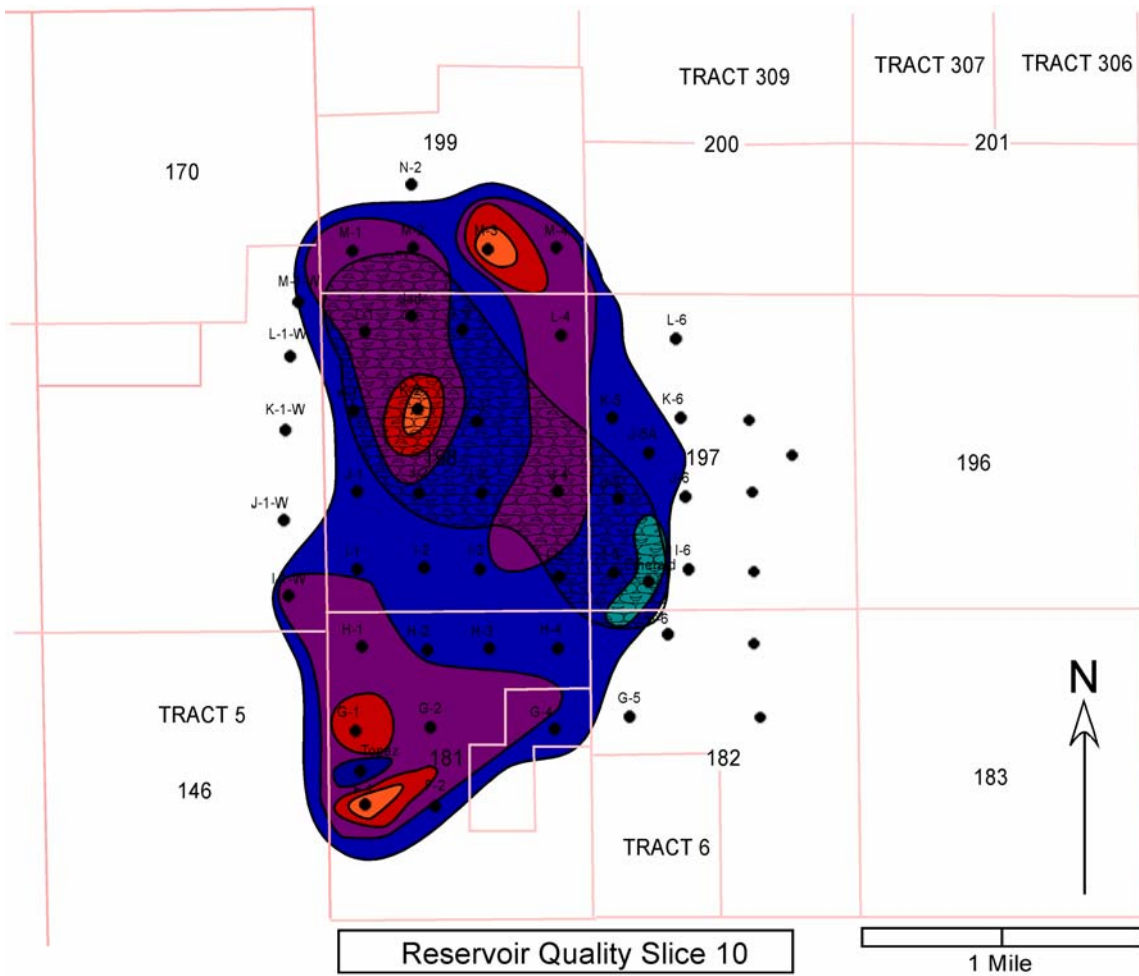
Figure C-42. Diamond M Flow Unit Map 90 to 100 ft Below Top of Reef
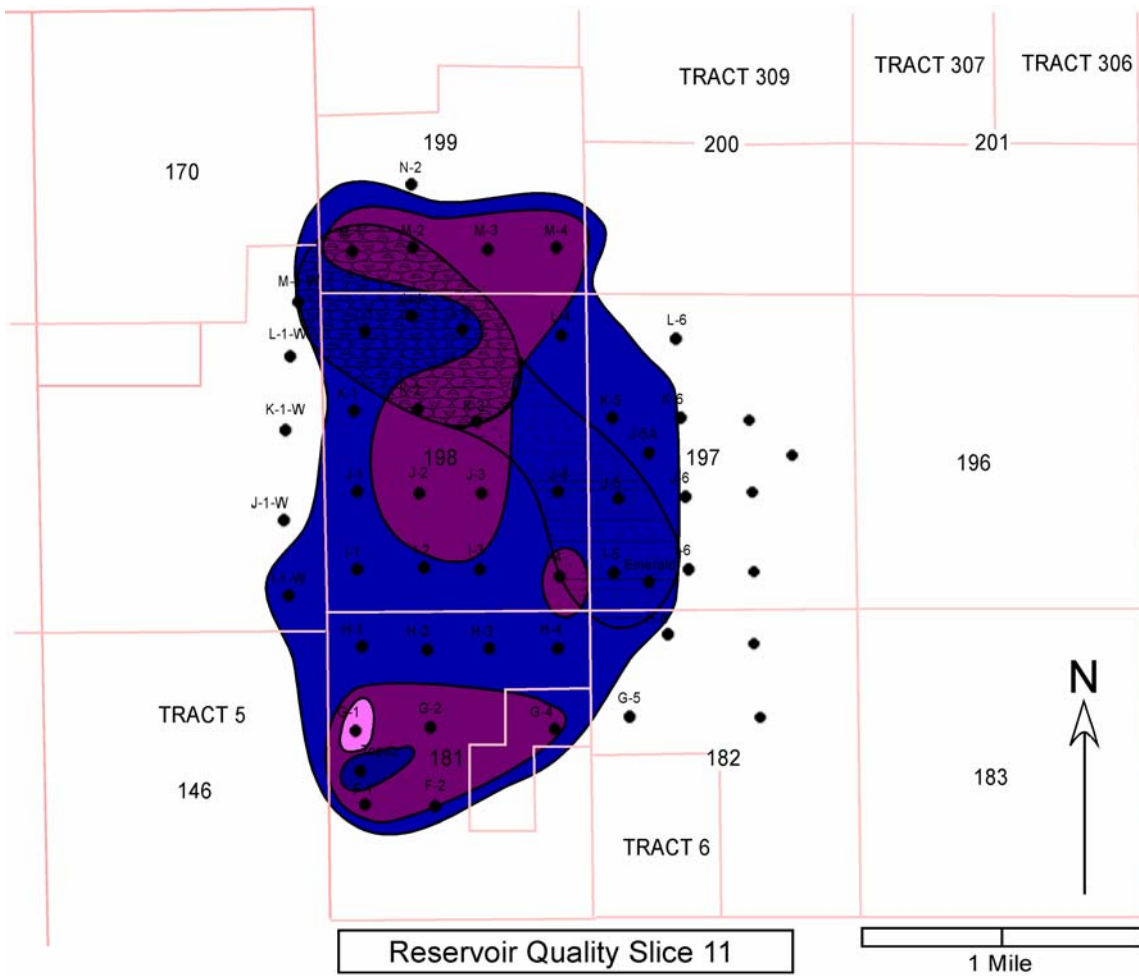
Figure C-43. Diamond M Flow Unit Map 100 to 110 ft Below Top of Reef
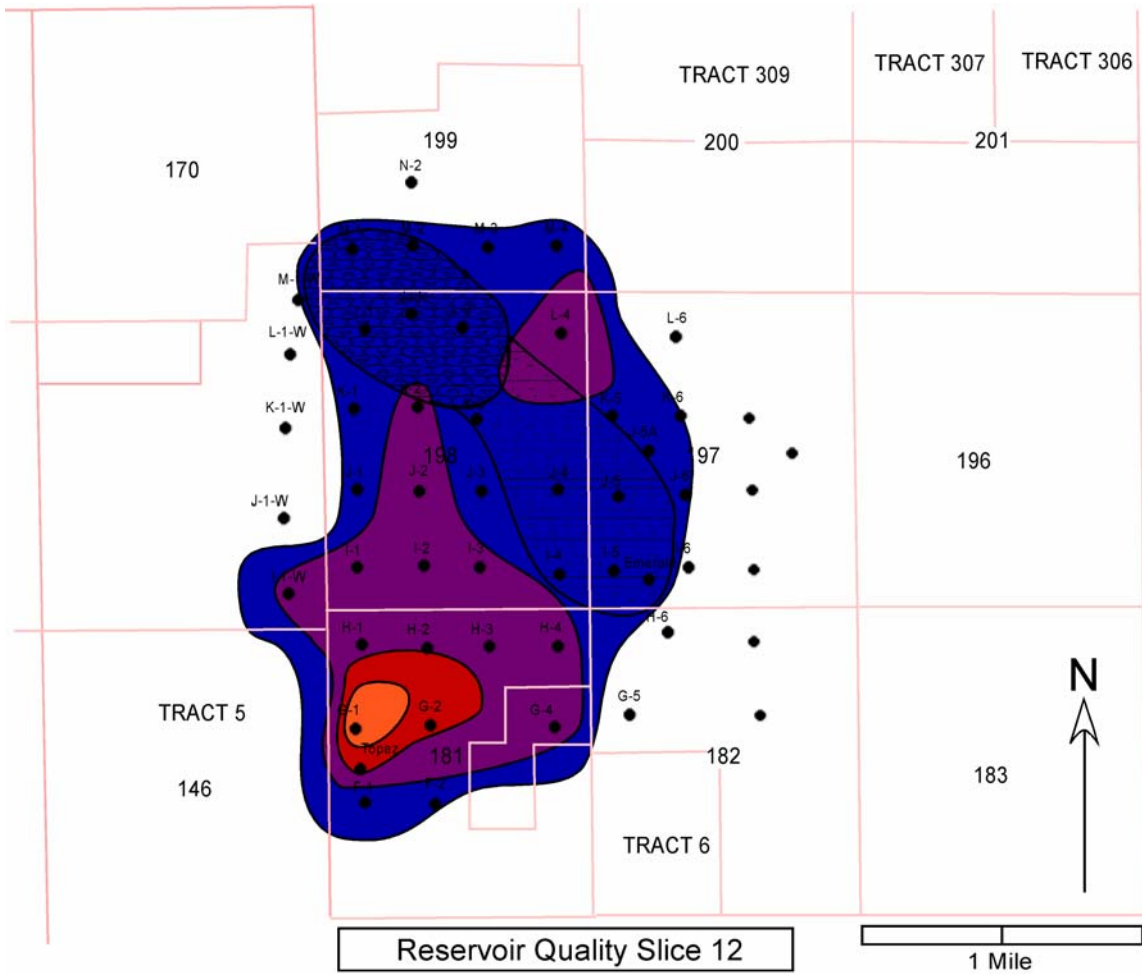
Figure C-44. Diamond M Flow Unit Map 110 to 120 ft Below Top of Reef

Figure C-45. Diamond M Flow Unit Map 120 to 130 ft Below Top of Reef

Figure C-46. Diamond M Flow Unit Map 130 to 140 ft Below Top of Reef

Figure C-47. Diamond M Flow Unit Map 140 to 150 ft Below Top of Reef

APPENDIX D

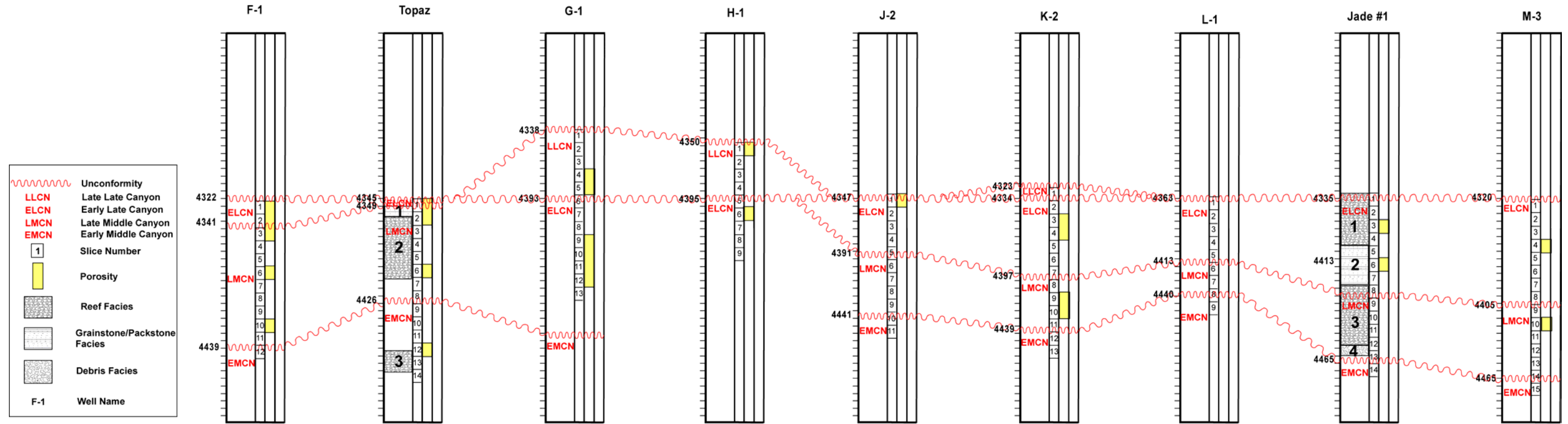**STRUCTURE AND STRATIGRAPHIC CROSS SECTIONS**
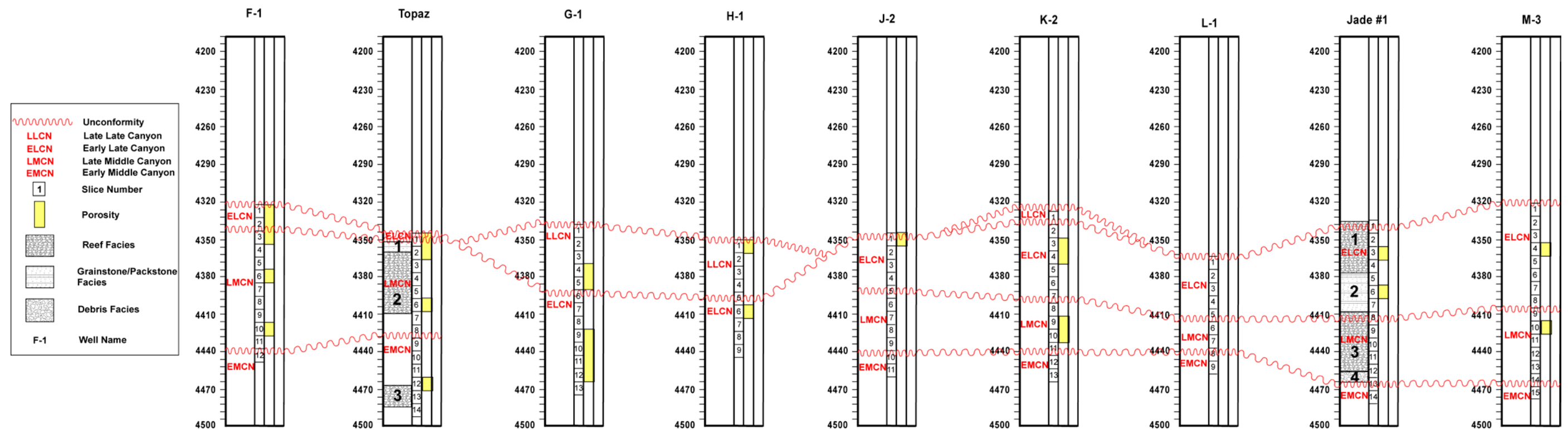
Figure D-1. N-S Structure

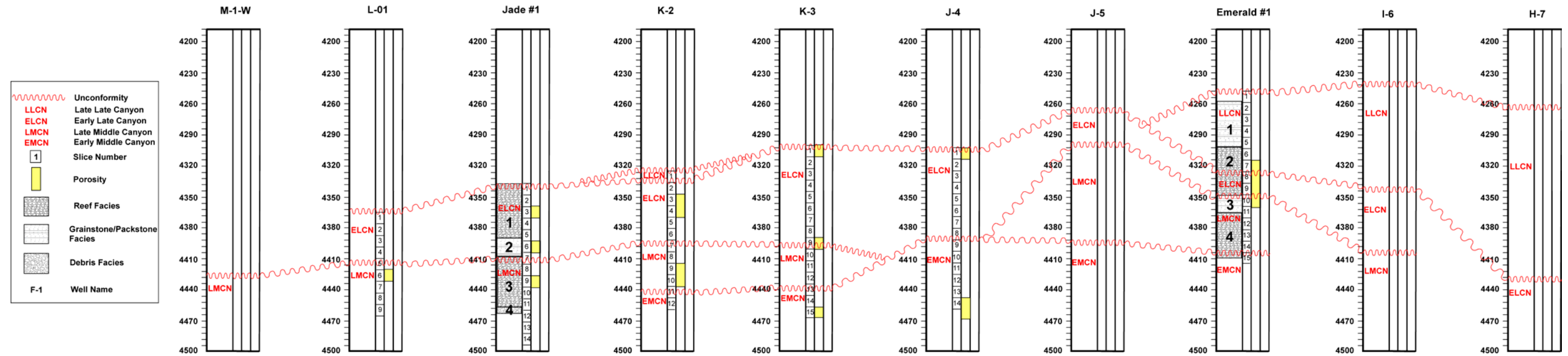**Figure D-2. N-S Stratigraphic**

Figure D-3. NW-SE Structure
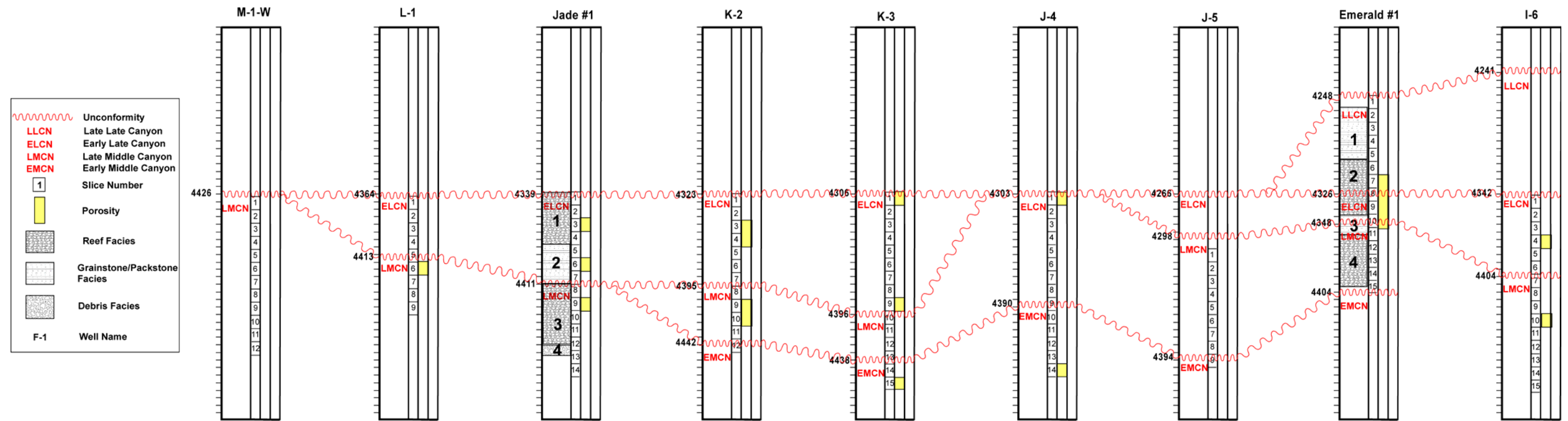
Figure D-4. NW-SE Stratigraphic
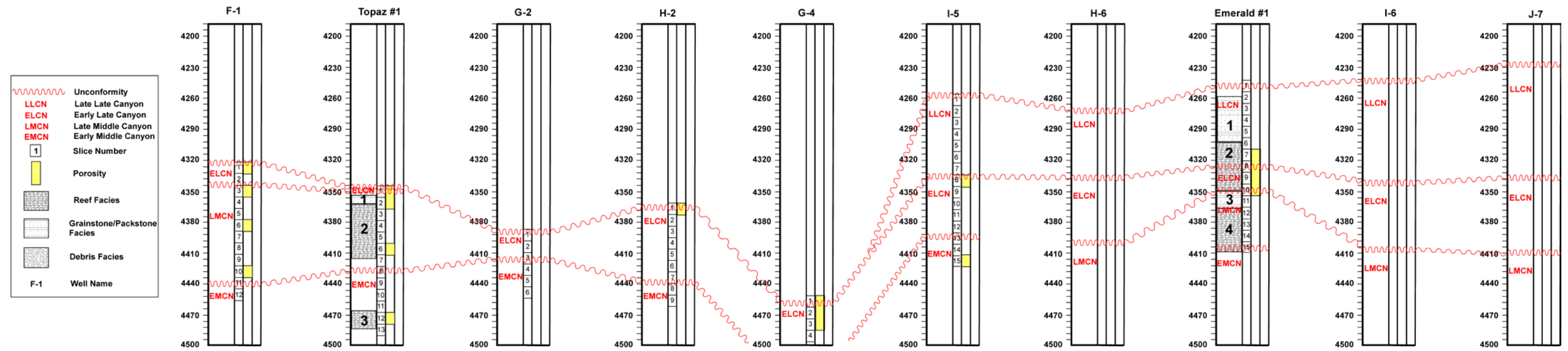
Figure D-5. SW-NE Structure

Figure D-6. SW-NE Stratigraphic

VITA
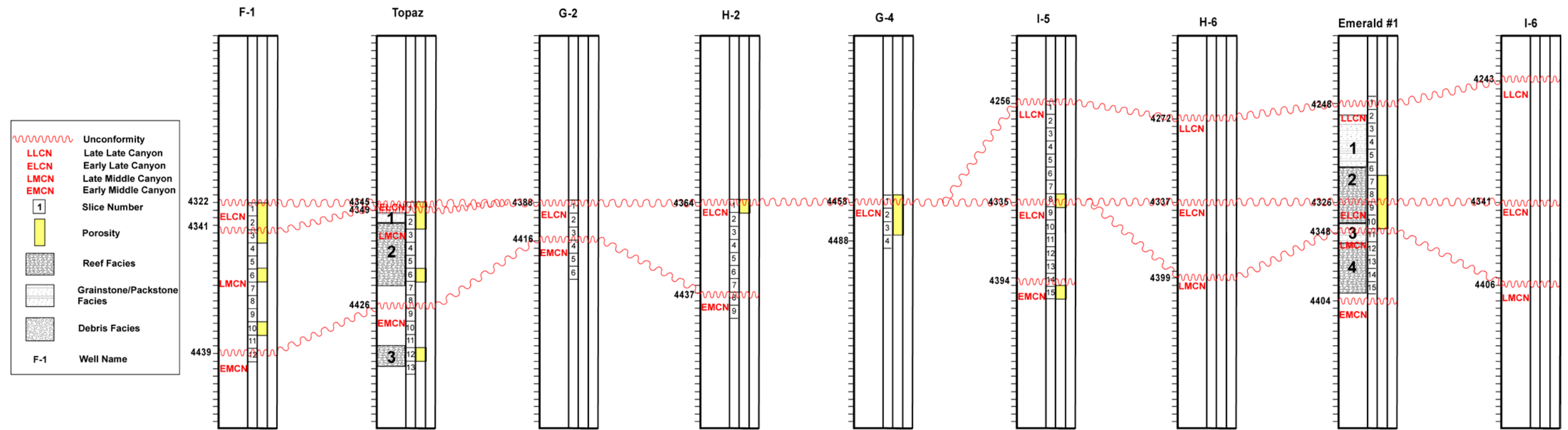
NAME   Aaron Jay Fisher

BIRTHPLACE   Norfolk, Nebraska

PARENTS   Jay and Denise Fisher

EDUCATION   University of Nebraska – Lincoln
                       Lincoln, Nebraska
                       B.S. Geology, 2002

                       Texas A&M University
                       College Station, Texas
                       M.S. Geology, 2005

PROFESSIONAL   U.S.G.S., Lincoln, Nebraska - Intern
EXPERIENCE   EnCana Oil & Gas, USA, Denver, Colorado – Intern

EMPLOYER   EnCana Oil & Gas, USA, Denver, Colorado

PERMANENT   2501 Grove #101
ADDRESS   Denver, CO 80211